Wake dynamics in buoyancy-driven flows: Steady-state–Hopf-mode interaction with O(2) symmetry revisited

Javier Sierra-Ausin,[1,2] David Fabre,[1] and Edgar Knobloch[3]
[1]*UPS-IMFT, Allée du Professeur Camille Soula, 31000 Toulouse, France*
[2]*Università degli Studi di Salerno, 132 Via Giovanni Paolo II, 84084 Fisciano, Salerno, Italy*
[3]*Department of Physics, University of California at Berkeley, Berkeley, California 94720, USA*

(Received 14 July 2023; accepted 9 November 2023; published 12 January 2024)

We present a detailed mathematical study of a truncated normal form relevant to the bifurcations observed in wake flow past axisymmetric bodies, with and without thermal stratification. We employ abstract normal form analysis to identify possible bifurcations and the corresponding bifurcation diagrams in parameter space. The bifurcations and the bifurcation diagrams are interpreted in terms of symmetry considerations. Particular emphasis is placed on the presence of attracting robust heteroclinic cycles in certain parameter regimes. The normal form coefficients are computed for several examples of wake flows behind buoyant disks and spheres, and the resulting predictions compared with the results of direct numerical flow simulations. In general, satisfactory agreement is obtained.

DOI: 10.1103/PhysRevE.109.014216

I. INTRODUCTION

Bifurcation, defined here as a transition between two states with different symmetry, is a key concept in many fields of modern physics. Generally speaking, the larger the symmetry of a problem, the greater is the number of ways the symmetry may be broken, leading to the richest collections of bifurcation scenarios. *Equivariant bifurcation theory* [1] constitutes a mathematical framework for studying such problems and predicts the possible states that may arise and the bifurcation routes between them. A key idea for the parameter space exploration of physical problems is the identification of points of *codimension two* (or greater), namely, sets of parameters at which two (or more) bifurcations arise simultaneously. The richest range of possible behavior is usually encountered in the vicinity of such points. The theory also provides a systematic procedure for constructing truncated dynamical systems called *normal forms* that enable a classification of all admissible states near such codimension-two points and their stability properties. This classification depends only on the symmetry properties of the problem and is thus common to all problems involving the same symmetry.

Fluid mechanics has proved to be a particularly rich playground for the investigation of bifurcations [2]. The classical problems for which bifurcation theory has proved both relevant and helpful include, among others, Taylor–Couette flow (TCF, [3,4]) and Rayleigh-Bénard convection (RBC, [5]). Bifurcation theory is also relevant to wake flows, with the wake of a fixed two-dimensional (2D) cylinder transverse to the flow providing the classic example. Here the wake experiences a Hopf bifurcation leading to the von Kármán vortex street beyond $\mathrm{Re} \approx 47$, where Re is a suitably defined Reynolds number. The case where the cylinder rotates was recently shown to give rise to a much richer range of behavior that was also successfully explained using bifurcation theory [6].

The present work is primarily devoted to transitions in *wake flows past axisymmetric objects* (WFA) within a homogeneous fluid. The geometry which attracted the largest number of studies is that of a sphere. Here experiments [7,8] and numerical investigations [9–11] reveal a primary steady-state bifurcation resulting in the loss of axisymmetry, followed by a secondary bifurcation leading to reflection-symmetric periodic states. The case of a rotating sphere, recently analyzed in [12], reveals a primary bifurcation leading to a rotating wave pattern. Secondary and tertiary bifurcations are therein interpreted as the result of an interaction between three rotating wave patterns. The cases of disks [13–15] and ellipsoids [15] have also been investigated, revealing a collection of new states and bifurcation scenarios involving the loss and recovery of planar symmetry.

Two other related classes of problems will also be considered here. The first is the path taken by objects in free motion, such as rising bubbles or falling solid disks (WFA-FO problem; see [16]). For falling or rising disks, experiments [16–19]) and simulations [20,21] reveal a rich range of possible behavior. As shown in [22], linear stability analysis predicts correctly the primary bifurcations for these flows, while weakly nonlinear analysis [23] reproduces the zigzag path observed in experiments. The case of a rising bubble proved to be more challenging. For bubbles of a fixed ellipsoidal shape, linear stability analysis predicts correctly the destabilization of the path observed in experiments [24], while [25] conducted a linear stability analysis for a deformable bubble, leading to the conclusion that shape deformation plays little role in the resulting dynamics.

The last class of problems considered here is closely related to the two previous ones and corresponds to wake flows past fixed objects in a thermally stratified background involving mixed convection due to Prandtl number effects

(WFA-MC). Motivated by interest in the transition to a turbulent wake in this system, the authors of Ref. [26] conducted a parameter study using numerical simulations at two different Prandtl numbers, $\mathrm{Pr} = 0.72$ and $\mathrm{Pr} = 7$. For both ellipsoids and disks [15], a large collection of states with various symmetry properties was revealed, closely related to the states found in the two previous sets of problems.

Fabre *et al.* [13] were the first to recognize that equivariant bifurcation theory is relevant to these sets of problems, and to note that the relevant spatial symmetry [corresponding to the mathematical group O(2)] is the same as that in Taylor-Couette flow, thus highlighting an unexpected analogy between both systems. Fabre *et al.* thus reconsidered the normal form initially introduced in [3,4] for the TCF problem, and showed that with an appropriate choice of the coefficients, the dynamics of the flow past a sphere and a thin disk are correctly reproduced. Auguste *et al.* [14] successfully applied the same approach to a thick disk. Subsequently, Meliga *et al.* [27] reconsidered the case of the sphere and the thick disk using a multiple scale analysis to determine the coefficients in the normal form. Their results are in agreement with the numerical simulations of [13], thereby confirming the relevance of the approach. However, their derivation method is not fully rigorous, as the problem is not strictly of codimension two. However, exact codimension-two points were detected in both the WFA-MC [26] and the WFA-FO [22] problems, indicating that in these problems a rigorous normal form derivation may be undertaken.

As previously mentioned, Golubitsky and collaborators [3,28] investigated solutions of the normal form corresponding to the state-state–Hopf interaction in the presence of O(2) symmetry, with application to the TCF problem, exploring the dynamics up to secondary bifurcations. However, they do not provide a systematic study of the problem, and many details are left to the reader. Their study also overlooks possible ternary bifurcation to states which are not observed in the TCF problem but are nonetheless relevant to the problems considered here. The purpose of this work is thus to revisit and extend these results and to explain how they can be applied to the TCF, WFA, and WFA-MC problems. Our method differs from that of Golubitsky *et al.* [3,28] in several aspects:

(1) The study is restricted to a truncated problem where only third-order nonlinearities are considered.

(2) Two systems are introduced: a polar coordinate representation that eliminates the two continuous symmetries of the system, and a second system written in its natural Hilbert basis which reduces the dynamics to its fundamental domain. These techniques, when systematically employed, reduce the six-dimensional system to four dimensions and the fixed-point solutions to a single representative of each group orbit and enable us to establish the presence of robust heteroclinic cycles in this system.

(3) The amplification rates λ_s and λ_h of the two primary modes are included explicitly in the unfolding of the problem. Golubitsky *et al.* considered the amplification rates as unspecified functions of a single control parameter only.

Our approach is thus much more in line with that used by Hirschberg and Knobloch [29,30] for the related problem of interaction of two steady-state modes with O(2) symmetry. There are strong similarities between these two situations, as emphasized in what follows.

The paper is organized as follows. Section II presents the normal form and introduces a reduction to polar coordinates that is used in what follows. Section III proposes a general nomenclature for the various solutions of the problem. Section IV reviews the fixed-point solutions of the normal form: pure modes, mixed modes, and possible bifurcations of higher order. Section V considers a degenerate case in which a number of details can be investigated analytically. Section VI presents a numerical exploration of various solutions of the truncated problem. Next, Sec. VII explains how the various results can be used to construct consistent stability diagrams, while Sec. VIII applies these results to the flow past a fixed axisymmetric object, in particular, a disk and a sphere. The paper concludes with a brief discussion in Sec. IX. Some technical details are relegated to a pair of Appendixes. Background to the techniques we use and their application to problems arising in fluid mechanics may be found in [2].

II. NORMAL FORM AND REDUCTION TO AMPLITUDE EQUATIONS

A. Problem parametrization

The flow state $\mathbf{q} = [\mathbf{u}, p]$ is specified by the velocity field $\mathbf{u}$ and the hydrodynamic pressure p (the WFA-MC also includes the temperature field T). Near the mode interaction (a codimension-two bifurcation) the flow state takes the form

$$\mathbf{q} = \mathbf{Q}_0 + \mathrm{Re}[a_0(t)e^{-i\theta}\hat{\mathbf{q}}_s] + \mathrm{Re}[a_1(t)e^{-i\theta}\hat{\mathbf{q}}_{h,-1} + a_2(t)e^{i\theta}\hat{\mathbf{q}}_{h,1}] + \mathrm{h.o.t.} \quad (1)$$

Here $\mathbf{Q}_0$ is the steady-state flow state that is invariant under the action of the whole O(2) group, $\hat{\mathbf{q}}_s$ is the steady mode, and $\hat{\mathbf{q}}_h$ is the Hopf (unsteady) mode. The ansatz in Eq. (1) takes into account the continuous (translation or rotation) symmetry via the terms $e^{\pm i\theta}$, where $\theta \in S^1$ is an angle-like variable in the periodicity direction; for axisymmetric problems it corresponds to the azimuthal angle, while in the TCF it corresponds to the axial direction: $\theta \equiv -2\pi x/\Lambda$, where Λ is the mode wavelength. Here without loss of generality the azimuthal wave number m is taken to be $m = 1$. Both the steady-state flow and the eigenmodes are functions of other spatial variables (radial distance and azimuthal angle for the TCF; radial and axial distances for axisymmetric wake problems), but this dependence is not of importance here.

In the following we shall be interested in the dynamics arising from the interaction between the amplitude a_0 of the steady mode and the amplitudes a_1, a_2 of the left- and right-rotating waves associated with the Hopf mode. All three amplitudes are in general complex functions of the time t, and their behavior near the mode interaction is described by normal form theory.

B. Universal normal form

The normal form is obtained in a standard way: provided the original system of equations is Γ-equivariant under the group $\Gamma \equiv \mathrm{O}(2) \times S^1$, the normal form must also be Γ-equivariant. The Hilbert-Weyl and Poénaru theorems, stated

in [28, Ch. 1], ensure the existence of a finite set of Γ-equivariant polynomials generating the Γ-equivariant Taylor expansion (at the origin) of any smooth mapping. The group Γ acts on $\mathbb{C}^3$, which decomposes into irreducibles $\mathbb{C} \oplus \mathbb{C}^2$ corresponding to the steady and Hopf modes. The action of the group Γ is generated by rotations R_α, reflection κ, and the temporal phase shift Φ of the Hopf mode. The canonical representation of these actions is as follows:

$$\begin{aligned} R_\alpha &: (a_0, a_1, a_2) \to (a_0 e^{i\alpha}, a_1 e^{i\alpha}, a_2 e^{-i\alpha}), \\ \Phi &: (a_0, a_1, a_2) \to (a_0, a_1 e^{i\phi}, a_2 e^{i\phi}), \\ \kappa &: (a_0, a_1, a_2) \to (\overline{a}_0, a_2, a_1). \end{aligned} \tag{2}$$

Based on these considerations, Golubitsky *et al.* [3,28] show that the resulting normal form can be written as follows:

$$\begin{aligned} \begin{pmatrix} \dot{a}_0 \\ \dot{a}_1 \\ \dot{a}_2 \end{pmatrix} &= (c^1 + i\delta c^2) \begin{pmatrix} a_0 \\ 0 \\ 0 \end{pmatrix} + (c^3 + i\delta c^4) \begin{pmatrix} \overline{a}_0 a_1 \overline{a}_2 \\ 0 \\ 0 \end{pmatrix} \\ &\quad + (p^1 + iq^1) \begin{pmatrix} 0 \\ a_1 \\ a_2 \end{pmatrix} + (p^2 + iq^2)\delta \begin{pmatrix} 0 \\ a_1 \\ -a_2 \end{pmatrix} \\ &\quad + (p^3 + iq^3) \begin{pmatrix} 0 \\ a_0^2 a_2 \\ \overline{a}_0^2 a_1 \end{pmatrix} + (p^4 + iq^4)\delta \begin{pmatrix} 0 \\ a_0^2 a_2 \\ -\overline{a}_0^2 a_1 \end{pmatrix}, \end{aligned} \tag{3}$$

where $\delta \equiv |a_2|^2 - |a_1|^2$, and the 12 real quantities c^i, p^i and q^i, $i = 1, 2, 3, 4$, are functions of the control parameters and of the five generators of the ring of invariant polynomials under the action of the group Γ:

$$\begin{aligned} &\rho \equiv |a_0|^2, \quad N \equiv |a_1|^2 + |a_2|^2, \quad \Delta \equiv (|a_2|^2 - |a_1|^2)^2, \\ &\eta \equiv \mathrm{Re}\big(a_0^2 \overline{a}_1 a_2\big), \quad \xi \equiv (|a_2|^2 - |a_1|^2)\mathrm{Im}\big(a_0^2 \overline{a}_1 a_2\big). \end{aligned} \tag{4}$$

Note that the term δ is not an invariant polynomial as its sign changes under the reflection κ. This feature is of importance when checking the equivariance properties of the normal form. That is, the terms of Eq. (3) proportional to δ are, in fact, Γ-equivariant.

C. Normal form in polar coordinates

Using the polar representation of the complex amplitudes $a_j = r_j e^{i\phi_j}$ for $j = 0, 1, 2$, Eq. (3) can be reduced to a system of four coupled equations governing the amplitudes r_0, r_1, r_2 and the phase $\Psi \equiv \phi_1 - \phi_2 - 2\phi_0$:

$$\begin{aligned} \dot{r}_0 &= [c^1 + c^3 r_1 r_2 \cos\Psi - c^4 \delta r_1 r_2 \sin\Psi] r_0, \\ \dot{r}_1 &= [p^1 + \delta p^2] r_1 + [(p^3 + \delta p^4)\cos\Psi + (q^3 + \delta q^4)\sin\Psi] r_0^2 r_2, \\ \dot{r}_2 &= [p^1 - \delta p^2] r_2 + [(p^3 - \delta p^4)\cos\Psi - (q^3 - \delta q^4)\sin\Psi] r_0^2 r_1, \\ \dot{\Psi} &= 2(q^2\delta - c^2\delta - c^3 \sin\Psi - c^4\delta\cos\Psi) \\ &\quad + \frac{r_0^2}{r_1 r_2}[(q^3 + Nq^4)\cos\Psi - (Np^3 + \Delta p^4)\sin\Psi]. \end{aligned} \tag{5}$$

This system is four-dimensional owing to the two continuous symmetries of the system (3). Invariance under the action of the phase shift Φ reduces the three angle-like variables (ϕ_0, ϕ_1, ϕ_2) to two $(\phi_0, \phi_1 - \phi_2)$; invariance under the rotations R_α then leads to the single phase Ψ.

The polar system is equivariant under the action of the group Γ_ρ which is isomorphic to the Pauli group $\Gamma_\rho \simeq D_4 \rtimes \mathbb{Z}_2$, where the symbol $\rtimes$ indicates the semidirect product between groups. The generators of the group are the reflection κ and $R_{\pi/2}\Phi_{\pi/2}$, the discrete rotation through $\pi/2$ with an equal time shift. For the sake of conciseness, let us introduce the action of the following group elements on the polar vector field:

$$\begin{aligned} \kappa &: (r_0, r_1, r_2, \Psi) \to (r_0, r_2, r_1, -\Psi), \\ R_{\pi/2}\Phi_{\pi/2} &: (r_0, r_1, r_2, \Psi) \to (r_0, -r_1, r_2, \Psi + \pi), \\ R_\pi \Phi_\pi &: (r_0, r_1, r_2, \Psi) \to (-r_0, r_1, r_2, \Psi), \\ R_{\pi/2}\Phi_{-\pi/2} &\quad (r_0, r_1, r_2, \Psi) \to (r_0, r_1, -r_2, \Psi + \pi), \end{aligned} \tag{6}$$

where $R_{\pi/2}\Phi_{-\pi/2} = \kappa \cdot (R_{\pi/2}\Phi_{\pi/2})^3 \cdot \kappa$ and $R_\pi \Phi_\pi = (R_{\pi/2}\Phi_{\pi/2})^2$. In the next section, we present a classification of the various solutions based on the polar representation.

D. Group-theoretic considerations

Branching of solutions is determined by the structure of the isotropy lattice acting on fixed points of the normal form (3). The isotropy subgroups of solutions that arise at primary bifurcations correspond to maximal isotropy subgroups of Γ, that is, isotropy subgroups that are not included in any other isotropy subgroup other than Γ itself. Similarly, solutions arising at secondary bifurcations have isotropy subgroups that are maximal in a subgroup strictly smaller than Γ. This process continues until the trivial group is reached, corresponding to the most general fixed point subspace of the normal form.

Prior to the introduction of the isotropy lattice of the normal form (3), let us introduce the following notation to denote some isotropy subgroups of Γ: the group of rotations $\widetilde{SO(2)}$:

$$\widetilde{SO(2)} \equiv \{R_\phi \Phi_{-\phi} \mid \phi \in [0, 2\pi)\}, \tag{7a}$$

and the group $\mathbb{Z}_n(g)$, a cyclic subgroup generated by the element g, satisfying $g^n = \mathrm{Id}$. In Sec. III we use the information extracted from this lattice to determine the types of invariant solutions admitted by the normal form. In addition to the isotropy subgroups of the complex normal form, Table III lists the isotropy subgroups of the solutions of the polar system (5).

E. Third-order normal form

Here we do not deal with the general case, and instead consider a truncated form retaining only nonlinearities of third order. Such a truncated system can be expressed in the following explicit form:

$$\begin{aligned} \dot{a}_0 &= \lambda_s a_0 + l_0 a_0 |a_0|^2 + l_1(|a_1|^2 + |a_2|^2)a_0 \\ &\quad + il_2(|a_2|^2 - |a_1|^2)a_0 + l_3 \overline{a}_0 \overline{a}_2 a_1, \end{aligned} \tag{8a}$$

$$\begin{aligned} \dot{a}_1 &= (\lambda_h + i\omega_h)a_1 + [B|a_1|^2 + (A + B)|a_2|^2]a_1 \\ &\quad + Ca_1|a_0|^2 + Da_0^2 a_2, \end{aligned} \tag{8b}$$

TABLE I. Correspondence of the real coefficients of the normal form (8) with the literature.

	λ_s	λ_h	ω_h	l_0	l_1	l_2	l_3
[3,28]	$c^1_\mu \cdot \mu$	$p^1_\mu \cdot \mu$	q^1_0	c^1_ρ	c^1_N	c^2_0	c^3_0
[4]	$\alpha_0\mu + \beta_0\nu$	$\alpha_1\mu + \beta_1\nu$	ω_0	c_0	$\mathrm{Re}(d_0)$	$-\mathrm{Im}(d_0)$	f_0

$$\dot{a}_2 = (\lambda_h + i\omega_h)a_2 + [B|a_2|^2 + (A+B)|a_1|^2]a_2 + Ca_2|a_0|^2 + D\bar{a}_0^2 a_1, \tag{8c}$$

where l_0, l_1, l_2, l_3 are real coefficients while A, B, C, D are complex. The correspondence with the notation of Golubitsky *et al.* [3,28] is reported in Tables I and II.

The system (8) thus corresponds to the polar equations

$$\dot{r}_0 = \left[\lambda_s + l_0 r_0^2 + l_1\left(r_1^2 + r_2^2\right)\right]r_0 + l_3 r_0 r_1 r_2 \cos\Psi, \tag{9a}$$

$$\dot{r}_1 = \left[\lambda_h + B_r r_1^2 + (A_r + B_r)r_2^2 + C_r r_0^2\right]r_1 + r_0^2 r_2(D_r \cos\Psi + D_i \sin\Psi), \tag{9b}$$

$$\dot{r}_2 = \left[\lambda_h + B_r r_2^2 + (A_r + B_r)r_1^2 + C_r r_0^2\right]r_2 + r_0^2 r_1(D_r \cos\Psi - D_i \sin\Psi), \tag{9c}$$

$$\dot{\Psi} = (A_i - 2l_2)\left(r_2^2 - r_1^2\right) - 2l_3 r_1 r_2 \sin\Psi + r_0^2 D_i \cos\Psi\left[\frac{r_2}{r_1} - \frac{r_1}{r_2}\right] - r_0^2 D_r \sin\Psi\left[\frac{r_2}{r_1} + \frac{r_1}{r_2}\right]. \tag{9d}$$

Interestingly, the polar system involves only nine of the 13 original coefficients, namely, l_0, l_1, l_3, A_r, B_r, C_r, D_r, D_i and $A_i - 2l_2$. The system (9) is decoupled from the evolution of the phase ϕ_0 and the "mean phase" of the Hopf component $\phi_m = (\phi_1 + \phi_2)/2$, which evolve according to

$$\dot{\phi}_0 = l_2\left(r_2^2 - r_1^2\right) + l_3 r_1 r_2 \sin\Psi, \tag{10a}$$

$$\dot{\phi}_m = \omega_h + \left(B_i + \frac{1}{2}A_i\right)\left(r_1^2 + r_2^2\right) + C_i r_0^2 + \frac{1}{2}r_0^2 D_i \cos\Psi\left[\frac{r_2}{r_1} + \frac{r_1}{r_2}\right] + \frac{1}{2}r_0^2 D_i \sin\Psi\left[\frac{r_1}{r_2} - \frac{r_2}{r_1}\right]. \tag{10b}$$

In addition, we introduce a system whose coordinates are invariant under the group action, except for the reflection symmetry in Ψ. The resulting system is useful for studying a particular degenerate case considered in Sec. V. The advantage of such a system is that the dynamics occur in the "fundamental domain," that is, there is only one representative of each group orbit. The system is defined in terms of the invariants

$$R = r_0^2,\ S = r_1^2 + r_2^2,\ P = r_1 r_2,\ Q = \cos\Psi. \tag{11}$$

In terms of these coordinates, the evolution equations become

$$\dot{R} = 2[\lambda_s + l_0 R + l_1 S + l_3 P]R, \tag{12a}$$

$$\dot{S} = 2[\lambda_h + B_r S + C_r R]S + 4[A_r P + D_r Q R]P, \tag{12b}$$

$$\dot{P} = [\lambda_h + B_r S + C_r R]P + 4[A_r P + D_r Q R]S - D_i R\sqrt{(1-Q^2)(S^2 - 4P^2)}, \tag{12c}$$

$$\dot{Q} = \left[2l_3 + \frac{D_r R S}{P}\right](1-Q^2) + \left[(A_i - 2l_2) - \frac{D_i R Q}{P}\right] \times \sqrt{(1-Q^2)(S^2-4P^2)}. \tag{12d}$$

In the study that follows, we take the nonlinear coefficients l_j ($j = 1, 2, 3, 4$) and A, B, C, D as constant and likewise for the frequency ω_h of the Hopf mode. The amplification rates λ_s and λ_h will be used as unfolding parameters. Our study provides predictions for the existence and stability of the possible solutions in the (λ_s, λ_h) plane. To apply these results to the flows we are interested in, we have to specify the dependence of the amplification rates on the control parameters of the problem. The WFA problem employs a single control parameter R, while the WFA-MC problem is specified by two control parameters R_1 and R_2 related to the magnitude of the incoming velocity and the temperature difference between the object and the background, respectively. In this case, the amplification rates can be assumed to have the following dependence:

$$\lambda_s = \alpha_s(R_1 - R_1^*) + \beta_s(R_2 - R_2^*),$$
$$\lambda_h = \alpha_h(R_1 - R_1^*) + \beta_h(R_2 - R_2^*), \tag{13}$$

where R_1^* and R_2^* are the threshold values given by the linear stability analysis of the axisymmetric steady state; for the WFA problem $\beta_s = \beta_h = 0$.

In the TCF problem R_1, R_2 are related to the angular velocities of the inner and outer cylinders; in the vicinity of the bicritical (codimension-two) point (R_1^*, R_2^*) the amplification rates can be assumed to depend linearly on the distance to this point:

$$\lambda_s = c^1_{R_1}(R_1 - R_1^*) + c^1_{R_2}(R_2 - R_2^*),$$
$$\lambda_h = p^1_{R_1}(R_1 - R_1^*) + p^1_{R_2}(R_2 - R_2^*). \tag{14}$$

Numerical values for (R_1^*, R_2^*) and for the parameters $c^1_{R_1}, c^1_{R_2}, p^1_{R_1}, p^1_{R_2}$ are tabulated in [3] for several values of the radius ratio $\eta < 1$ (i.e., the ratio of the radii of the inner and outer cylinders).

TABLE II. Correspondence of the complex coefficients of the normal form (8) with the literature.

	A	B	C	D
[3,28]	$2(p_0^2 + iq_0^2)$	$(p_N^1 - p_0^2) + i(q_N^1 - q_0^2)$	$p_\rho^1 + iq_\rho^1$	$p_0^3 + iq_0^3$
[4]	$e_1 - d_1$	d_1	c_1	f_1

III. CLASSIFICATION OF THE SOLUTIONS

The nomenclature used to classify the various solutions is given in Tables III and IV. We describe every possible solution, although emphasis will be put on solutions that arise generically in the third-order problem and in the degenerate case considered in Sec. V.

To illustrate the various solutions graphically, we project the four-dimensional phase space into a plane spanned either

TABLE III. Nomenclature and symmetry groups of the steady-state solutions of the system (5).

Name	Representative	Isotropy group (complex)	Isotropy group (polar)	Frequency
Pure modes				
TS	$(0, 0, 0, nd)$	$\mathrm{O}(2) \times S^1$	$D_4 \rtimes \mathbb{Z}_2(\kappa)$	0
SS	$(r_a, 0, 0, nd)$	$\mathbb{Z}_2(\kappa) \times S^1$	$\mathbb{Z}_2(\kappa) \times \mathbb{Z}_2(\Phi_\pi)$	0
RW	$(0, r_a, 0, nd)$	$\widetilde{SO(2)}$	$\mathbb{Z}_4(R_{\pi/2}\Phi_{\pi/2})$	1
SW	$(0, r_a, r_a, nd)$	$\mathbb{Z}_2(\kappa) \times \mathbb{Z}_2(R_\pi \Phi_\pi)$	$\mathbb{Z}_2(\kappa) \times \mathbb{Z}_2(R_\pi \Phi_\pi)$	1
Mixed modes				
MM_0	$(r_a, r_b, r_b, 0)$	$\mathbb{Z}_2(\kappa)$	$\mathbb{Z}_2(\kappa)$	1
MM_π	(r_a, r_b, r_b, π)	$\mathbb{Z}_2(\kappa \cdot R_\pi \Phi_\pi)$	$\mathbb{Z}_2(\kappa \cdot R_\pi \Phi_\pi)$	1
MW	$(0, r_a, r_b, \Psi)$	$\mathbb{Z}_2(R_\pi \Phi_\pi)$	$\mathbb{Z}_2(R_\pi \Phi_\pi)$	2
Precessing waves				
General	(r_a, r_b, r_c, Ψ)	$\mathbb{1}$	$\mathbb{1}$	2
Type A	(r_a, r_b, r_b, Ψ)	$\mathbb{1}$	$\mathbb{1}$	2
Type B	$(r_a, r_b, r_c, 0 \text{ or } \pi)$	$\mathbb{1}$	$\mathbb{1}$	2
Type C	$(r_a, r_b, 0, \Psi)$	$\mathbb{1}$	$\mathbb{1}$	2

by the complex amplitude $A(t)$ or by $A'_j(t)$ for $j = 0, 1$, where

$$A(t) \equiv a_0(t) + a_1(t) + \overline{a}_2(t),$$
$$A'_j(t) \equiv A(t)e^{-i\phi_j(t)}, \text{ for } j = 0, 1, \tag{15}$$

hereafter referred to as the A projection and the A' projection, respectively.

The function A provides a global measure of the dynamics of the system and combines contributions from both the steady and unsteady components. In the wake problem, the real and imaginary parts of A can be identified with the leading order contribution to the lift forces in the y and z directions, respectively. In the TCF problem they represent, for example, the vorticity levels at two points located a quarter of a wavelength apart in the periodicity direction.

The solutions that are stationary in the polar representation are summarized in Table III. The simplest solution is the trivial solution [TS: $(a_0, a_1, a_2) = (0, 0, 0)$]. This solution corresponds to Couette flow in the TCF problem, and to the axisymmetric solution in the WFA and WFA-MC problems. In the A projection this solution corresponds to the origin [Fig. 1(a)]. There are three primary solutions: steady-state modes (SSs), rotating waves (RWs), and standing waves (SWs). The steady-state mode (SS) takes the form $(a_0, 0, 0)$, $a_0 \neq 0$. This state corresponds to the Taylor vortex state in the TCF problem and the steady shedding mode in the wake problems. In the A projection, this state is represented by an off-center point [Fig. 1(b)]. As shown in Table V and in Fig. 1(b) using a thin dashed-dotted line, there is a circle of such states related by the rotations R_{ϕ_0}; each state is in addition reflection-symmetric.

The RW and SW solutions arise in a primary Hopf bifurcation of the trivial state. Because of the O(2) symmetry, the eigenvalues at the Hopf bifurcation are doubled, and the Hopf bifurcation produces simultaneously a branch of rotating waves [RWs: $(a_0, a_1, a_2) = (0, a_1, 0)$] and standing waves [SWs: $(a_0, a_1, a_2) = (0, a_1, a_1)$]. The RWs break reflection symmetry; consequently, there are two RWs, rotating in opposite directions and related by reflection. In contrast, the SWs are reflection-symmetric oscillations with zero mean. In the TCF problem the RWs correspond to the spiral vortex state, while in the wake problem they correspond to the spiral

TABLE IV. Nomenclature and symmetry groups of limit cycle solutions of the system (5).

Name of solution	Representative in polar coordinates	Isotropy group	Frequencies in primitive coordinates
$\widetilde{\mathrm{MM}}_{0,\pi}$	$(r_a(t), r_b(t), r_b(t), 0 \text{ or } \pi)$	$\mathbb{1}$	2
IMM	$(0, r_b, r_c, \Psi(t))$	$\mathbb{1}$	2
PuWs	$(r_a(t), r_b(t), r_c(t), \Psi(t))$ with $\overline{r}_b = \overline{r}_c$ and $\overline{\sin \Psi} = 0$	$\mathbb{1}$	2
3-frequency waves (3FW)			
General	$(r_a(t), r_b(t), r_c(t), \Psi(t))$	$\mathbb{1}$	3
Type A	$(r_a(t), r_b(t), r_b(t), \Psi(t))$ with $\overline{\sin \Psi} \neq 0$	$\mathbb{1}$	3
Type B	$(r_a(t), r_b(t), r_c(t), 0 \text{ or } \pi)$ with $\overline{r}_b \neq \overline{r}_c$	$\mathbb{1}$	3
Type C	$(0, r_b(t), r_c(t), \text{nd}^{\text{a}})$ with $\overline{r}_b \neq \overline{r}_c$	$\mathbb{1}$	3
Type D	$(r_a(t), r_b(t), 0, \Psi(t))$ with $\overline{\sin \Psi} \neq 0$	$\mathbb{1}$	3

[a] 'nd' refers to 'not defined'.

TABLE V. Defining equations and eigenvalues of primary branches in the third-order normal form (8).

Name of solutions (condition for supercriticality)	Definition	Eigenvalues	Notes
Pure modes:			
TS	$r_0 = r_1 = r_2 = 0$	λ_s (twice)	Bif. to SS
		$\lambda_h \pm i\omega_h$ (twice each)	Bif. to SW and RW
SS	$r_0 = \sqrt{-\frac{\lambda_s}{l_0}} \equiv r_P$	0	Inv. under rotation
$l_0 < 0$	ϕ_0 arbitrary	$2l_0 r_P^2$	Bif. from TS
	$r_1 = r_2 = 0$	$\lambda_h + i\omega_h + (C+D)r_P^2$ and c.c.	Bif. to MM_0
		$\lambda_h + i\omega_h + (C-D)r_P^2$ and c.c.	Bif. to MM_π
SW	$r_1 = r_2 = \sqrt{-\frac{\lambda_h}{(2B_r + A_r)}} \equiv r_S$	0	Inv. under time shift
$2B_r + A_r < 0$	$r_0 = 0$	0	Inv. under rotation
	$\phi_1 - \phi_2$ arbitrary	$(4B_r + 2A_r)r_S^2$	Bif. from TS
	$\dot{\phi}_1 = \dot{\phi}_2 = \omega_h + (2B_i + A_i)r_S^2$	$-2A_r r_S^2$	Bif. to RW
		$\lambda_s + (2l_1 + l_3)r_S^2$	Bif. to MM_0
		$\lambda_s + (2l_1 - l_3)r_S^2$	Bif. to MM_π
RW	$r_1 = \sqrt{-\frac{\lambda_h}{B_r}} \equiv r_R$	0	Inv. under time shift + rotation
$B_r < 0$	$r_0 = r_2 = 0$	$2B_r r_R^2$	Bif. from TS
	$\dot{\phi}_1 = \omega_h + B_i r_R^2$	Ar_R^2 and c.c.	Bif. to SW
		$\lambda_s + (l_1 + il_2)r_R^2$ and c.c.	Bif. to PrW

shedding state, observed, for example, in the wake of a rising bubble [31]. In the A projection, the RW state corresponds to a limit cycle centered at the origin [Fig. 1(c)], while the SW state is represented by a radial oscillation through the origin [Fig. 1(d)]. In the TCF problem, the SWs correspond to the ribbon state, while in the wake problem they correspond to the symmetric periodic shedding state observed, for example, in the wake of a disk when $R \approx 150$. As for SS, there is a circle of SW states related by rotations; see Fig. 1(d). Each of these solutions corresponds to a one-dimensional fixed point

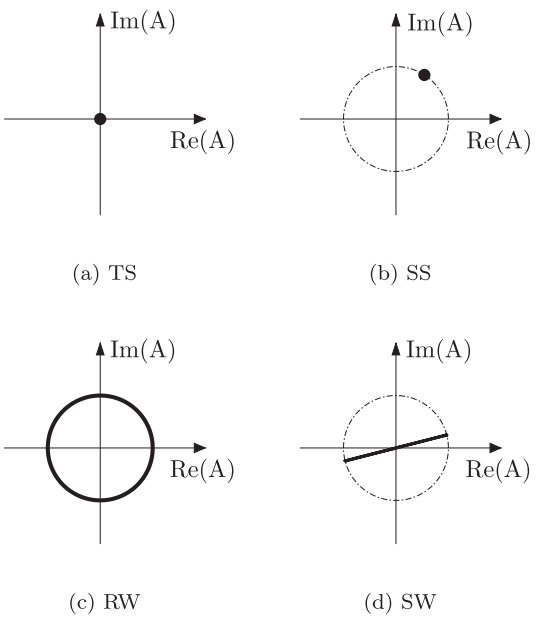

FIG. 1. (a) Trivial state TS and primary branching solutions (b) SS, (c) RW, and (d) SW in the complex A plane.

subspace spanned either by a_0 or a_1, and their presence is therefore guaranteed by the equivariant branching lemma.

Secondary bifurcations may lead to states with a higher-dimensional fixed point subspace. These states correspond to the next rung of the lattice of isotropy subgroups. An example is provided by mixed mode states that correspond to a (nonlinear) superposition of the SS and SW modes. There are two possible states of this type. The first is denoted by MM_0 and corresponds, respectively, to a pattern called twisted vortices in the TCF problem and to the reflection symmetry-preserving mode (RSP) in the wake problem. In the A projection the solution oscillates back and forth in the radial direction but now with nonzero mean [Fig. 2(a)]. The second mixed mode, MM_π, corresponds, respectively, to wavy vortices in the TCF problem and to the reflection symmetry-breaking mode (RSB) in the wake problem. In the A projection, this solution corresponds to a back-and-forth along a line segment perpendicular to the radial direction [Fig. 2(b)]. The phase ϕ_0 of both these states is arbitrary. In other words, there is a circle of solutions of each type, as indicated in Fig. 2(a) and Fig. 2(b). Finally, one can also find a mixed mode state involving the Hopf modes, referred to as a modulated wave state (MW), consisting of a (nonlinear) superposition of two rotating wave modes, and characterized in [32]. This state is referred to as the modulated spiral mode (MSP) in the TCF problem and the modulated wave mode (MW) in the wake problem. It is a state with two temporal frequencies, which are in general incommensurate, and so corresponds to a 2-torus as sketched in Fig. 2(c). This type of solution does not occur generically in the third-order system, although it arises in higher order normal forms or in the degenerate case corresponding to $A_r = 0$ [33].

The last solution type, that is, a state arising in a tertiary bifurcation, corresponds to a fixed point in the (r_0, r_1, r_2, Ψ) coordinates with no further symmetry. According to Eq. (10), in such states the phase ϕ_0 of the steady mode generically

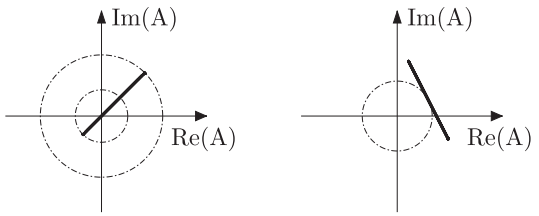

(a) MM_0 (b) $MM\pi$

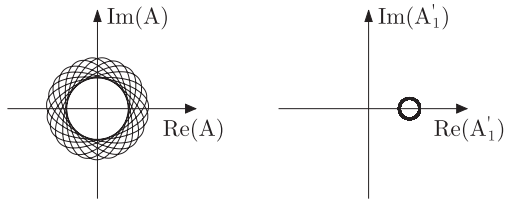

(c) MW: A-projection (d) MW: A'_1-projection

FIG. 2. Secondary states (a) MM_0, (b) MM_π, and (c) MW in the complex A plane. (d) A'_1 projection of the MW state.

precesses at a constant rate given by $\dot{\phi}_0$. Consequently, states of this type display two frequencies, one of which is close to the critical Hopf frequency while the other is a low frequency given by Eq. (10a). Such modes have been called "modulated rotating waves" in [3], but here we prefer to avoid the ambiguous word "modulated," which has been used to describe a large variety of very different states in the past. Instead, these solutions will be referred to as precessing waves (PrWs) or "drifting waves."

The precession of these states is best appreciated in the A' projection, showing the state in a frame of reference precessing with the steady-state component a_0. In this frame of reference, the PrW is periodic and takes the form of an ellipse [Fig. 3(b)]. Note that in this representation the polar coordinates (r_0, r_1, r_2, Ψ) can be interpreted graphically: r_0 is the distance of the center of the ellipse to the origin, $(r_1 + r_2)/2$ and $(r_1 - r_2)/2$ are the major and minor axes, and Ψ is twice the angle between the major axis of the ellipse and the direction of the steady-state component.

There are in fact four types of PrWs, as explained in Table III. The general solution, PrW general, occurs generically in the third-order normal form and corresponds to the most general fixed-point solution of Eq. (9). In addition, there

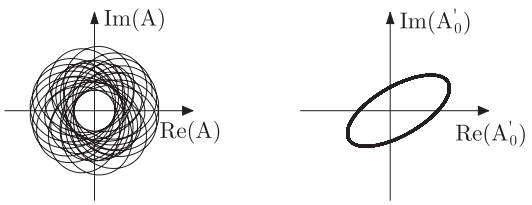

(a) A-projection of PrW (b) A'_0-projection of PrW

FIG. 3. Tertiary state PrW. (a) A projection. (b) A'_0 projection.

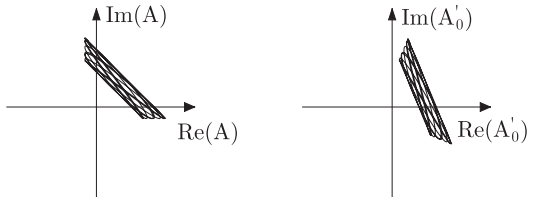

(a) A-projection of $\widetilde{MM}_\pi$ (b) A'_0-projection of $\widetilde{MM}_\pi$

FIG. 4. The modulated mixed mode $\widetilde{MM}_\pi$ in the complex A plane. (a) A projection. (b) A'_0 projection.

are special PrW states. The first two, called PrW type A and type B, do not occur generically in the third-order problem, but they are found in normal forms of higher order or in the degenerate case considered in Sec. V. The third solution, PrW type C, is another degenerate solution that arises in the third-order normal form but only when the three conditions $A_i - 2l_2 = D_r = D_i = 0$ are satisfied. The solutions that are periodic in the polar representation are summarized in Table IV. We distinguish three types of solutions. The first type is referred to as a modulated mixed mode, since it displays the same spatial symmetries as the mixed modes already described. For example, in the A projection the modulated mixed mode state $\widetilde{MM}_\pi$ evolves on a 2-torus, whose shape resembles that of MM_π [Fig. 4(a)]. The A'_0 projection [Fig. 4(b)] yields an identical but rotated picture, indicating that the phase of the steady-state component remains constant. The related state $\widetilde{MM}_0$ is not displayed, since its A projection is identical to that of the MM_0 state. Its modulus $|A|$, however, pulsates with two independent frequencies.

We also find periodic states we call pulsating waves (PuWs). In such states, the polar coordinates (r_0, r_1, r_2, Ψ) all oscillate periodically in time, but the pulsation retains a certain symmetry. Specifically, $\bar{r}_1 = \bar{r}_2$ and $\overline{\sin\Psi} = 0$, where the overbar indicates an average over the pulsation period. According to Eq. (10) the phase ϕ_0 of the steady-state component also pulsates periodically, but the average value of its derivative over one pulsation period vanishes. Consequently, the pattern does not precess. In the A projection, the solution evolves on a 2-torus that remains confined within a given angular sector [Fig. 5(a)], indicating the absence of net precession. The A'_0 projection [Fig. 5(b)] also reveals a 2-torus, albeit of different form.

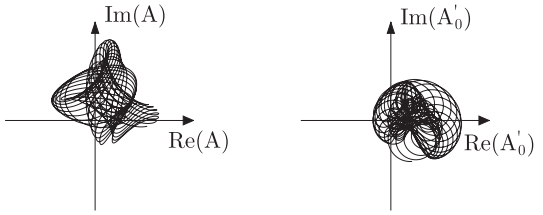

(a) A-projection of PuW (b) A'_0-projection of PuW

FIG. 5. Pulsating wave PuW in the complex A plane. (a) A projection. (b) A'_0 projection.

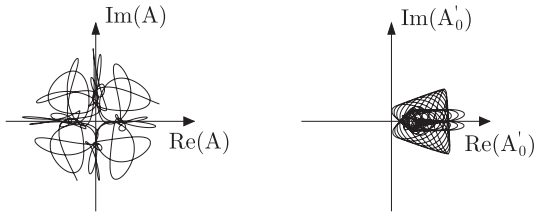

(a) A-projection of 3FW (b) A_0'-projection of 3FW

FIG. 6. Three-frequency wave 3FW in the complex A plane. (a) A projection. (b) A_0' projection.

The last type of periodic solution corresponds to the case where the (r_0, r_1, r_2, Ψ) variables are once again time-periodic, but the conditions $\bar{r}_1 = \bar{r}_2$ and $\overline{\sin\Psi} = 0$ are violated. In the A projection, this state appears irregular [Fig. 6 a], while the A_0' projection [Fig. 6(b)] revels a 2-torus. In fact, this solution actually evolves on a 3-torus, owing to net drift in the phase ϕ_0. We call these states three-frequency waves (3FWs), since they are characterized by a frequency near the critical Hopf frequency, the pulsation frequency, and finally the precession frequency.

The classification of the solutions of the generic steady-Hopf interaction with O(2) symmetry presented by Golubitsky *et al.* [3,28] and covered in Sec. II D is based on maximal isotropy subgroups of the symmetry group $O(2) \times S^1$ of the normal form. The isotropy lattice of the normal form (3) is represented in Fig. 7. This technique predicts the existence up to tertiary bifurcations of fixed points of the complex normal form (3). These isotropy subgroups correspond to the symmetries of the solutions within the fixed point subspace of each isotropy group (cf. Table III). However, several of the states identified here have trivial symmetry (denoted by $\mathbb{1}$), and their existence cannot be established by group-theoretic arguments alone. Thus, the polar representation introduced here is helpful for the explicit computations required to establish the presence of these more complex states.

IV. DYNAMICS OF THE SOLUTIONS

In this section we describe the various solutions of the truncated third-order system (8). We summarize not only the solutions but also their stability properties, assuming that all necessary nondegeneracy conditions hold.

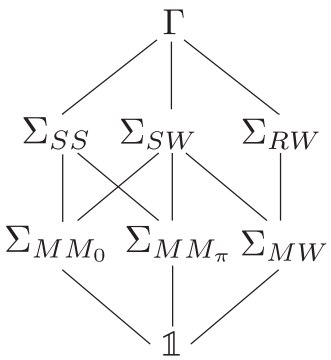

FIG. 7. Lattice of isotropy subgroups of the symmetry group Γ (resp. Γ_ρ).

A. Pure modes

Table V contains the definition and eigenvalues of the trivial state and of the pure modes. Since the polar angle Ψ is undefined for these states, the results are obtained from the primitive amplitude equations (8). Therefore, six eigenvalues are listed for each branch. The condition for supercriticality of the primary branch is also given. This can be deduced from elementary considerations. For example, the SS branch is supercritical if $l_0 < 0$, as can be seen in both the equation for the branch (which is then defined for $\lambda_s > 0$) and the first nonzero eigenvalue (which is then negative, implying that stability has been transferred to the SS branch). The conditions for supercriticality also provide the conditions for the subcriticality (if the corresponding parameter has the opposite sign) and nondegeneracy (if the corresponding quantity is nonzero).

The bifurcation at $\lambda_h = 0$ is the standard Hopf bifurcation with O(2) symmetry and so gives rise simultaneously to branches of RWs and SWs. The RWs rotate counterclockwise (clockwise) when $\omega_h > 0$ ($\omega_h < 0$). Reflection symmetry implies that for each RW $(r_1, r_2) = (r_1, 0)$ there is also a RW $(r_1, r_2) = (0, r_1)$ rotating in the opposite direction. The condition $A_r = 0$ represents a degeneracy that is analyzed theoretically in [1,2,33,34]. In the vicinity of this degeneracy, two-frequency states are present, and these are analyzed in Appendix B.

B. Mixed modes

The defining equations for the mixed modes are given in Table VI. We differentiate between nondegenerate solutions of the third-order truncated normal form, which are the mixed modes of type $MM_{0,\pi}$, and degenerate solutions, which are the modulated wave modes (MWs) briefly discussed in Appendix B. The nondegeneracy conditions for the existence of MM branches are $\Delta_\pm = (2B_r + A_r)l_0 - (2l_1 \pm l_3)(C_r \pm D_r) \neq 0$, with the positive sign for MM_0 and the negative sign for MM_π. Inspection shows that these states bifurcate supercritically from the SS branch if $\Delta_\pm l_0 < 0$ and from the SW branch if $\Delta_\pm(2B_r + A_r) < 0$. Modulated wave modes (MWs) are degenerate solutions of the third order normal form (9) and exist when $A_r = 0$ and $l_3 \sin\Psi \neq 0$.

At this point, it is interesting to point out the similarities between the present problem and the related problem of the interaction between two steady-state modes with opposite parity analyzed by Hirschberg and Knobloch [29,30]. The latter problem has two pure modes and two mixed modes, which are defined by equations similar to those defining our SS and SW pure modes and our mixed modes. So, if we restrict to the subspace generated by the SS and SW pure modes, all the results of Hirschberg and Knobloch [29,30] can be directly applied to the present case. This is not so, however, within the system (8), which reveals the presence of additional secondary bifurcations (see below).

TABLE VI. Defining equations and eigenvalues of mixed modes in the third-order normal form (8).

Name of solutions (condition for supercriticality)	Definition	Eigenvalues	Notes
MM_0	$r_a^2 = \frac{(2l_1+l_3)\lambda_h-(2B_r+A_r)\lambda_s}{\Delta_+}$	eigs of M_a^+	Bif. to $\widetilde{\mathrm{MM}}_0$
$\Delta_+ \neq 0$	$r_b^2 = \frac{(C_r+D_r)\lambda_s-l_0\lambda_h}{\Delta_+}$	eigs of M_b^+	Bif. to PrW and/or PuWs
	$\Delta_+ = (2B_r + A_r)l_0 - (2l_1 + l_3)(C_r + D_r)$		
MM_π	$r_a^2 = \frac{(2l_1-l_3)\lambda_h-(2B_r+A_r)\lambda_s}{\Delta_-}$	eigs of M_a^-	Bif. to $\widetilde{\mathrm{MM}}_\pi$
$\Delta_- \neq 0$	$r_b^2 = \frac{(C_r-D_r)\lambda_s-l_0\lambda_h}{\Delta_-}$	eigs of M_b^-	Bif. to PrW and/or PuWs
	$\Delta_- = (2B_r + A_r)l_0 - (2l_1 - l_3)(C_r - D_r)$		
MW	$r_a^2 = \frac{1}{2}[-\frac{A_r}{2p_N^2} - \sqrt{\frac{\chi}{4p_\Delta^1 p_N^2}}]$	$-2r_{\mathrm{SW}}^2(A_r + 4r_{\mathrm{SW}}^2 p_N^2)$	Bif. from/to SW
$2B_r + A_r < 0, A_r > 0$	$r_b^2 = \frac{1}{2}[-\frac{A_r}{2p_N^2} + \sqrt{\frac{\chi}{4p_\Delta^1 p_N^2}}]$	$-r_{\mathrm{RW}}^2(A_r - 2r_{\mathrm{RW}}^2 p_N^2)$	Bif. from/to RW
$p_N^2 < 0,\ p_\Delta^1 < 0$		$\lambda_s - l_1\frac{A_r}{p_N^2}$	Bif. to PrW or 3FW
Existence I: $A_r/p_N^2 < 0$			
Existence II: $0 < \frac{\chi}{p_\Delta^1 p_N^2} < \frac{A_r^2}{(p_N^2)^2}$	$\chi = A_r(A_r + 2B_r) - 4p_N^2 - A_r\frac{p_{N^2}^1}{p_N^2}\lambda_h$		

C. Stability of mixed modes and tertiary bifurcations

Higher order bifurcations can be detected by linearizing the normal form (8) around the mixed modes in Table VI. Working with the primitive equations, as done in Golubitsky *et al.* [28], leads to the same results, but the procedure is more involved. Within the polar representation four eigenvalues need to be computed; the remaining eigenvalues are both zero owing to the two continuous symmetries representing the invariance of the mixed modes under rotation and time translation.

1. Mixed modes

To obtain the results listed in Table VI, consider the following expansion: $r_0 = r_a + x_0$, $r_1 = r_b + x_1$, $r_2 = r_b + x_2$, and $\Psi = \Psi_0 + \psi$, with either $\Psi_0 = 0$ for MM_0 or $\Psi_0 = \pi$ for MM_π; in either case we suppose the perturbation is infinitesimal, $|x_0|, |x_1|, |x_2|, |\psi| \ll 1$. In terms of the quantities $\rho = x_1 - x_2$ and $x_M = (x_1 + x_2)/2$ the resulting liner stability problem is block-diagonal:

$$\begin{pmatrix}\dot{x}_0\\ \dot{x}_M\end{pmatrix} = M_a^\pm\begin{pmatrix}x_0\\ x_M\end{pmatrix} \text{ with}$$

$$M_a^\pm = 2\begin{pmatrix} l_0 r_a^2 & (2l_1 \pm l_3)r_a r_b \\ (C_r \pm D_r)r_a r_b & (2B_r + A_r)r_b^2\end{pmatrix},$$

$$\begin{pmatrix}\dot{\rho}\\ \dot{\psi}\end{pmatrix} = M_b^\pm\begin{pmatrix}\rho\\ \psi\end{pmatrix} \text{ with}$$

$$M_b^\pm = 2\begin{pmatrix} -A_r r_b^2 \mp D_r r_a^2 & \pm D_i r_a^2 r_b \\ (2l_2 - A_i)r_b \mp D_i r_a^2/r_b & \mp\left(D_r r_a^2 + l_3 r_b^2\right)\end{pmatrix}, \tag{16}$$

with the upper sign applying to MM_0 and the lower one to MM_π. The matrices M_a^+, M_b^+, M_a^-, M_b^- correspond, respectively, to the matrices denoted M_0, M_1, N_0, and N_1 in Golubitsky *et al.* [28] but are obtained here in a much more straightforward way. The expressions are identical, except for the prefactor 2, which is missing in Golubitsky *et al.* and an overall change of sign in their matrix M_1.

Let us first discuss the situation in the subspace (x_0, x_M), which is governed by the system (16a). This system is completely analogous to that studied by Hirschberg and Knobloch [29], since it involves perturbations within the SS/SW invariant subspace of the problem. In particular, the determinant of the matrix $M_a^\pm$ (i.e., the product of the eigenvalues) is $4r_a r_b \Delta_\pm$. It follows that a steady-state bifurcation cannot occur along either mixed mode within the SS/SW subspace. This fact could have been anticipated by noting that this subspace does not admit symmetry-breaking bifurcations of these states. As a result, only Hopf bifurcations are possible. It follows that the eigenvalues of the matrix $M_a^\pm$ are either real with constant sign, or complex conjugate with a possible Hopf bifurcation. Inspection shows that the situation depends upon the signs of the quantities l_0, $2B_r + A_r$, and $\Delta_\pm$. If $\Delta_\pm < 0$, both eigenvalues are real and their product is negative. Therefore, one of the eigenvalues is stable and the other unstable. This means that the corresponding branch $\mathrm{MM}_{0,\pi}$ is always less stable than the primary SS and SW branches. In the case $\Delta_\pm > 0$, the product of the eigenvalues is positive, and their sum is given by the trace of the matrix, i.e., $2[l_0 r_a^2 + (2B_r + A_r)r_b^2]$. When $l_0 < 0$ and $2B_r + A_r < 0$, i.e., when both primary bifurcations are supercritical, the trace remains negative, indicating that both eigenvalues are stable along the whole mixed mode branch. Similarly, when $l_0 > 0$, and $2B_r + A_r > 0$, i.e., when both primary bifurcations are subcritical, the trace remains positive, indicating that both eigenvalues are unstable along the whole branch. The last possibility, $l_0(2B_r + A_r) < 0$, arises when one of the primary bifurcations is subcritical while the other is supercritical. In this case, the real part of the eigenvalues changes sign somewhere along the branch, signaling the occurrence of a Hopf bifurcation. The solution born at such a Hopf bifurcation is referred to here as a modulated mixed mode ($\widetilde{\mathrm{MM}}_{\Psi_0}$; see Table IV). The frequency of oscillation of the modulated mixed mode at the Hopf bifurcation is given by the determinant of the matrix $M_a^\pm$ and may be expressed in terms of r_a^2 as

follows:

$$\omega_a^2 = -\frac{l_0\Delta_\pm}{2B_r + A_r} r_a^4. \tag{17}$$

According to Hirschberg and Knobloch [29], the corresponding bifurcation is degenerate within the third-order truncation, and higher order terms are required to determine whether it is subcritical or supercritical.

Consider now the situation in the (ρ, ψ) subspace, governed by the system (16b). Inspection shows that the matrix $M_b^\pm$ may have complex or real eigenvalues. So, in this subspace, each of the mixed modes can experience steady bifurcations (associated with the vanishing of a single eigenvalue of $M_b^\pm$) and/or Hopf bifurcations (associated with the vanishing of the real part of a pair of complex eigenvalues of $M_b^\pm$). To discuss the nature of the solutions born at these tertiary bifurcations, it is useful to note that the phase drift $\dot\phi_0$ of the steady mode component is related to these quantities by the equation

$$\dot\phi_0 = -2l_2 r_b \rho \pm l_3 r_b^2 \psi + O(\rho^3, \rho^2\psi, \psi^2\rho, \psi^3), \tag{18}$$

obtained from Eq. (10a).

A steady-state bifurcation will generically give rise to a branch with constant, nonzero (ρ, ψ), and according to Eq. (18) such a state will therefore precess at a constant angular velocity. The corresponding bifurcation will be referred to as a parity-breaking bifurcation, and the states produced as precessing waves (PrWs; see Table III). On the other hand, a Hopf bifurcation will generically give rise to a limit cycle in the (ρ, ψ) plane. Since this cycle is symmetric about $(\rho, \psi) = (0, 0)$, Eq. (18) implies that the resulting state will drift back and forth with zero net drift. The result is a direction-reversing wave [35], and we refer here to states of this type as pulsating waves (PuWs; see Table IV).

These predictions are in agreement with those of Golubitsky *et al.* except for their expectation that the symmetry-breaking Hopf bifurcation (i.e., the Hopf bifurcation in the (ρ, ψ) subspace) gives rise to a 3-frequency state. We see that while the bifurcation is indeed associated with translations of the pattern and hence motion along a three-torus, this motion is in fact a two-frequency motion (in the original variables).

The eigenvalues of the matrix $M_b^\pm$ solve a quadratic equation which cannot be simplified easily and generally has to be investigated on a case-by-case basis. However, it is instructive to consider the situation in the vicinity of the bifurcation points of the mixed modes from the pure modes. In the vicinity of the bifurcation from the SS mode one has $r_b \ll r_a$, and the eigenvalues of $M_b^\pm$ are, at leading order, $(\mp 2Dr_a^2, \mp\bar{D}r_a^2)$. Thus, if $D_r > 0$ (resp. $D_r < 0$), the MM_0 is more (resp. less) stable than the MM_π mode in the vicinity of the bifurcation from the SS mode. Similarly, near the bifurcation from the SW mode, the requirement $r_a \ll r_b$ shows that the eigenvalues of $M_b^\pm$ are, at leading order, $(-2A_r r_b^2, \mp 2l_3 r_b^2)$. The first eigenvalue indicates stability for both MM_0 and MM_π modes provided $A_r > 0$. Recall that the parameter A_r also determines if the SW branch is more or less stable than the RW branch. Thus, the mixed modes inherit this property from the SW branch in the vicinity of the bifurcation point. The second eigenvalue likewise implies that if $l_3 > 0$ (resp. $l_3 < 0$), the MM_0 is more (resp. less) stable than the MM_π in the vicinity of the bifurcation from the SW mode.

D. Bifurcation from rotating waves to precessing waves

As indicated in Table III, the RW branch has a couple of complex eigenvalues, which may lead to a bifurcation to a precessing wave (PrW). This situation was investigated by Crawford *et al.* [36] using the primitive sixth-order system. The derivation was lengthy and required the demonstration of an extension of the Hopf theorem to complex equations. The use of the polar representation introduced here leads to substantial simplifications because, within this representation, this bifurcation is in fact a steady-state one, and the resulting precessing wave is a stationary solution of the polar equations.

We consider here the clockwise $(\omega_h > 0)$ RW with $(r_1, r_2) \equiv (r_R, 0)$, where r_R is given in Table III. According to the table, a bifurcation occurs along this branch when the bifurcation parameter, defined by

$$\sigma_R \equiv \lambda_s + l_1 r_R^2, \tag{19}$$

vanishes. Inspection shows that the corresponding eigenvector breaks the symmetry of the mixed mode (i.e., it points in the a_0 direction). We expect, therefore, that the branch originating in this bifurcation will be characterized by $r_0 = O(\sigma_R^{1/2})$. We further anticipate that $r_2 = O(\sigma_R)$ and $r_1 = r_R + x_1$ with $x_1 = O(\sigma_R)$. We also assume that Ψ has a finite limit in the vicinity of the bifurcation point. With these assumptions, the stationary solutions of the polar system (12) obey the following equations at leading order:

$$\sigma_R + l_0 r_0^2 + 2l_1 r_R x_1 + l_3 r_R r_2 \cos\Psi = 0, \tag{20a}$$

$$2B_r r_R x_1 + C_r r_0^2 = 0, \tag{20b}$$

$$A_r r_R r_2 = -r_0^2 (D_r \cos\Psi - D_i \sin\Psi), \tag{20c}$$

$$(A_i - 2l_2) r_R r_2 = -r_0^2 (D_i \cos\Psi + D_r \sin\Psi). \tag{20d}$$

To solve these equations, we add the squares of Eqs. (20c) and (20d) to obtain

$$\left[A_r^2 + (A_i - 2l_2)^2 r_R^2 r_2^2\right] = |D|^2 r_0^4. \tag{21}$$

This equation allows us to express r_2 in terms of r_0. Eliminating $\sin\Psi$ from Eqs. (20c) and (20d) leads to

$$\cos\Psi = -\frac{D_r A_r + D_i(A_i - 2l_2)}{|D|\sqrt{A_r^2 + (A_i - 2l_2)^2}}. \tag{22}$$

Finally, x_1 is easily expressed as a function of r_0 from Eq. (20b). Introducing these expressions into Eq. (20a) yields a classical branching equation which can be cast in the form

$$\sigma_R + H^r r_0^2 = 0,$$
$$\text{with } H^r = l_0 - l_1 \frac{C_r}{B_r} - l_3 \frac{D_r A_r + D_i(A_i - 2l_2)}{A_r^2 + (A_i - 2l_2)^2}. \tag{23}$$

It follows that in the vicinity of the bifurcation point, the precessing waves are given by the branching equation $r_0 \approx (-\sigma_R/H^r)^{1/2}$, and the bifurcation is then supercritical if $H^r < 0$.

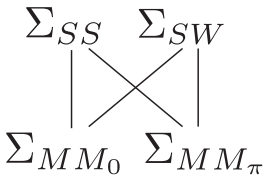

FIG. 8. Structure within in the isotropy lattice suggesting that there may exist of a robust heteroclinic cycle.

The precession rate corresponding to this solution is given by Eq. (10a) and reads

$$\dot{\phi}_0 = -l_2 r_R^2 + H^i r_0^2$$
$$\text{with} \quad H^i = l_2 \frac{C_r}{B_r} + l_3 \frac{D_i A_r - D_r(A_i - 2l_2)}{A_r^2 + (A_i - 2l_2)^2}. \tag{24}$$

Note that the branching parameter H^r and the term H^i correspond, respectively, to the real and imaginary parts of the complex Hopf coefficient H computed in [36], at the end of a much lengthier analysis.

E. Robust heteroclinic cycles

As already mentioned, one may expect the presence of structurally stable or robust heteroclinic cycles in our system in view of its similarity to the mode interaction problem studied in [29,30] when written in polar coordinates. More generally, a heteroclinic cycle is a set of trajectories $\{(\overline{r}_0^{(j)}(t), \overline{r}_1^{(j)}(t), \overline{r}_2^{(j)}(t), \overline{\Psi}^{(j)}(t))\}_{j=1,2,\ldots,m}$ that connect equilibrium solutions $\{(r_0^{(j)}, r_1^{(j)}, r_2^{(j)}, \Psi^{(j)})\}_{j=1,2,\ldots,m}$ with the property that $(\overline{r}_0^{(j)}(t), \overline{r}_1^{(j)}(t), \overline{r}_2^{(j)}(t), \overline{\Psi}^{(j)}(t))$ is backward asymptotic to $(r_0^{(j)}, r_1^{(j)}, r_2^{(j)}, \Psi^{(j)})$ and forward asymptotic to $(r_0^{(j+1)}, r_1^{(j+1)}, r_2^{(j+1)}, \Psi^{(j+1)})$ with the convention $(r_0^{(m+1)}, r_1^{(m+1)}, r_2^{(m+1)}, \Psi^{(m+1)}) = (r_0^{(1)}, r_1^{(1)}, r_2^{(1)}, \Psi^{(1)})$. Such cycles are *robust* if each connection is robust, i.e., cannot be destroyed by changing parameters. Robust heteroclinic cycles do not exist in general nonsymmetric vector fields. However, they may exist in symmetric systems such as ours. First examples of robust heteroclinic cycles connecting saddle points were found in [37,38]. Afterwards, Melbourne, Krupa, and collaborators [39,40] established a general approach to the existence and stability of structurally stable heteroclinic cycles in Γ-equivariant systems. The existence of a robust heteroclinic cycle requires the following conditions:

(1) Each saddle solution sits on a flow-invariant line l_j, say, and each such line is the fixed-point subspace of the isotropy subgroup of the saddle solution, i.e., $l_j = \mathrm{Fix}(\Sigma_{j-1}) \cap \mathrm{Fix}(\Sigma_j)$.

(2) The isotropy subgroups of the invariant lines are maximal isotropy subgroups.

(3) The invariant plane containing the invariant line is the fixed point subspace of a maximal isotropy subgroup.

The proof of this result is based on the existence of cycles in the isotropy lattice, such as Fig. 8 for the present case.

The isotropy lattice in Fig. 8 suggests the existence of a robust heteroclinic cycle between the steady-state mode SS and the standing wave mode SW. Such a heteroclinic cycle possesses two connections that lie within the $\mathrm{Fix}(\mathbb{Z}(\kappa))$ and $\mathrm{Fix}(\mathbb{Z}[\kappa \cdot (\pi, \pi)])$ subspaces. In our notation, the heteroclinic connections lie in the invariant subspaces of the two MM solutions. Melbourne *et al.* [41] found that in the supercritical case such a cycle exists whenever the steady-state mode SS is a saddle (resp. sink) in the fixed-point subspace $\mathrm{Fix}(\mathbb{Z}(\kappa))$ of the isotropy subgroup of the MM_0 mode and a sink (resp. saddle) in the fixed-point subspace $\mathrm{Fix}(\mathbb{Z}[\kappa \cdot (\pi, \pi)])$ of the isotropy subgroup of the MM_π mode. Similarly, the SW mode must be a sink (resp. saddle) in $\mathrm{Fix}(\mathbb{Z}(\kappa))$ and a saddle (resp. sink) in $\mathrm{Fix}(\mathbb{Z}[\kappa \cdot (\pi, \pi)])$. These conditions are satisfied if the first three existence conditions in Table VII are satisfied. In addition, no other fixed point solutions can be present in either of the fixed point subspaces, and solutions starting in the neighborhood of the trivial mode are required to remain bounded, a condition that is satisfied if the last two existence conditions in Table VII hold.

The necessary and sufficient conditions for the asymptotic stability of a particular type of robust heteroclinic cycle referred to as *Type A* are derived in [40]. This type of heteroclinic cycle is constructed in such a way that each trajectory connecting two fixed-point solutions lies within the fixed point subspace of an isotropy group isomorphic to $\mathbb{Z}_2$. Because of this the necessary and sufficient condition for asymptotic stability is

$$\prod_{j=1}^{m} \min\left(-\nu_j^c, \nu_j^e - \nu_j^t\right) > \prod_{j=1}^{m} \nu_j^e, \tag{25}$$

where ν_j^c, ν_j^e, ν_j^t, ν_j^r denote the contracting, expanding, transversal, and radial eigenvalues of the solution j. The *contracting* eigenvalue of the solution j corresponds to the minimum eigenvalue (maximum $-\nu_j$) in the fixed point subspace of solution j; the *expanding* eigenvalue corresponds to the eigenvalue with the largest real part among the eigenvalues restricted to the fixed point subspace of the backward asymptotic heteroclinic connection; the *radial* eigenvalue is the eigenvalue with the smallest real part (largest $-\nu_j^r$) within the intersection between the two previous fixed point subspaces and the *transverse* eigenvalue correspond to the eigenvalue with the largest real part among the eigenvalues restricted to the orthogonal complement. The proof of the identity (25) is based on the use of a set of Poincaré return maps to obtain global estimates of stability from local ones. For more details, the reader is referred to [39,40]. Application of Eq. (25) to our case shows that the heteroclinic cycle $\mathrm{Het}_{\mathrm{SS-SW}}$ is asymptotically stable provided condition (ii) and either condition (i-a) or (i-b) in Table VII hold. This possibility was not considered in [28].

V. THE DEGENERATE CASE $D_i = 0, A_i - 2l_2 = 0$

In this section, we consider the scenario where the parameters D_i and $A_i - 2l_2$ both vanish. This situation arises when all the nonlinear coefficients in Eq. (8) are real. This case is of basic theoretical interest since it corresponds to the case where an additional $\mathbb{Z}_2$ symmetry is present in the primitive amplitude equations. In this case Eq. (8) reduces to a special case of the equations studied in generality by Silber and Knobloch [42] provided we also take $l_0 = A_r + 2B_r$, $\lambda_s = \lambda_h$.

TABLE VII. Definining conditions for structurally and asymptotically stable heteroclinic cycles connecting SS and SW with $\nu_{SS}^{\pm} \equiv \lambda_h + (C_r \pm D_r) r_P^2$ and $\nu_{SW}^{\pm} \equiv \lambda_s + (2l_1 \pm l_3) r_S^2$.

Name of solution (condition for supercriticality)	Existence	Asymptotic stability [Asymp. stable if (ii) and either (i-a) or (i-b)]
Het_{SS-SW}	$\nu_{SS}^{+}\nu_{SS}^{-} < 0$	(i-a) $\nu_{SS}^{+}\nu_{SW}^{-} < -\nu_{SS}^{-}\min(-\nu_{SW}^{+}, \nu_{SW}^{-} + 2A_r r_s^2)$
$l_0 > 0$	$\nu_{SW}^{+}\nu_{SW}^{-} < 0$	(i-b) $\nu_{SS}^{-}\nu_{SW}^{+} < -\nu_{SS}^{+}\min(-\nu_{SW}^{+}, \nu_{SW}^{+} + 2A_r r_s^2)$
$A_r + 2B_r > 0$	$\nu_{SS}^{+}\nu_{SW}^{-} > 0$	(ii) $A_r > 0$
	$\frac{\lambda_s}{\lambda_h}\frac{(C_r+D_r)}{l_0} + \frac{\lambda_h}{\lambda_s}\frac{(2l_1+l_0)}{(2B_r+A_r)} > -2$	
	$\frac{\lambda_s}{\lambda_h}\frac{(C_r-D_r)}{l_0} + \frac{\lambda_h}{\lambda_s}\frac{(2l_1-l_0)}{(2B_r+A_r)} > -2$	

In this case, the equations in polar coordinates take the form

$$\dot{r}_0 = \left[\lambda_s + l_0 r_0^2 + l_1\left(r_1^2 + r_2^2\right) + l_3 r_1 r_2 \cos\Psi\right] r_0, \tag{26a}$$

$$\dot{r}_2 + \dot{r}_1 = \left[\lambda_h + B_r\left(r_1^2 + r_2^2\right) + A_r r_1 r_2 + r_0^2(C_r + D_r\cos\Psi)\right](r_1 + r_2), \tag{26b}$$

$$\dot{r}_2 - \dot{r}_1 = \left[\lambda_h + B_r\left(r_1^2 + r_2^2\right) - A_r r_1 r_2 + r_0^2(C_r - D_r\cos\Psi)\right](r_2 - r_1), \tag{26c}$$

$$\dot{\Psi} = -\left[2l_3 r_1 r_2 + D_r r_0^2 \frac{r_1^2 + r_2^2}{r_1 r_2}\right]\sin\Psi, \tag{26d}$$

while the $PQRS$ equations take the form

$$\dot{R} = 2[\lambda_s + l_0 R + l_1 S + l_3 PQ]R, \tag{27a}$$

$$\dot{S} = 2[\lambda_h + B_r S + C_r R]S + 4[A_r P + D_r RQ]P, \tag{27b}$$

$$\dot{P} = 2[\lambda_h + B_r S + C_r R]P + [A_r P + D_r RQ]S, \tag{27c}$$

$$\dot{Q} = [2l_3 P^2 + D_r RS]\frac{1 - Q^2}{P}. \tag{27d}$$

The former possess an additional reflection symmetry

$$\kappa_r : (r_0, r_1, r_2, \Psi) \to (r_0, r_2, r_1, \Psi) \tag{28}$$

responsible for a reflection symmetry in Ψ:

$$(\kappa_r \cdot \kappa) \cdot (r_0, r_1, r_2, \Psi) = (r_0, r_1, r_2, -\Psi).$$

This symmetry has several consequences. First, the isotropy group of the polar normal form is now $\Gamma_\rho^{(d)} \simeq \mathbb{Z}_2^2 \rtimes D_4 \simeq \mathbb{Z}_2^4 \rtimes \mathbb{Z}_2$. Its isotropy lattice, depicted in Fig. 9, displays new isotropy groups whose fixed point subspaces are of dimension three, *viz.*, Σ_{PrW_A}, Σ_{PrW_B}, Σ_{IMM}. The fixed point subspaces $\mathrm{Fix}(\Sigma_{\mathrm{PrW}_A})$ and $\mathrm{Fix}(\Sigma_{\mathrm{PrW}_B})$ are characterized by $r_1 = r_2$ and $\sin\Psi = 0$, respectively, and are of dimension four in the space of complex amplitudes, i.e., they display two-frequency behavior; see Table VIII. In contrast, the fixed point subspace $\mathrm{Fix}(\Sigma_{\mathrm{IMM}})$ is characterized by $r_0 = 0$. Strictly speaking this is not an invariant subspace of the cubic truncation (since $A_r \neq 0$) but it does become so when the truncation is extended to fifth order; cf. Appendix B. This subspace is also of dimension four and is spanned by solutions of the form $(0, a_1, a_2)$, i.e., by $r_1 \neq r_2$ and the corresponding phases (ϕ_1, ϕ_2).

In addition, it turns out that the isotropy subgroups associated to the mixed waves Σ_{MW_0} and Σ_{MW_π} are not conjugates of each other, i.e., these solutions are distinct, just as in the case of the mixed modes MM_0 and MM_π. The reason behind the distinction between the subgroups Σ_{SW_0}, Σ_{SW_π} (resp. Σ_{RW_0}, Σ_{RW_π}) is algebraic: these isotropy groups are not conjugate of each other, although their fixed point representatives are of the same type. This is because the phase Ψ is undefined for both rotating waves and standing waves, a consequence of the fact that for these states $a_0 = 0$. However, we find it convenient to distinguish between SW_0 and SW_π (resp. RW_0 and RW_π) based on the limiting behavior of the mixed modes (resp. mixed waves) as $r_0 \to 0$, as indicated in the isotropy lattice in Fig. 9.

In this degenerate case the conditions for higher order bifurcations, as well as the complete definition of all possible branches of precessing waves, can be obtained explicitly. The corresponding results are tabulated in Table IX. It is found that there are at most three branches of precessing waves. The first two are denoted PrW_A and PrW_B, while the third kind is generic with no additional symmetry and hence trivial isotropy, and is denoted PrW_G.

A. Bifurcations from mixed modes and rotating waves

Bifurcations from mixed modes are governed by the eigenvalues of the matrices $M_b^{\pm}$ defined in Sec. IV C (apart from the possible bifurcation to a modulated mixed mode if $l_0(2B_r + A_r) < 0$). In the present case, the matrix is diagonal with real

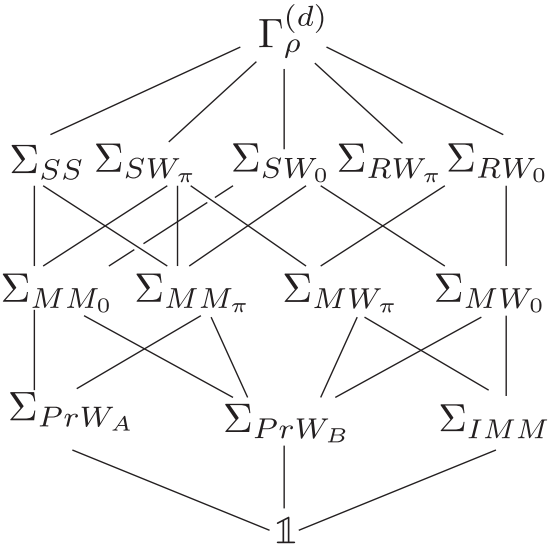

FIG. 9. Lattice of isotropy groups of the degenerate normal form.

TABLE VIII. Nomenclature and symmetry groups of steady-state solutions of the system (26).

Name	Representative	Isotropy group (polar)	Frequency
Primary bifurcations			
SS	$(r_a, 0, 0, nd)$	$\mathbb{Z}_2(\kappa_r) \times \mathbb{Z}_2(\kappa) \times \mathbb{Z}_2(\Phi_\pi)$	0
RW_0	$(0, r_a, 0, nd)$	$D_4(R_{\pi/2}\Phi_{\pi/2}, \kappa \cdot \kappa_r)$	1
RW_π	$(0, r_a, 0, nd)$	$D_4(R_{\pi/2}\Phi_{\pi/2}, \kappa \cdot \kappa_r \cdot \Phi_\pi)$	1
SW_0	$(0, r_a, r_a, nd)$	$\mathbb{Z}_2(\kappa_r) \times \mathbb{Z}_2(\kappa) \times \mathbb{Z}_2(R_\pi\Phi_\pi)$	1
SW_π	$(0, r_a, r_a, nd)$	$\mathbb{Z}_2(\kappa_r\Phi_\pi) \times \mathbb{Z}_2(\kappa) \times \mathbb{Z}_2(R_\pi\Phi_\pi)$	1
Secondary bifurcations			
MM_0	$(r_a, r_b, r_b, 0)$	$\mathbb{Z}_2(\kappa_r) \times \mathbb{Z}_2(\kappa)$	1
MM_π	(r_a, r_b, r_b, π)	$\mathbb{Z}_2(\kappa_r\Phi_\pi) \times \mathbb{Z}_2(\kappa \cdot R_\pi\Phi_\pi)$	1
MW_0	$(0, r_a, r_b, 0)$	$\mathbb{Z}_2(\kappa_r \cdot \kappa) \times \mathbb{Z}_2(R_\pi\Phi_\pi)$	1
MW_π	$(0, r_a, r_b, \pi)$	$\mathbb{Z}_2(\kappa_r \cdot \kappa \cdot \Phi_\pi) \times \mathbb{Z}_2(R_\pi\Phi_\pi)$	1
Tertiary bifurcations			
PrW_A	(r_a, r_b, r_b, Ψ)	$\mathbb{Z}_2(\kappa_r)$	2
PrW_B	$(r_a, r_b, r_c, 0 \text{ or } \pi)$	$\mathbb{Z}_2(\kappa_r \cdot \kappa)$	2
IMM	$(0, r_a, r_b, \Psi(t))$, $\Psi(t) = \phi_1(t) - \phi_2(t)$	$\mathbb{Z}_2(R_\pi\Phi_\pi)$	2

eigenvalues. Therefore, symmetry-breaking bifurcations from MM can lead only to PrWs (precessing waves), excluding the possibility of PuWs (pulsating waves). The number of such bifurcations follows from the eigenvalues of $M_b^\pm$. The first of these is $2(-A_r r_b^2 \mp D_r r_a^2)$, and this quantity changes sign along the MM_0 (MM_π) branch. The second eigenvalue of $M_b^\pm$ is $\mp 2(l_3 r_b^2 + D_r r_a^2)$. Thus, if $l_3 D_r > 0$, this eigenvalue remains of one sign for both mixed modes. On the other hand, if $l_3 D_r < 0$, it changes sign somewhere along both branches. So the number of branching points to precessing waves along the MM branches is either one (if $l_3 D_r > 0$) or three (if $l_3 D_r < 0$). These results are restated in the top part of Table IX, where the conditions for a zero eigenvalue are stated in terms of λ_s and λ_h instead of r_a and r_b using Table VI.

We also report in the table the branching point from the RW branch, investigated in Sec. IV D. This point exists generically, and the corresponding branch has $\Psi = 0$ (resp. $\Psi = \pi$) if $A_r D_r < 0$ (resp. $A_r D_r > 0$). We end up with a total number of either two or four bifurcation points to precessing waves.

The IMM solution is degenerate, as was the case already for the generic third-order normal form. The addition of higher order terms, as done in Appendix B, leads to the existence of the solution IMM, which in this degenerate case is a heteroclinic connection between the mixed waves MW_0 and MW_π. This last statement follows from the integration of Eq. (26d) with $r_0 = 0$, which leads to $\Psi \to 0$ as $t \to \infty$ and $\Psi \to \pi$ as $t \to -\infty$ if $l_3 r_a r_b > 0$ and to $\Psi \to \pi$ as $t \to \infty$ and $\Psi \to 0$ as $t \to -\infty$ if $l_3 r_a r_b < 0$.

TABLE IX. Higher order bifurcations in the degenerate case $D_i = 0, A_i - 2l_2 = 0$. [(1)]Results relevant to the PrW of type A also hold in the less degenerate case to $D_i = 0, A_i - 2l_2 \neq 0$. [(2)]Results for bifurcations to modulated mixed modes hold in the generic case. [(3)]The bifurcation from rotating waves leads to a PrW_B in the present case, and to a general PrW in the generic case. [(4)]The conditions listed for the existence of Hopf bifurcations ensure an odd number of Hopf lines (1 or 3). The condition for an odd number of Hopf lines in the case of a termination at the MM_π fixed point is $\Delta_+ \Lambda_B^+ > 0$.

Branch	New solution	Bifurcation point	Condition for existence of new solution
MM_0	$PrW_A^{(1)}$	$\sigma_{0A} \equiv [l_3(C_r + D_r) - D_r(2B_r + A_r)]\lambda_s + [(2l_1 + l_3)D_r - l_0 l_3]\lambda_h = 0$	$l_3 D_r < 0$
	PrW_B	$\sigma_{0B} \equiv -[A_r C_r - 2B_r D_r]\lambda_s + [A_r l_0 - D_r(2l_1 + l_3)]\lambda_h = 0$	$A_r D_r < 0$
	$\widetilde{MM}_0^{(2)}$	$2(B_r + A_r)(C_r + D_r - l_0)\lambda_s + l_0(2l_1 + l_3 - 2B_r - A_r)\lambda_h = 0$	$(2B_r + A_r)l_0 < 0$
MM_π	$PrW_A^{(1)}$	$\sigma_{\pi A} \equiv [l_3(C_r - D_r) - D_r(2B_r + A_r)]\lambda_s + [(2l_1 - l_3)D_r - l_0 l_3]\lambda_h$	$l_3 D_r < 0$
	PrW_B	$\sigma_{\pi B} \equiv -[A_r C_r + 2B_r D_r]\lambda_s + [A_r l_0 + D_r(2l_1 - l_3)]\lambda_h = 0$	$A_r D_r > 0$
	$\widetilde{MM}_\pi^{(2)}$	$(2B_r + A_r)(C_r + D_r - l_0)\lambda_s + l_0(2l_1 + l_3 - 2B_r - A_r)\lambda_h = 0$	$(2B_r + A_r)l_0 < 0$
RW	$PrW_B^{(2,3)}$	$\sigma_R \equiv \lambda_s - l_1\lambda_h/B_r = 0$	Generic
PrW_A	PrW_G	$\sigma_{AG} \equiv [l_3(\sigma_{0A} + \sigma_{\pi A}) - A_r(\sigma_{\pi A} - \sigma_{0A})]/(\Sigma_A l_3) = 0$	$l_3 D_r < 0, A_r^2 < l_3^2$
	3FW(A)	$H_A = 0$	Eq. (38)
PrW_B	PrW_G	$\sigma_{BG} \equiv [2l_3 B_r D_r - A_r^2 C_r]\lambda_s + [A_r^2 l_0 - 2l_1 l_3 D_r - l_3 A_r D_r]\lambda_h = 0$	If $A_r D_r < 0, A_r^2 - A_r l_3 < 0$, If $A_r D_r > 0, A_r^2 + A_r l_3 < 0$
	3FW(B)[(4)]	$H_B = 0$	Eq. (49)
PrW_G	3FW	$\Omega^4 - I I_G \Omega^2 + D_G = 0, \quad T_G \Omega^2 - I_G = 0$	–

B. The subspace $r_1 = r_2$

The dynamics within the invariant subspace $\mathrm{Fix}(\Sigma_{\mathrm{PrW}_A})$, defined in polar coordinates as

$$\mathrm{Fix}(\Sigma_{\mathrm{PrW}_A}) = \{(r_0, r_1, r_2, \Psi) : r_1 = r_2\}, \tag{29}$$

take the form

$$\dot{r}_0 = \left[\lambda_s + l_0 r_0^2 + 2l_1 r_1^2 + l_3 r_1^2 \cos\Psi\right] r_0, \tag{30a}$$

$$\dot{r}_1 = \left[\lambda_h + (A_r + 2B_r) r_1^2 + (C_r + D_r \cos\Psi) r_0^2\right] r_1, \tag{30b}$$

$$\dot{\Psi} = -2\left[l_3 r_1^2 + D_r r_0^2\right] \sin\Psi. \tag{30c}$$

The RPQ coordinates can also be used in this subspace (which corresponds to $S = 2P$):

$$\dot{R} = 2[\lambda_s + l_0 R + (2l_1 + l_3 Q)P]R, \tag{31a}$$

$$\dot{P} = 2[\lambda_h + (2B_r + A_r)P + (C_r + D_r Q)R]P, \tag{31b}$$

$$\dot{Q} = 2[l_3 P + D_r R](1 - Q^2). \tag{31c}$$

The resulting systems are formally identical to those governing the interaction of two steady-state modes with opposite parity studied by Hirschberg and Knobloch, Eq. (10) of [29], given by the correspondence

$$r_0 \equiv r,\ r_1 \equiv \rho,\ \Psi \equiv 2\Psi,\ \lambda_s \equiv \lambda,\ \lambda_h \equiv \mu,\ l_0 \equiv a,$$
$$2l_1 \equiv b,\ l_3 \equiv e,\ 2B_r + A_r \equiv d,\ C_r \equiv c,\ D_r \equiv f. \tag{32}$$

The results of [29,30] can therefore be applied to the system (30). We use these results to conclude that when $D_r l_3 < 0$ the two branches of mixed modes are connected by a tertiary branch of the form $r_0 \neq 0$, $r_1 = r_2 \neq 0$, $\sin\Psi \neq 0$. In the nomenclature of the present manuscript, this branch corresponds to a precessing wave of type A (see Table III). The defining equations for this solution are

$$R = r_0^2 = \frac{\sigma_{0A} - \sigma_{\pi A}}{2D_r \Sigma_A}, \tag{33a}$$

$$P = r_1^2 = r_2^2 = -\frac{\sigma_{0A} - \sigma_{\pi A}}{2l_3 \Sigma_A}, \tag{33b}$$

$$Q = \cos\Psi = \frac{\sigma_{\pi A} + \sigma_{0A}}{\sigma_{\pi A} - \sigma_{0A}}, \tag{33c}$$

where

$$\Sigma_A \equiv (2B_r + A_r + 2l_1)D_r - l_3(C_r + l_0) \neq 0,$$
$$\Sigma_A^a \equiv D_r(A_r + 2B_r) - l_0 l_3,$$
$$H_A^{0,\pi} \equiv (\Delta_+ + \Delta_-) - 4D_r l_3\left(1 - \Sigma_A/\Sigma_A^a\right),$$
$$\tfrac{1}{2}(\sigma_{0A} + \sigma_{\pi A}) \equiv [(2B_r + A_r)D_r - C_r l_3]\lambda_s + (2D_r l_1 - l_0 l_3)\lambda_h,$$
$$\tfrac{1}{2}(\sigma_{0A} - \sigma_{\pi A}) \equiv D_r l_3(\lambda_s + \lambda_h), \tag{33d}$$

as in Eq. (17) of [29]. The range of existence of this connecting branch in the (λ_s, λ_h) plane is obtained by imposing the requirement $\cos\Psi \in [-1, 1]$ on Eq. (33c); the conditions obtained from $\cos\Psi = \pm 1$ are identical to the conditions obtained from the vanishing of the second eigenvalue of $M_b^{\pm}$ and displayed in Table IX, confirming that the PrW_A branch connects the two mixed mode branches.

The stability of all the solutions within the invariant subspace $\mathrm{Fix}(\Sigma_{\mathrm{PrW}_A})$ is determined as in Ref. [29]. The linearized dynamics within this subspace are governed by a 3×3 matrix with determinant D_A, trace T_A and second invariant I_A given below:

$$D_A = -\frac{4}{D_r \Sigma_A^2 l_3}\sigma_{\pi A}\sigma_{0A}(\sigma_{\pi A} - \sigma_{0A}), \tag{34a}$$

$$T_A = \frac{\Sigma_A^a(\sigma_{\pi A} - \sigma_{0A})}{D_r l_3 \Sigma_A}, \tag{34b}$$

$$I_A = -\frac{\Delta_+\sigma_{\pi A}^2 + \Delta_-\sigma_{0A}^2}{D_r l_3 \Sigma_A^2} + \frac{(-4D_r l_3 + \Delta_+ + \Delta_-)}{D_r l_3 \Sigma_A^2}\sigma_{\pi A}\sigma_{0A}. \tag{34c}$$

Since $-1 < Q < 1$ along the PrW_A branch, the quantity $\sigma_{\pi A} - \sigma_{0A} \equiv -2D_r l_3(\lambda_s + \lambda_h)$ cannot vanish along it. As a consequence, D_A vanishes only at the bifurcations to mixed modes (defined by $Q = \pm 1$), and no steady-state bifurcations occur within the invariant subspace Σ_{PrW_A} along the branch. The necessary and sufficient conditions for the stability of the branch within its fixed point subspace are $D_A < 0$, $T_A < 0$, $I_A > 0$, and $H_A \equiv I_A - D_A/T_A > 0$. Inspection of Eq. (34a) shows that the determinant is negative (resp. positive) whenever $\sigma_{\pi A} - \sigma_{0A} > 0$, which occurs when $l_3 > 0$, $D_r < 0$ (resp. $l_3 < 0$, $D_r > 0$) corresponding to the bifurcation of PrW_A from the MM_π mode (resp. MM_0). When the determinant is negative, the trace is negative if and only if $\Sigma_A \Sigma_A^a > 0$. If these two conditions are satisfied, the necessary and sufficient condition of the positivity of the second invariant I_A all along the branch is that $\Delta_+ \geqslant 0$ and $\Delta_- \geqslant 0$ (defined in Table VI), since $\sigma_{0A}\sigma_{\pi A} \leqslant 0$ all along the branch. The fourth condition is as follows:

$$0 < H_A \equiv \frac{1}{D_r l_3 \Sigma_A^2}\big[-\Delta_+\sigma_{\pi A}^2 - \Delta_-\sigma_{0A}^2 + \sigma_{\pi A}\sigma_{0A}(\Delta_+ + \Delta_- - 4D_r l_3\left(1 - \Sigma_A/\Sigma_A^a\right)\big]. \tag{35}$$

Thus, if the previous three conditions are satisfied, the necessary and sufficient condition for $H_A > 0$ all along the branch is

$$\left|\left(1 - \frac{\Sigma_A}{\Sigma_A^a}\right) - \frac{\Delta_+ + \Delta_-}{4D_r l_3}\right| \geqslant -\frac{\sqrt{\Delta_+\Delta_-}}{2D_r l_3}, \tag{36}$$

which is immediately satisfied if $0 < \Sigma_A/\Sigma_A^a < 1$. Summarizing, the necessary and sufficient conditions for the stability of the branch within the invariant subspace Σ_{PrW_A} are

$$\Delta_+ > 0, \quad \Delta_- > 0, \quad 0 < \frac{\Sigma_A^a}{\Sigma_A} < 1, \quad l_3 > 0. \tag{37}$$

The condition $\frac{\Sigma_A}{\Sigma_A^a} < 1$ can be replaced by Eq. (36).

The quantity $H_A(\sigma_{0A}, \sigma_{\pi A})$ can be interpreted as the distance to a Hopf bifurcation of the PrW_A branch, which is located at $H_A(\sigma_{0A}, \sigma_{\pi A}) = 0$. In particular, because the trace T_A divides D_A, we have at most two Hopf bifurcations. There is a supercritical Hopf from the PrW_A branch leading to a stable 3FW if the following conditions are satisfied:

$$\Delta_+ > 0, \quad \Delta_- > 0, \quad l_3 D_r < 0,$$
$$\frac{\sqrt{\Delta_+\Delta_-}}{2D_r l_3} \leqslant \left(1 - \frac{\Sigma_A}{\Sigma_A^a}\right) - \frac{\Delta_+ + \Delta_-}{4D_r l_3} \leqslant -\frac{\sqrt{\Delta_+\Delta_-}}{2D_r l_3}. \tag{38}$$

The case of a single Hopf bifurcation arises when the following two degeneracy conditions hold, $\Delta_-\Delta_+ = 0$ and $\Sigma_A = \Sigma_A^a$. Therefore, whenever Eq. (38) is satisfied and $\Delta_+\Delta_- \neq 0$ we have two Hopf bifurcations in the $(\sigma_{0A}, \sigma_{\pi A})$ plane, located at

$$\sigma_{\pi A} = K^{\pm}_{A,H}\sigma_{0A},$$
$$K^{\pm} \equiv \frac{H_A^{0,\pi}}{2\Delta_+} \pm \frac{1}{\Delta_+}\left[\left(H_A^{0,\pi}\right)^2 - 4\Delta_+\Delta_-\right]^{\frac{1}{2}}, \tag{39}$$

with $H_A^{0,\pi}$ defined in Eq. (33d).

In the present situation, we also need to determine one additional eigenvalue that describes the stability in the $r_2 - r_1$ direction. This eigenvalue, hereafter σ_{AG}, is given by

$$\sigma_{AG} \equiv 2P(l_3 Q - A_r) = \frac{l_3(\sigma_{0A} + \sigma_{\pi A}) - A_r(\sigma_{\pi A} - \sigma_{0A})}{\Sigma_A l_3}. \tag{40}$$

A necessary and sufficient condition ensuring the existence of a steady-state bifurcation associated with the vanishing of σ_{AG} is that the signs of σ_{AG} at either end of the branch are opposite. This leads to the condition reported in the last column of Table IX.

C. The subspace sin Ψ = 0

The second fixed point subspace corresponds to $\sin\Psi = 0$. At first glance, this subspace corresponds to two distinct cases, $\Psi = 0$ and $\Psi = \pi$. However, because of the symmetry of the polar equations, a jump in Ψ by π is equivalent to a change of sign of either r_1 or r_2. As a consequence, to investigate this subspace, we may set $\Psi = 0$ but allow arbitrary signs of r_1 and r_2. Both mixed mode solutions belong to this subspace (MM_π corresponds to $\Psi = 0$, $r_2 = -r_1$). The pure modes can also be considered as part of this subspace, even though Ψ is not defined for these branches. Within this subspace, the equations take the form

$$\dot r_0 = \left[\lambda_s + l_0 r_0^2 + l_1\left(r_1^2 + r_2^2\right) + l_3 r_1 r_2\right] r_0, \tag{41a}$$
$$\dot r_1 = \left[\lambda_h + B_r r_1^2 + (A_r + B_r) r_2^2 + C_r r_0^2\right] r_1 + D_r r_0^2 r_2, \tag{41b}$$
$$\dot r_2 = \left[\lambda_h + B_r r_2^2 + (A_r + B_r) r_1^2 + C_r r_0^2\right] r_2 + D_r r_0^2 r_1, \tag{41c}$$

$$\dot R = 2[\lambda_s + l_0 R + l_1 S + l_3 P]R, \tag{42a}$$
$$\dot S = 2[\lambda_h + B_r S + C_r R]S + 4[A_r P + D_r R]P, \tag{42b}$$
$$\dot P = 2[\lambda_h + B_r S + C_r R]P + [A_r P + D_r R]S. \tag{42c}$$

To detect the existence of precessing waves in the present subspace, we look for steady solutions of the above equations. From Eqs. (42b) and (42c) we obtain the conditions

$$\lambda_h + B_r S + C_r R = 0, \quad A_r P + D_r R = 0. \tag{43}$$

The precessing waves in question belong to this subspace, leading to

$$R = r_0^2 = -\frac{A_r}{D_r}\frac{\sigma_{0B} - \sigma_{\pi B}}{4\Sigma_B}, \tag{44a}$$
$$S = r_1^2 + r_2^2 = -\frac{\sigma_{0B} + \sigma_{\pi B}}{2\Sigma_B}, \tag{44b}$$
$$P = r_1 r_2 = \frac{\sigma_{0B} - \sigma_{\pi B}}{4\Sigma_B}, \tag{44c}$$

where
$$\Sigma_B \equiv B_r(A_r l_0 - D_r l_3) - l_1(A_r C_r) \neq 0,$$
$$\sigma_R \equiv \lambda_s - \frac{l_1}{B_r}\lambda_h,$$
$$\sigma_{0B} + \sigma_{\pi B} \equiv 2[(A_r C_r)\lambda_s + (l_3 D_r - A_r l_0)\lambda_h],$$
$$\sigma_{0B} - \sigma_{\pi B} \equiv 4B_r D_r \sigma_R. \tag{44d}$$

These expressions define a single branch of precessing waves, referred to as the PrW_B branch. One may check that the conditions obtained on imposing $P = 0$ and $S = 2|P|$ yield, respectively, the conditions listed in Table IX for the bifurcation from rotating waves and the relevant mixed mode, confirming that the PrW_B branch connects these two branches. Note that the sign of P is given by $A_r D_r$. So, had we adopted the convention that both r_1 and r_2 are positive and Ψ is either 0 or π, we would have arrived at the conclusion that PrW_B is associated with $\Psi = 0$ if $A_r D_r < 0$ and $\Psi = \pi$ if $A_r D_r > 0$. Note that the precession frequency given by Eq. (10a) vanishes when $l_2 = 0$. In this case the resulting mode will actually be singly periodic in the primitive variables, instead of a two-frequency wave. However, this property is not visible when working with the polar variables. The stability of the PrW_B branch within its invariant subspace $\mathrm{Fix}(\Sigma_{\mathrm{PrW}_B})$ can be determined by studying its characteristic polynomial in a similar manner as done for PrW_A in Sec. V B. The invariants of the 3×3 stability matrix are the determinant D_B, trace T_B and I_B given below:

$$D_B = -4\Sigma_B R(2P - S)(2P + S) = \frac{A_r}{D_r \Sigma_B^2}\sigma_{\pi B}\sigma_{0B}(\sigma_{\pi B} - \sigma_{0B}), \tag{45a}$$
$$T_B = 2l_0 R + (A_r + 2B_r)S = \frac{A_r l_0(\sigma_{\pi B} - \sigma_{0B}) - D_r(A_r + 2B_r)(\sigma_{0B} + \sigma_{\pi B})}{2D_r\Sigma_B}, \tag{45b}$$
$$I_B = R[\Delta_+(2P + S) + \Delta_-(-2P + S)] + 2A_r B_r(S^2 - 4P^2) = \frac{A_r}{4D_r\Sigma_B^2}\left(\Delta_-\sigma_{\pi B}^2 - \Delta_+\sigma_{0B}^2\right) + \frac{A_r}{4D_r\Sigma_B^2}(8B_r D_r + \Delta_+ - \Delta_-)\sigma_{0B}\sigma_{\pi B}. \tag{45c}$$

The vanishing of σ_R coincides with the origin of the PrW_B branch along the RW branch. Note that the vanishing of σ_R implies $\sigma_{0B} = \sigma_{\pi B}$. Similarly, one of the quantities σ_{0B} or $\sigma_{\pi B}$ vanishes at the termination of the PrW_B branch on one of the mixed modes. One may verify that the third point where D_B vanishes is located outside the existence interval of the branch, confirming that no parity-breaking bifurcation occurs along the branch. In addition, one may confirm that $\sigma_{0B}\sigma_{\pi B} > 0$, except at the termination point. The necessary conditions for

stability within the Fix(PrW$_B$) subspace are $D_B < 0$, $T_B < 0$, $I_B > 0$ and $H_B \equiv I_B - D_B/T_B > 0$. From Eq. (45a) one may easily verify that the determinant is negative if and only if $\Sigma_B < 0$. Similarly, the trace has a negative sign if $A_r + 2B_r < 0$ and $l_0 < 0$, which are the conditions for the supercriticality of standing waves and the steady-state mode, respectively. If instead $l_0(A_r + 2B_r) < 0$, then the trace changes sign within the region of existence of the PrW$_B$ solution. Analogously, the necessary conditions for a positive sign of the second invariant I_B everywhere along the branch are

$$\begin{aligned} &A_rB_r > 0 \quad \text{and} \quad \Delta_+ > 0 \quad \text{if} \quad A_rD_r < 0 \\ &\text{or } \Delta_- > 0 \quad \text{if} \quad A_rD_r > 0. \end{aligned} \tag{46}$$

The first condition ensures that the second invariant is positive at its birth from the RW branch, while the second condition ensures that I_B is positive at its termination on the corresponding MM branch. To ensure that $I_B > 0$ along the whole PrW$_B$ branch it suffices to have $\Delta_- > -\Delta_+$ if $A_rD_r < 0$, a condition that depends only on Δ_+ and B_rD_r, or $\Delta_+ > -\Delta_-$ if $A_rD_r > 0$ for $\Delta_- > 0$, a condition that depends only on Δ_- and B_rD_r. The PrW$_B$ branch is stable when $H_B > 0$. If H_B changes sign along the PrW$_B$ branch, a Hopf bifurcation with frequency Ω takes place ($H_B = 0$), characterized by the following set of conditions:

$$T_B\Omega^2 - D_B = 0, \quad \Omega^2 - I_B = 0. \tag{47}$$

These equations yield the conditions for the presence of a Hopf bifurcation along the PrW$_B$ branch stated above. In terms of the eigenvalues $\sigma_{0B}(\lambda_s, \lambda_h)$ and $\sigma_{\pi B}(\lambda_s, \lambda_h)$ of the mixed modes the Hopf distance H_B is given by

$$\begin{aligned} H_B \equiv &-\frac{A_r}{8D_r^2\Sigma_B^3}\big\{\Delta_-\Lambda_B^-\sigma_{\pi B}^3 - \Delta_+\Lambda_B^+\sigma_{0B}^3 \\ &+ [\Lambda_B^+(8B_rD_r - \Delta_-) + 2A_rl_0\Delta_+ - 8D_r\Sigma_B]\sigma_{\pi B}\sigma_{0B}^2 \\ &+ [\Lambda_B^-(8B_rD_r + \Delta_+) + 2A_rl_0\Delta_- + 8D_r\Sigma_B]\sigma_{\pi B}^2\sigma_{0B}\big\}, \\ \Lambda_B^\pm \equiv &\, D_r(A_r + 2B_r) \pm A_rl_0. \end{aligned} \tag{48}$$

The condition $H_B = 0$ describes a planar cubic algebraic curve in $(\sigma_{0B}, \sigma_{\pi B})$. A possible procedure is to determine the type of the planar curve isomorphic to one of the five canonical forms [43] and then determine the number of solutions from it. Instead of following this procedure, we prefer to provide a sufficient condition for the appearance of a Hopf bifurcation along this branch. Provided Eq. (46) holds, the frequency Ω is real, and there exists an odd number (one or three) of Hopf bifurcations whenever H_B has opposite signs at the two endpoints of the branch. This occurs when

$$\Delta_-\Lambda_B^- < 0 \quad (\text{MM}_0), \quad \Delta_+\Lambda_B^+ > 0 \quad (\text{MM}_\pi). \tag{49}$$

When Eq. (49) does not hold, the number of Hopf bifurcations is even (none or two). In such a case one can distinguish between the different scenarios using, for instance, the Descartes sign rule for positive roots. In addition to the three eigenvalues governing the stability of the PrW$_B$ branch within the $\sin\Psi = 0$ subspace discussed above, there is a fourth eigenvalue governing the stability in the orthogonal direction, given by

$$\sigma_{\text{BG}} = -(2l_3P - A_rS). \tag{50}$$

The vanishing of this eigenvalue leads to the birth of a branch of general precessing waves. The resulting condition in terms of λ_s and λ_h is listed in Table IX. A condition ensuring that such a bifurcation occurs somewhere along the branch is that σ_{BG} has opposite signs at its termination points on RW and the relevant MM. This leads to the condition reported in the last column of Table IX. This condition is the same as for the bifurcation from PrW$_A$.

D. The third branch of precessing waves

As demonstrated in the previous sections, two bifurcations can occur along the precessing waves of type A and B giving rise to a precessing wave with no symmetry called PrW$_G$. Here we investigate this branch as well as its stability. We look for a steady solution of the polar equations with $r_0 \neq 0$, $r_1 \neq r_2$ and $\sin\Psi \neq 0$; cf. Table VIII. The same manipulations as before lead to the following conditions:

$$\begin{aligned} 0 &= PQl_3 + Rl_0 + Sl_1 + \lambda_s, \\ 0 &= B_rS + C_rR + \lambda_h, \\ 0 &= A_rP + D_rQR, \\ 0 &= D_rRS + 2P^2l_3. \end{aligned} \tag{51}$$

The solution of this system yields the conditions for the presence of the PrW$_G$ branch:

$$\begin{aligned} R &= \frac{2B_r\lambda_s - (2l_1 + A_r)\lambda_h}{\Sigma_G}, \\ S &= 2\frac{C_r\lambda_s - l_0\lambda_h}{\Sigma_G}, \\ P &= \frac{-1}{l_3\Sigma_G}\{D_rl_3[B_r\lambda_s - (2l_1 + A_r)\lambda_h](C_r\lambda_s - l_0\lambda_h)\}^{\frac{1}{2}}, \\ Q &= A_r\left\{\frac{C_r\lambda_s - l_0\lambda_h}{D_rl_3[2B_r\lambda_s - (2l_1 + A_r)\lambda_h]}\right\}^{\frac{1}{2}}, \end{aligned}$$

where $\Sigma_G = C_r(A_r + 2l_1) - 2B_rl_0 \neq 0$. (52)

These expressions define a single solution branch. One may check that imposing $Q^2 = 1$ and $S = 2|P|$ yields, respectively, the same conditions as found for the steady bifurcations from the PrW$_A$ and PrW$_B$ branches listed in Table IX, confirming that the PrW$_G$ solution indeed links these two branches. The invariants of the stability matrix are

$$\begin{aligned} T_G &= 2Rl_0 + S(A_r + 2B_r) \\ &= \frac{2[\sigma_S(A_r + 2B_r) + l_0\sigma_R]}{\Sigma_G}, \\ D_G &= 8\Sigma_GD_rl_3R^2(4P^2 - S^2)(Q^2 - 1) \\ &= \frac{32}{\Sigma_G^3l_3}\sigma_S\sigma_R\big(A_r^2\sigma_S + D_rl_3\sigma_R\big)(D_r\sigma_R + \sigma_Sl_3), \\ I_G &= \frac{4A_r}{\Sigma_G^2}\big[2(B_r - A_r)\sigma_S^2 - D_r^2\sigma_R^2\big] \\ &\quad + \frac{\sigma_S\sigma_R}{\Sigma_G^2l_3}\big[4D_r\big(2A_rB_r - 3l_3^2\big) + 4l_0l_3(A_r + 2B_r)\big] \end{aligned}$$

TABLE X. Defining conditions for structurally and asymptotically stable heteroclinic cycles connecting mixed modes or standing waves and a mixed mode.

Name of solution (comments)	Existence conditions	Asymptotic stability [Asymp. stable if either (i-a) or (i-b)]
$\mathrm{Het}_{\mathrm{MM}_0-\mathrm{MM}_\pi}$		
Stable radial dir.	$\Delta_+ > 0, \quad \Delta_- > 0, l_0 < 0, \quad A_r + 2B_r < 0$	(i-a) $\sigma_{\pi A} + \sigma_{\pi B} < 0$
Sink-saddle conditions	$\sigma_{0A}\sigma_{0B} > 0, \quad \sigma_{\pi A}\sigma_{\pi B} < 0, l_3 D_r < 0, \quad A_r D_r > 0$	(i-b) $\sigma_{0A} - \sigma_{0B} > 0$
Nonattractivity of PrW	$2l_1 \pm l_3 > 0, \quad C_r \pm D_r > 0$	
$\mathrm{Het}_{\mathrm{SW}-\mathrm{MM}_\pi}$		
Stable radial dir.	$\Delta_- > 0, l_0 < 0, A_r + 2B_r < 0, A_r > 0$	(i-a) $2(2B_r + A_r)\lambda_s - (2l_1 - A_r)\lambda_h > 0$
SW saddle in $\mathrm{Fix}(\Sigma_{\mathrm{MM}_\pi})$	$\sigma^-_{\mathrm{SW}} > 0, \sigma^+_{\mathrm{SW}} < 0$	(i-b) $\sigma_{\pi A} + \sigma_{\pi B} < 0$
MM_π saddle in $\mathrm{Fix}(\Sigma_{\mathrm{PrW}_B})$	$\sigma_{\pi A}\sigma_{\pi B} < 0, A_r D_r > 0$	
$\mathrm{Het}_{\mathrm{SW}-\mathrm{MM}_0}$		
Stable radial dir.	$\Delta_+ > 0, l_0 < 0, A_r + 2B_r < 0, A_r > 0$	(i-a) $2(2B_r + A_r)\lambda_s - (2l_1 - A_r)\lambda_h > 0$
SW saddle in $\mathrm{Fix}(\Sigma_{\mathrm{MM}_0})$	$\sigma^-_{\mathrm{SW}} < 0, \sigma^+_{\mathrm{SW}} > 0$	(i-b) $\sigma_{\pi A} - \sigma_{\pi B} > 0$
MM_0 saddle in $\mathrm{Fix}(\Sigma_{\mathrm{PrW}_B})$	$\sigma_{0A}\sigma_{0B} > 0, A_r D_r < 0$	

$$
\begin{aligned}
&- 4\frac{\sigma_S\sigma_R}{\Sigma_G^2 l_3}[(A_r + 2l_1)(A_r D_r + C_r l_3)],\\
II_G = &-\frac{8}{\Sigma_G^3}\left(D_r^2 l_0 \sigma_R^3 + 4A_r^2 B_r \sigma_S^3\right)\\
&+ \frac{8D_r\sigma_S\sigma_R^2}{\Sigma_G^3 l_3}\left[2\Sigma_B + l_3(\Sigma_A - 4B_r D_r) - l_0\left(A_r^2 + l_3^2\right)\right]\\
&+ \frac{8\sigma_S^2\sigma_R}{\Sigma_G^3 l_3}\left(A_r l_3 \Sigma_G - 6B_r D_r l_3^2\right)\\
&+ \frac{8\sigma_S^2\sigma_R}{\Sigma_G^3 l_3}A_r^2[D_r A_r + 2D_r(l_1 - B_r) - 2l_3 l_0]. \qquad (53)
\end{aligned}
$$

The determinant D_G only vanishes at the termination points, that is, whenever $Q^2 = 1$ or $S = 2|P|$, which rules out the possibility of a steady-state bifurcation. Thus there can only be Hopf bifurcations along the PrW_G branch. The frequency Ω solves the following equations obtained from the characteristic polynomial

$$\Omega^4 - II_G\Omega^2 + D_G = 0, \quad T_G\Omega^2 - I_G = 0, \qquad (54)$$

leading to the following sixth-order equation in terms of λ_s and λ_h:

$$II_G^2 - II_G I_G T_G + T_G^2 D_G = 0. \qquad (55)$$

E. A robust heteroclinic cycle

The isotropy lattice (see Fig. 9) of the degenerate case under discussion suggests the possibility that new heteroclinic cycles may exit. One of the most intriguing possibilities is a connection between the isotropy subspace of mixed modes and the subspaces of precessing waves A and B, corresponding to a cycle of type C in the classification of Krupa and Melbourne [40]. The conditions for the existence of a robust heteroclinic cycle connecting mixed modes consists in demanding that MM_0 is a saddle whose unstable manifold is of dimension one (resp. sink) within Σ_{PrW_B} and a sink (resp. saddle) within Σ_{PrW_A}. Then MM_π would need to be a sink (resp. saddle) within Σ_{PrW_B} and a saddle (resp. sink) within Σ_{PrW_A}. However, for the mixed mode MM_π to be a saddle within Σ_{PrW_A} and the mixed mode MM_0 to be a sink it is necessary that $\sigma_{\pi A} - \sigma_{0A} < 0$ with $D_r l_3 < 0$, conditions that indicate that there is a fixed point within the invariant subspace Σ_{PrW_A}, i.e., PrW_A (resp. PrW_B). Despite the existence of a fixed point within the invariant subspace Σ_{PrW_A} (resp. Σ_{PrW_B}), a robust heteroclinic cycle may still exist; cf. [44]. In the case of an invariant fixed point subspace of dimension two the existence of heteroclinic cycles relies on the use of the Poincaré-Bendixson theorem; see, for instance, [41]. In this case, the fixed-point subspace is required to be free of any other fixed point other than those connected by the heteroclinic cycle. Instead, when the dimension is three, one may use the invariant sphere theorem, or more generally a Lyapunov functional, to establish attraction. In our case, the presence of a robust heteroclinic cycle requires that the coefficients $C_r \pm D_r$ and $2l_1 \pm l_3$ should both be positive, since otherwise the precessing waves A and B are globally attracting except possibly within a ball of size $O(\lambda_s, \lambda_h)$ in the subspace R, P, S. These conditions are listed in Table X. Note that our reasoning does not exclude the existence of a small heteroclinic cycle within the $O(\lambda_s, \lambda_h)$ ball near PrW, although such a state (if it exists) would require a larger set of defining conditions and would be restricted to a small region of phase space. If the conditions listed in Table X are satisfied, then there exists a robust heteroclinic cycle between the mixed modes, which bifurcates to a 3FW in the case $A_i - 2l_2 \neq 0$ and $D_i = 0$, and to a PuWs or 3FW in the case with $A_i - 2l_2 \neq 0$ and $D_i \neq 0$; see Fig. 10. Finally, the application of the theory of Krupa and Melbourne [40] also allows one to establish the existence of heteroclinic cycles between standing waves and mixed modes, whose existence and stability conditions are listed in Table X. As for the heteroclinic cycles between mixed modes, these heteroclinic cycles persist in the form of limit cycles of the polar normal form when the degeneracy conditions are not satisfied; see Fig. 11.

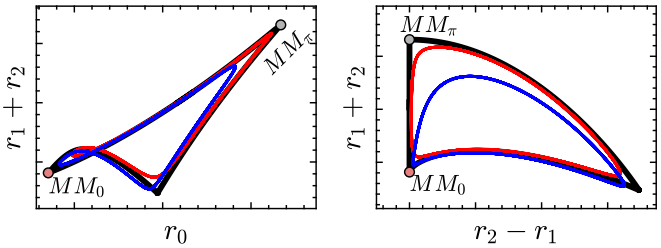

(a) A-projection of PuW (b) A_0'-projection of PuW

FIG. 10. Heteroclinic cycle between MM_0 and MM_π in the polar normal form (9) with $A_i - 2l_2 = D_i = \sin\Psi = 0$ (black line) and corresponding results when $A_i - 2l_2 \neq 0$ and $D_i = 0$ (red line) or $D_i \neq 0$ and $A_i - 2l_2 = 0$ (blue line). (a) $(r_0, r_1 + r_2)$ projection. (b) $(r_2 - r_1, r_1 + r_2)$ projection.

VI. NUMERICAL EXPLORATION OF THE THIRD-ORDER NORMAL FORM (9)

Section V has shown the existence of multiple fixed points with additional symmetries, e.g., PrW_A and PrW_B, in the degenerate case [equivariant under the group $O(2) \times \mathbb{Z}_2 \times S^1$]. The additional $\mathbb{Z}_2$ symmetry is characteristic of mode interactions in O(2) symmetric systems with strong resonance conditions (1:2 [44], 1:3 [45]). Departure from the degeneracy conditions ($A_i - 2l_2 = D_i = 0$) breaks this additional $\mathbb{Z}_2$ symmetry and may be responsible for destroying the Het_{SS-SW} heteroclinic cycle, leading to more complex dynamics. This section is devoted to the numerical exploration of the degenerate case $A_i - 2l_2 = D_i = 0$ and the implications of the departure from this condition ($A_i - 2l_2 \neq 0$ and/or $D_i \neq 0$). For this purpose, we choose generic values for the normal form coefficients, listed in Table XI. These coefficients are chosen in such a way that primary bifurcations, that is, bifurcations leading to SS, SW, and RW, are supercritical, and the flow is globally stable, that is, there is no finite-time blow-up. As the bifurcation parameter, we have selected the polar angle θ such that the unfolding parameters are $\lambda_S = \rho\cos\theta$ and $\lambda_H = \rho\sin\theta$, with $\rho = (0, \infty)$ and $\theta \in [0, 2\pi)$. In contrast to [44] the bifurcation diagram barely depends on ρ, and we have fixed the value of ρ at $\rho = 0.5$. The numerical continuation of the polar normal form is carried out with the numerical continuation software MATCONT [46]. In the following, we

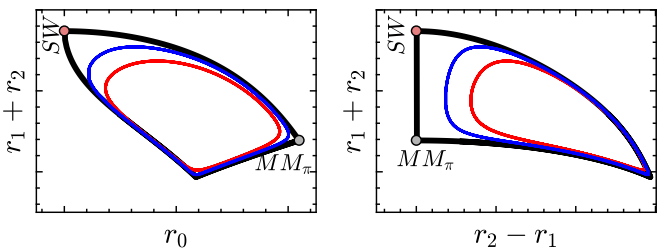

(a) A-projection of PuW (b) A_0'-projection of PuW

FIG. 11. Heteroclinic cycle (black) between MM_π and SW in the polar normal form (9) with $A_i - 2l_2 = D_i = \sin\Psi = 0$ (black line) and corresponding results with $A_i - 2l_2 \neq 0$ (red line) or $D_i \neq 0$ (blue line). (a) $(r_0, r_1 + r_2)$ projection. (b) $(r_2 - r_1, r_1 + r_2)$ projection.

TABLE XI. Cubic coefficients of the normal form.

l_0	l_1	l_3	A_r	B_r	C_r	D_r
−6.19	−1.4	−1.7	0.96	−1.08	4	10

show the bifurcation diagrams associated with the degenerate and nondegenerate cases. There are two major differences. First, the two connected branches of symmetric precessing waves (PrW_A and PrW_B) are a characteristic feature of the degenerate case [symmetry $O(2) \times \mathbb{Z}_2 \times S^1$]. In the nondegenerate case, these two branches split into two disconnected branches of general precessing waves PrW_G. Second, in the degenerate case we observe Het_{SS-SW} cycles, which break apart as the orbit intersects the invariant subspace $r_1 = r_2$. Instead, in the nondegenerate case, we have identified complex heteroclinic cycles around Het_{PrW_A}. Such a feature was also observed by Porter and Knobloch [44], who concluded that the transition from Het_{SS-SW} cycles to this second set is a characteristic of systems with $O(2) \times \mathbb{Z}_2$ symmetry where the $\mathbb{Z}_2$ symmetry is weakly broken.

A. The degenerate case $A_i - 2l_2 = D_i = 0$

Figure 12 shows the bifurcations of the fixed point branches of the polar normal form with the parameters listed in Table XI and the degeneracy conditions $A_i - 2l_2 = D_i = 0$. Along this particular path, the trivial state first loses stability at $\theta = -\pi/2$ in a primary pitchfork bifurcation to the SS mode, which terminates at $\theta = \pi/2$. The SS mode gives birth to the MM_0 branch when $\theta = \arctan(C_r + D_r)/l_0 \approx -1.15$ and to the MM_π branch when $\theta = \arctan(C_r - D_r)/l_0 \approx 0.77$ (Table V). The mixed mode MM_0 subsequently produces the PrW_A branch in a symmetry-breaking bifurcation when $\sigma_{0A} = 0$ (Table IX) and then terminates on the SW branch. A magnified visualization is displayed in Fig. 13(a), where we can see the PrW_A branch which terminates on the MM_π branch and eventually gives birth to a general precessing wave PrW_G via a symmetry-breaking bifurcation when $\sigma_{AG} = 0$. The PrW_G mode experiences a Hopf bifurcation that leads to a 3FW (blue point in Fig. 12); Fig. 14 illustrates the stable periodic orbit (3FW) with a thick black line and the stable manifold of PrW_A with a thin gray line. The existence of a global attractor (PrW_A) in the invariant subspace $r_1 = r_2$ pre-

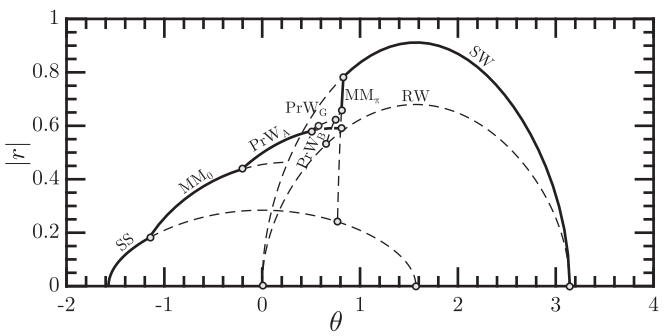

FIG. 12. Bifurcation diagram in the degenerate case when $\rho = 0.5$, showing $|r| = \sqrt{r_0^2 + r_1^2 + r_2^2}$ as a function of the angle θ.

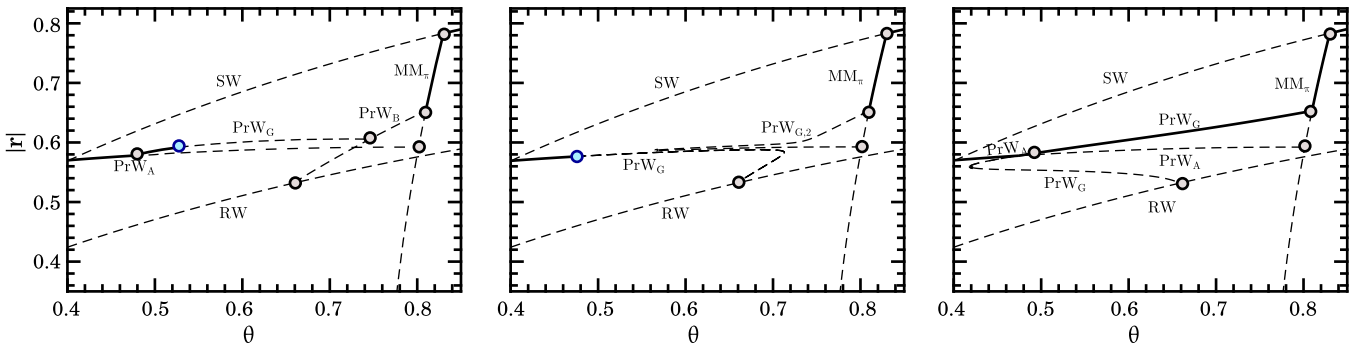

(a) A_i-$2l_2 = 0$, $D_i = 0$ (b) A_i-$2l_2 = 0$, $D_i = 0.35$ (c) A_i-$2l_2 = -1$, $D_i = 0$

FIG. 13. Bifurcation diagram in the degenerate case when $\rho = 0.5$, showing $|r| = \sqrt{r_0^2 + r_1^2 + r_2^2}$ as a function of the angle θ. Legend: Solid (dashed) lines correspond to stable (unstable) fixed points. Symmetry-breaking bifurcations are illustrated with gray points, and Hopf bifurcations with blue points. Note: In (a) as well as in Fig. 12 the PrW$_G$ branch has been artificially displaced upwards to visually differentiate it from the PrW$_A$ branch.

vents the existence of a true heteroclinic cycle $\text{Het}_{\text{SS}-\text{SW}}$, but allows the existence of shadowing stable periodic orbits that approximate it; see Fig. 14. These orbits exist in $0.52 < \theta < 0.592$ and collapse in a global bifurcation when the limit cycle intersects the invariant subspace $r_1 = r_2$ at $\theta \approx 0.592$. Once a trajectory intersects the $r_1 = r_2$ subspace, it is trapped within it and so is attracted to the only attractor in this subspace, i.e., the PrW$_A$ state. The same phenomenon occurs in the small region of coexistence of MM$_\pi$ and the heteroclinic cycle, $0.78 < \theta < 0.82$. The PrW$_G$ branch terminates on the PrW$_B$ branch, which connects RW and MM$_\pi$. Finally, the MM$_\pi$ branch is stable between its endpoint on the SW branch and its symmetry-breaking bifurcation that leads to the PrW$_B$ branch. For $0.82 < \theta \leqslant \pi$ the only stable state is the SW branch.

B. Nondegenerate case $A_i - 2l_2 = -1$, $D_i = 0.35$

The general picture of the bifurcation scenario, depicted in Fig. 12, remains qualitatively unchanged. However, the precessing wave branches are modified. We first examine the case when one of the two degeneracy conditions is still satisfied. The case $A_i - 2l_2 = 0$ but $D_i \neq 0$ is illustrated in Fig. 13(b) and reveals the existence of two distinct PrW$_G$ branches. This case corresponds to an imperfect bifurcation, where the two symmetry-breaking pitchfork bifurcations leading to the PrW$_G$ branch in the degenerate case are replaced by a saddle-node bifurcation on each branch. The second case, $D_i = 0$ but $A_i - 2l_2 \neq 0$, illustrated in Fig. 13(c), shows the presence of PrW$_A$ and PrW$_G$ branches, the latter replacing the symmetric PrW$_B$ branch. These branches connect via a transcritical bifurcation, which is responsible, in this case, for the stability of the whole upper section of the PrW$_G$ branch since no Hopf bifurcation takes place. We next turn our attention to the nondegenerate case $A_i - 2l_2 \neq 0$, $D_i \neq 0$. The bifurcation diagram of the fixed points of the polar normal form is depicted in Fig. 15. The figure displays two disconnected branches of general precessing waves PrW$_G$. The first of these, referred to as PrW$_{G,1}$ in the figure, becomes unstable through a Hopf bifurcation, leading to a 3FW branch (not shown). The second PrW$_G$ branch, labeled PrW$_{G,2}$, bifurcates from and terminates on the MM$_\pi$ branch with a saddle-node

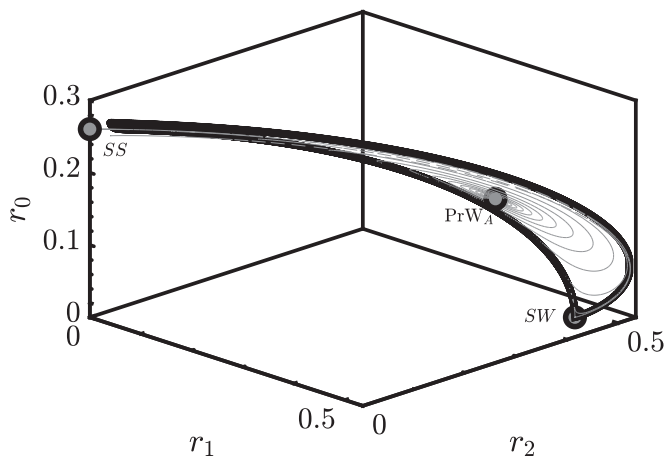

FIG. 14. Example of the heteroclinic cycle SS-SW (thick line). The gray line corresponds to the stable manifold of PrW$_A$.

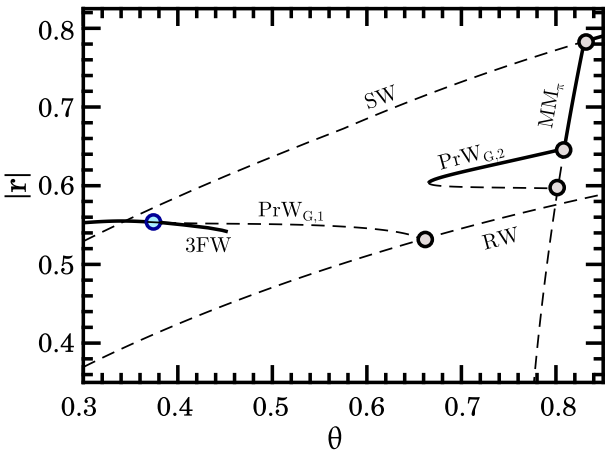

FIG. 15. Bifurcation scenario in the nondegenerate case, showing $|r| = \sqrt{r_0^2 + r_1^2 + r_2^2}$ as a function of the angle θ with the same legend as in Fig. 13. The end point of PrW$_{G,1}$ is located at $\theta \approx 0.6581$ (gray point), i.e., below θ_{SN} but above the global bifurcation at $\theta \approx 0.6454$ (not shown). Note: The blue point and the associated 3FW branch have been artificially displaced, so the crossing point between the SW and PrW$_{G,1}$ and the blue Hopf point do not coincide.

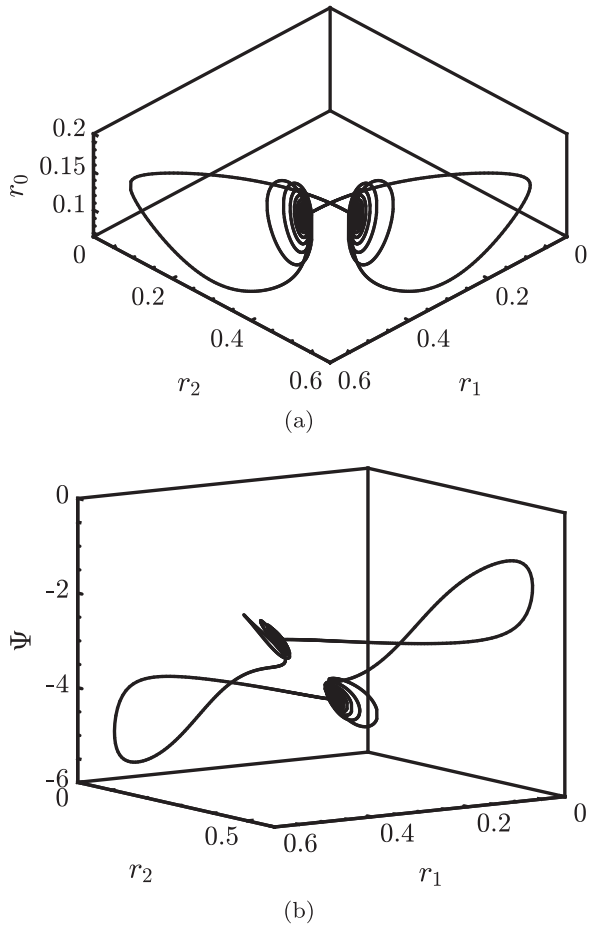

FIG. 16. Heteroclinic cycle at $\theta_{\rm SN} \approx 0.663445$.

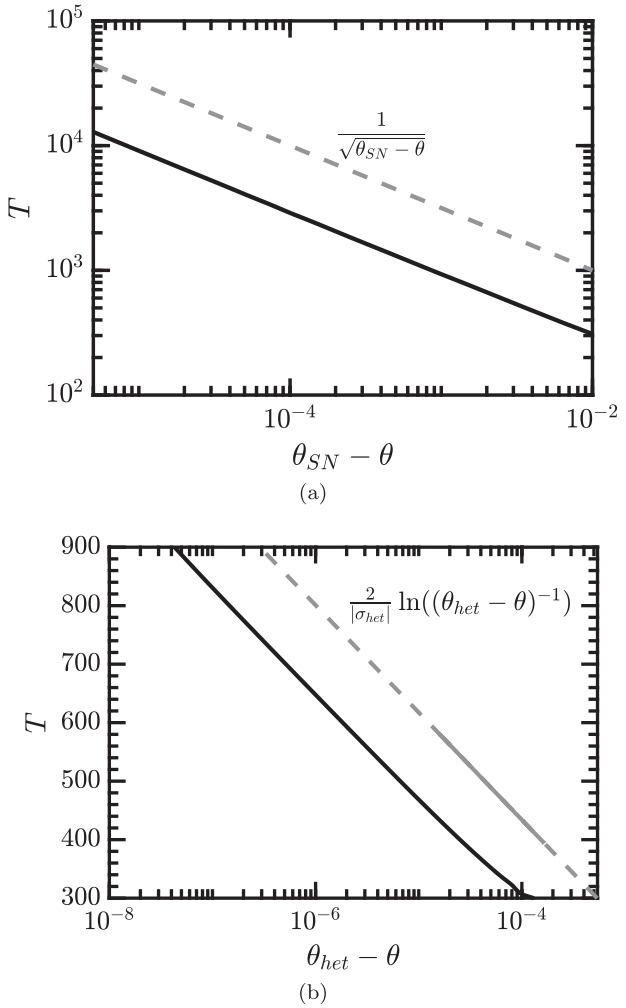

FIG. 17. (a) Evolution of the period of the stable limit cycles shadowing the heteroclinic cycle as a function of the distance $\theta_{\rm SN} - \theta$ to the saddle-node bifurcation. (b) Evolution of the period near the heteroclinic bifurcation at $\theta_{\rm het}$, where $\sigma_{\rm het} = -0.0251$ is the leading stable eigenvalue of the $\mathrm{PrW}_{G,1}$ fixed point.

bifurcation in between: the upper section is stable, whereas the lower is unstable. Because of the symmetry under the reflection κ, there is in fact a pair of such saddle-node bifurcations, $\mathrm{PrW}^{\pm}_{G,2}$, both occurring at $\theta = \theta_{\rm SN} \approx 0.663445$. Moreover, each is of saddle-node-in-a-periodic-orbit (SNIPER) type but with complex leading eigenvalues at the fold points $\mathrm{PrW}^{\pm}_{G,2}$: $(0, -0.6795, -0.0182 \pm 0.4418i)$. For a study of this situation in the absence of κ symmetry, see [47]. In the presence of this symmetry, this case can either lead to a pair of symmetry-related homoclinics to $\mathrm{PrW}^{\pm}_{G,2}$ or, as in this case, to a heteroclinic cycle connecting $\mathrm{PrW}^{+}_{G,2}$ to $\mathrm{PrW}^{-}_{G,2}$ and vice versa, a consequence of the intertwined nature of the stable and unstable manifolds of $\mathrm{PrW}^{\pm}_{G,2}$. In the former case the near-homoclinic orbit to the left of $\mathrm{PrW}^{\pm}_{G,2}$ contains a certain number of decreasing oscillations as it approaches and leaves $\mathrm{PrW}^{\pm}_{G,2}$, the number of these oscillations depending on the speed with which the trajectory passes through the $\mathrm{PrW}^{\pm}_{G,2}$ neighborhood, and hence on the distance of θ from $\theta_{\rm SN}$. In the latter case the unstable manifold associated with the degenerate eigenvalue injects the trajectory into the image fold point, and the same local behavior there leads to reinjection back into the original fold, generating a κ-symmetric heteroclinic cycle; cf. [48]. Figure 16 shows such an orbit in two projections, computed for θ just below $\theta_{\rm SN} \approx 0.663445$. At this θ the $\mathrm{PrW}^{\pm}_{G,2}$ points are absent, and the orbit shown is actually a long period periodic orbit. Figure 17(a) shows the period of such orbits as a function of $\theta_{\rm SN} - \theta$, confirming the expected relation $T \sim (\theta_{\rm SN} - \theta)^{-1/2}$. This divergence is a consequence of a slowdown of the trajectory in the vicinity of the phase space location where the $\mathrm{PrW}_{G,2}$ appear when θ increases through $\theta_{\rm SN}$, resulting in increased accumulation of turns as this point is approached. Note that these orbits inherit the stability of the (upper) $\mathrm{PrW}_{G,2}$ branch (cf. Fig. 15) and hence represent attractors of the system. Figure 18 shows sample attractors found on decreasing θ further. Figure 18(a) shows a stable symmetric orbit at $\theta = 0.663$, followed by asymmetric chaotic attractors (with a positive Lyapunov exponent) generated with increasing distance from $\theta_{\rm SN}$. The absence of chaotic states near $\theta_{\rm SN}$ is a consequence of the fact the flow in this region is locally contracting. To understand the origin of these states, we examine the behavior of a typical periodic orbit associated with the SNIPER bifurcation. As already explained this orbit depends sensitively on the value of $\theta < \theta_{\rm SN}$. In Fig. 19(a) we show the period T of this orbit as a function of θ obtained using numerical

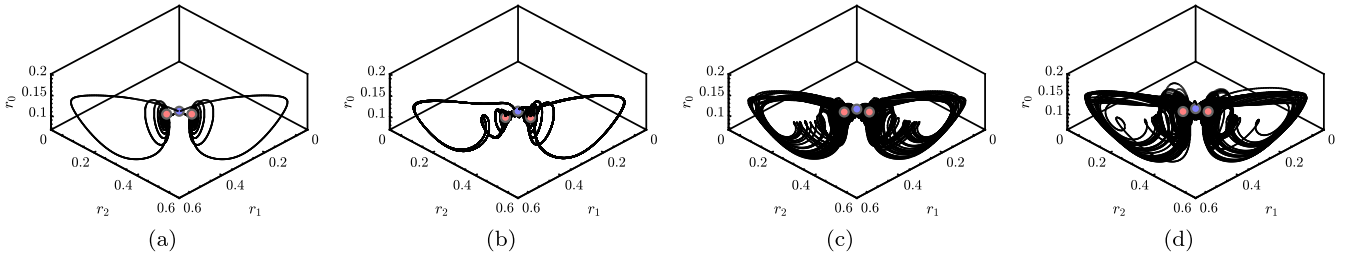

FIG. 18. Stable attractors in a (r_0, r_1, r_2) projection for (a) $\theta = 0.663$ (symmetric periodic orbit); (b) $\theta = 0.647$ (asymmetric orbit); (c) $\theta = 0.645$ (asymmetric orbit); (d) $\theta = 0.643$ (asymmetric orbit). The symmetry-related $\mathrm{PrW}_{G,2}$ fixed points corresponding to the saddle node at $\theta \approx 0.663445$ are indicated by red points, with the PrW_A point (present in the degenerate case only) depicted as a blue point; these are shown for orientation only.

continuation. This period diverges as $\theta \to \theta_{\mathrm{SN}}$ from below and the orbit approaches the heteroclinic cycle shown in Fig. 16. As θ decreases, the period T decreases, although this decrease is interrupted by a series of back-to-back folds. Each such pair is responsible for the elimination of one small amplitude turn of the trajectory (not shown), resulting in a gradual unwinding of the trajectory. As θ decreases towards the leftmost fold and beyond, the trajectory develops small loops in the vicinity of $\mathrm{PrW}_{G,1}$ (Fig. 20) and its period begins to diverge again, this time logarithmically [Fig. 17(b)], indicating approach to a heteroclinic connection involving $\mathrm{PrW}_{G,1}$ and located at $\theta = \theta_{\mathrm{het}} \approx 0.6454$. Since the leading unstable eigenvalues of $\mathrm{PrW}_{G,1}$ at this parameter values are complex, $0.2446 \pm 0.3661i$, while the leading stable eigenvalue is real, -0.0251, these points are both saddle foci. The complex unstable eigenvalues account for the oscillatory approach to

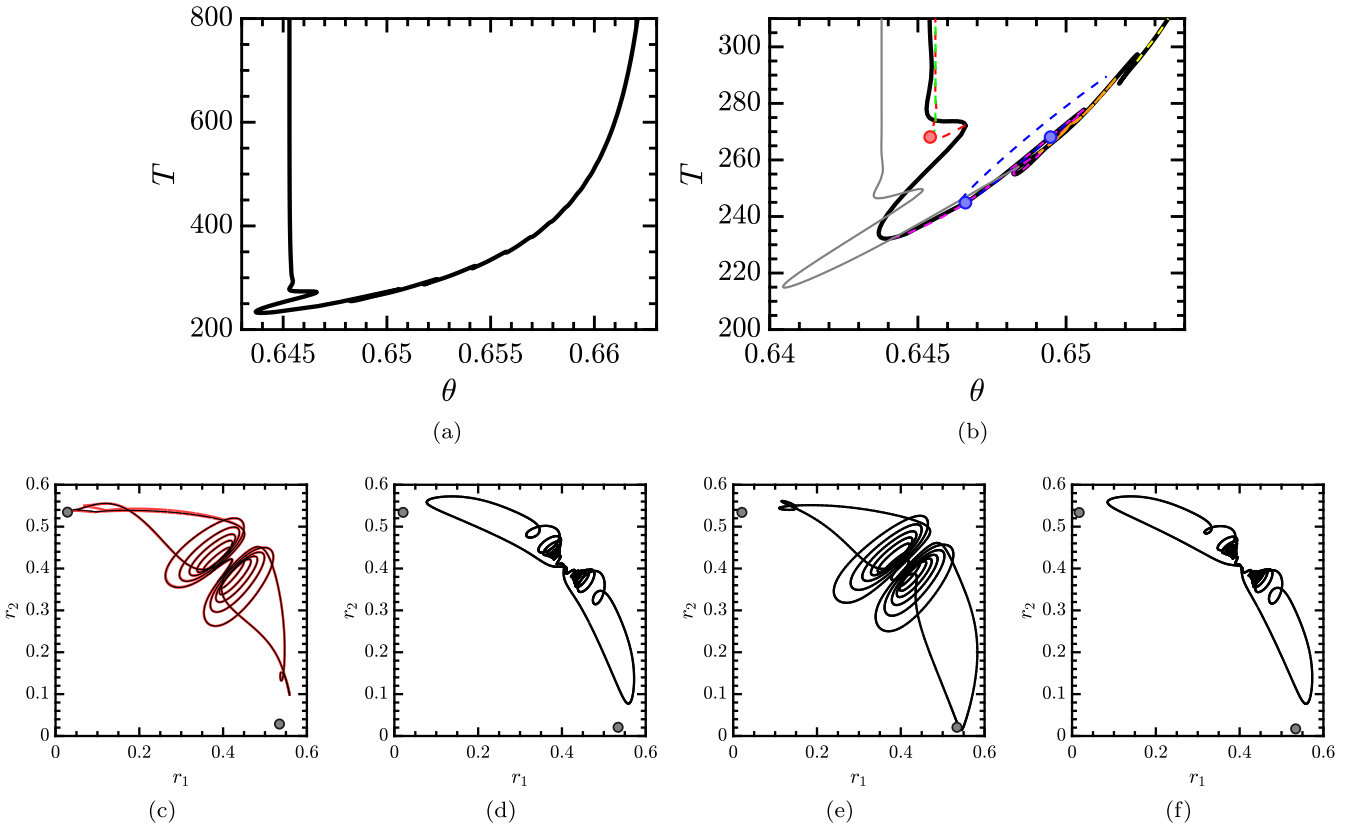

FIG. 19. (a) Evolution of the period T of a symmetric periodic orbit born in the SNIPER bifurcation $\theta \approx 0.663445$ and terminating in a heteroclinic bifurcation at $\theta \approx 0.6454$ (thick solid line). Secondary branches of asymmetric states are displayed in thin lines: solid line for the branch whose period diverges at $\theta \approx 0.64377$ and dashed lines for the other branches; see panel (b) for more detail. The secondary branches are accompanied by back-to-back period-doubling cascades (three period-doubling points are indicated with solid circles of the same color as the branch), which open up via the formation of subsidiary homoclinic orbits as in panel (c), black line; the superposed red curve shows an accompanying period-doubled solution. Panels (d)–(f) display the (r_1, r_2) projection at $\theta = 0.65$ for the dashed magenta, blue, and orange branches in (b) showing a symmetric and two asymmetric periodic orbits, respectively. The location of $\mathrm{PrW}^{\pm}_{G,1}$ is indicated with a small circle in (c)–(f). Only (c) is close to homoclinic; the proximity of orbit (e) to the lower fixed point is a projection effect.

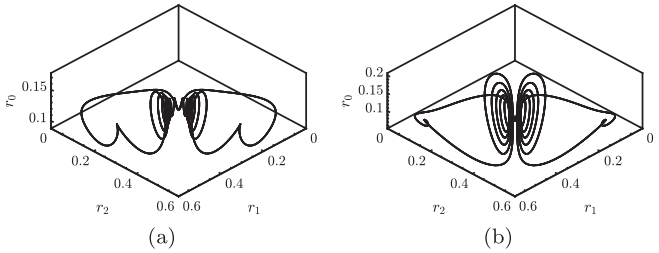

FIG. 20. Periodic orbit at the seventh and eighth folds from the right in Fig. 19(b), with a period-doubling bubble in between (not shown). (a) $\theta = 0.6437$; (b) $\theta = 0.6466$.

the global bifurcation at $\theta \approx 0.6454$ while the fact that the flow near $\mathrm{PrW}_{G,1}$ is locally expanding implies that we should expect stable chaotic dynamics near this parameter value, as in the classical example of Shil'nikov where the signs of the eigenvalues are reversed [49–51]. In Fig. 19(a) the solid line tracks the period of the κ-symmetric orbit. As $\theta \to \theta_{\mathrm{het}} \approx 0.6454$ from above, this orbit collides with $\mathrm{PrW}_{G,1}$, forming a heteroclinic connection from $\mathrm{PrW}_{G,1}$ to its image under κ and back again. Near θ_{het} this orbit is accompanied by back-to-back symmetry-breaking bifurcations, generating asymmetric periodic orbits [Fig. 19(b)]. These asymmetric orbits are free to period-double into chaos, resulting in "bubbles" of chaotic behavior, as described in [52] and references therein. Close to the primary heteroclinic bifurcation, these bubbles "burst" via the formation of pairs of subsidiary homoclinic orbits. The red dashed and thin solid lines in Fig. 19(b) show examples of this generic behavior in our problem; Fig. 19(c) compares the homoclinic orbit at the green dashed asymptote with the corresponding period-doubled orbit on the red dashed branch at the same θ value. Further details are omitted. Thus, the primary symmetric periodic orbit is associated with a number of chaotic intervals located around subsidiary homoclinic orbits originating in global bifurcations of asymmetric orbits associated with it; cf. Fig. 18. In particular, stable chaotic motion is also observed for θ *below* the primary heteroclinic bifurcation at $\theta_{\mathrm{het}} \approx 0.6454$.

We mention that the periodic orbit originating from the Hopf point on the $\mathrm{PrW}_{G,1}$ branch ($\theta \approx 0.3841$, blue point in Fig. 15) is stable from the Hopf point to $\theta \approx 0.4518$, where the first of several Neimark-Sacker bifurcations takes place. These are interspersed with additional global bifurcations and intervals of chaos as θ increases towards $\theta_{\mathrm{het}} \approx 0.6454$. Some sample solutions are shown in Fig. 21 to whet the appetite. The details depend on the parameters used and are omitted.

VII. NORMAL FORM REDUCTION

The process of reducing the governing equations to normal form near a multiple bifurcation is based on center manifold reduction followed by a series of near-identity variable changes to simplify the dynamical equations on the center manifold. The resulting equations are then *unfolded* by introducing parameters that break apart the multiple bifurcation in a generic way. In infinite-dimensional problems, such as those arising in fluid mechanics, it is preferable to employ multiple scales techniques to compute both the normal form and the

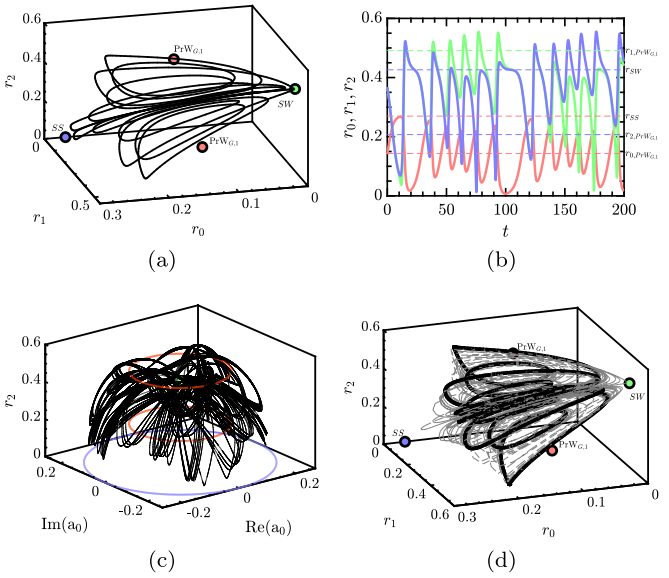

FIG. 21. (a) Phase portrait of a near-homoclinic orbit to the SW state in the (r_0, r_1, r_2) space at $\theta = 0.452$, and (b) the corresponding time series showing $r_0(t)$ (red), $r_1(t)$ (green), and $r_2(t)$ (blue). Near the homoclinic connection r_1 approaches r_2 and r_0 falls to zero. (c) A trajectory at $\theta = 0.457$ in the $(\mathrm{Re}(a_0), \mathrm{Im}(a_0), r_2)$ space showing that the trajectory intermittently visits SW states with different phases ϕ, each visit resulting in a switch between an oscillation about one $\mathrm{PrW}_{G,1}$ state to an oscillation about the other; red circles represent the group orbit of the two $\mathrm{PrW}_{G,1}$ states while the blue circle represents the group orbit of the SS states [53]. (d) Chaotic attractor at $\theta = 0.49$ (thin dashed gray line) together with an (unstable) κ-symmetric periodic orbit computed at $\theta \approx 0.4896$.

coefficients within it as part of the same calculation. We employ here this technique to determine all the coefficients in the third-order normal form (8). First, let us introduce the following formal expression for the governing equations on a domain Ω:

$$\mathbf{B}\frac{\partial \mathbf{q}}{\partial t} = \mathbf{F}(\mathbf{q}, \boldsymbol{\eta}) \equiv \mathbf{L}\mathbf{q} + \mathbf{N}(\mathbf{q}, \mathbf{q}) + \mathbf{G}(\mathbf{q}, \boldsymbol{\eta}), \ \mathbf{x} \in \Omega,$$
$$\mathbf{D}_{bc}\mathbf{q}(\mathbf{x}) = \mathbf{q}_{\partial\Omega}, \ \mathbf{x} \in \partial\Omega. \tag{56}$$

Here $\partial\Omega$ represents the domain boundary. This form of the governing equations takes into account a linear dependence on the state variable $\mathbf{q}$ through $\mathbf{L}$ and a quadratic dependence on the state variable and the parameters $\boldsymbol{\eta}$ through the operators $\mathbf{G}(\cdot,\cdot)$ and $\mathbf{N}(\cdot,\cdot)$. Equation (56) formally includes the incompressible Navier-Stokes equations written in cylindrical coordinates for the TCF and WFA problems, whereas for WFA-MC one must consider the Boussinesq approximation of the incompressible Navier-Stokes equations written in cylindrical coordinates as well. For this set of equations, the operators in Eq. (56) take the following form:

$$\mathbf{L}\mathbf{q} = \begin{pmatrix} -\nabla P \\ \nabla \cdot \mathbf{U} \\ 0 \end{pmatrix},$$
$$\mathbf{N}(\mathbf{q}_1, \mathbf{q}_2) = -\begin{pmatrix} \mathbf{U}_1 \cdot \nabla \mathbf{U}_2 \\ 0 \\ \mathbf{U}_1 \cdot \nabla T \end{pmatrix},$$

$$\mathbf{G}(\mathbf{q},\boldsymbol{\eta}) = \begin{pmatrix} \frac{1}{\mathrm{Re}}\nabla\cdot\left(\nabla\mathbf{U}+(\nabla\mathbf{U})^T\right)+\mathrm{Ri}\,T\,\mathbf{e}_z \\ 0 \\ \frac{1}{\mathrm{Re}\,\mathrm{Pr}}\nabla^2 T \end{pmatrix}. \quad (57)$$

In red we have included the modification for the WFA-MC problem with respect to the WFA problem. The set of parameters $\boldsymbol{\eta}\in\mathbb{R}^{N_p}$, where N_p is the number of parameters, is composed of the two dimensionless angular velocities of the cylindrical annulus for TCF, the inverse Reynolds number for WFA, and the inverse Reynolds number together with the Richardson and Prandtl numbers for WFA-MC. In the following, we will consider the most general case, that is, the WFA-MC case where the vector of parameters takes the form $\boldsymbol{\eta}\equiv[\eta_0,\eta_1,\eta_2]=[\mathrm{Re}^{-1},\mathrm{Ri},\mathrm{Pr}]^T$. The Reynolds number is defined as the ratio of inertial and viscous forces, i.e., $\mathrm{Re}=\frac{U_\infty D}{\nu}$, with U_∞ the uniform velocity at the far field, D the diameter of the bluff body, and ν the kinematic viscosity; the Prandtl number, $\mathrm{Pr}=\frac{\nu}{\kappa}$, is the ratio of viscosity and the thermal diffusivity κ. The Richardson number is defined as $\mathrm{Ri}=-\frac{\beta(\mathbf{e}_{U_\infty}\cdot\mathbf{g})(T_b-T_\infty)D}{U_\infty^2}$, with β the thermal expansion coefficient, $\mathbf{e}_{U_\infty}=\mathbf{U}_\infty/U_\infty$ the unit vector in the direction of the far field velocity, $\mathbf{g}$ the gravitational acceleration, and T_b and T_∞ the temperature of the bluff body and in the far field, respectively. Finally, we suppose that the dependence of the solution restricted to the boundary of the domain is linear, i.e., we take $\mathbf{D}_{bc}$ to be a linear boundary condition operator. One can also consider the dependence of the boundary conditions on parameters, that is, either $\mathbf{D}_{bc}(\boldsymbol{\eta})$ or $\mathbf{q}_{\partial\Omega}(\boldsymbol{\eta})$, which may be used, for instance, for modeling of a moving wall. For the sake of simplicity this possibility is not considered. The multiple scales expansion of the solution $\mathbf{q}$ of Eq. (56) consists of an expansion of Eq. (1) in powers of a small parameter $\varepsilon\ll 1$:

$$\mathbf{q}(t,\tau)=\mathbf{Q}_0+\varepsilon\mathbf{q}_{(\varepsilon)}(t,\tau)+\varepsilon^2\mathbf{q}_{(\varepsilon^2)}(t,\tau)+O(\varepsilon^3). \quad (58)$$

The departure $\boldsymbol{\eta}-\boldsymbol{\eta}_c$ of the parameters from criticality is assumed to be of second order, i.e., $\eta_i-\eta_{i,c}=O(\varepsilon^2)$ for $i=0,1,2$. The expansion (58) encompasses a two-scale expansion of the original time, $t\mapsto t+\varepsilon^2\tau$, that incorporates the fast time scale t of the self-sustained instability and the slow timescale τ of the evolution of the amplitudes $a_i(\tau)$ in Eq. (1), for $i=0,1,2$. The resulting expansion of the left side of Eq. (56) up to third order is given by

$$\varepsilon\mathbf{B}\frac{\partial\mathbf{q}_{(\varepsilon)}}{\partial t}+\varepsilon^2\mathbf{B}\frac{\partial\mathbf{q}_{(\varepsilon^2)}}{\partial t}+\varepsilon^3\left[\mathbf{B}\frac{\partial\mathbf{q}_{(\varepsilon^3)}}{\partial t}+\mathbf{B}\frac{\partial\mathbf{q}_{(\varepsilon)}}{\partial\tau}\right], \quad (59)$$

while the right side is

$$\mathbf{F}(\mathbf{q},\boldsymbol{\eta})=\mathbf{F}_{(0)}+\varepsilon\mathbf{F}_{(\varepsilon)}+\varepsilon^2\mathbf{F}_{(\varepsilon^2)}+\varepsilon^3\mathbf{F}_{(\varepsilon^3)}. \quad (60)$$

The resulting problem is solved order by order.

1. Order ε^0

The leading order solution $\mathbf{Q}_0$ of the multiple scales expansion (58) is the steady state of the governing equations evaluated at the threshold of instability, i.e., $\boldsymbol{\eta}=\boldsymbol{\eta}_c$,

$$\begin{aligned}\mathbf{0}&=\mathbf{F}(\mathbf{Q}_0,\mathbf{0}),\quad \mathbf{x}\in\Omega,\\ \mathbf{D}_{bc}\mathbf{Q}_0(\mathbf{x})&=\mathbf{Q}_{0,\partial\Omega},\quad \mathbf{x}\in\partial\Omega.\end{aligned} \quad (61)$$

2. Order ε^1

The first-order correction $\mathbf{q}_{(\varepsilon)}(t,\tau)$ in the multiple-scale expansion (58) is composed of the eigenmodes of the linearized system

$$\begin{aligned}\mathbf{q}_{(\varepsilon)}(t,\tau)\equiv&\,\mathrm{Re}[a_0(\tau)e^{-im_0\theta}\hat{\mathbf{q}}_0]\\ &+\mathrm{Re}[a_1(\tau)e^{-i\omega t}e^{-im_1\theta}\hat{\mathbf{q}}_1]\\ &+\mathrm{Re}[a_2(\tau)e^{-i\omega t}e^{-im_2\theta}\hat{\mathbf{q}}_2],\end{aligned} \quad (62)$$

where the reflection symmetry in O(2) imposes the requirement $m_2=-m_1$. Each term $\hat{\mathbf{q}}_\ell$ in the first-order expansion (62) solves the corresponding linear problem:

$$\begin{aligned}\mathbf{J}_{(\omega_\ell,m_\ell)}\hat{\mathbf{q}}_\ell&=\left(i\omega_\ell\mathbf{B}-\left.\frac{\partial\mathbf{F}}{\partial\mathbf{q}}\right|_{\mathbf{q}=\mathbf{Q}_0,\boldsymbol{\eta}=\boldsymbol{\eta}_c}\right)\hat{\mathbf{q}}_\ell=\mathbf{0},\quad \mathbf{x}\in\Omega,\\ \mathbf{D}_{bc}\hat{\mathbf{q}}_\ell(\mathbf{x})&=0,\quad \mathbf{x}\in\partial\Omega,\end{aligned} \quad (63)$$

where $\frac{\partial\mathbf{F}}{\partial\mathbf{q}}|_{\mathbf{q}=\mathbf{Q}_0,\boldsymbol{\eta}=\boldsymbol{\eta}_c}\hat{\mathbf{q}}_\ell=\mathbf{L}_{m_\ell}\hat{\mathbf{q}}_\ell+\mathbf{N}_{m_\ell}(\mathbf{Q}_0,\hat{\mathbf{q}}_\ell)+\mathbf{N}_{m_\ell}(\hat{\mathbf{q}}_\ell,\mathbf{Q}_0)$. The subscript m_ℓ indicates the azimuthal wave number used for the evaluation of the operator.

3. Order ε^2

The second-order expansion term $\mathbf{q}_{(\varepsilon^2)}(t,\tau)$ is determined from the resolution of a set of forced linear systems, with the forcing terms evaluated in terms of the (known) zeroth- and first-order terms. The expansion in terms of amplitudes $a_i(\tau)$ of $\mathbf{q}_{(\varepsilon^2)}(t,\tau)$ is assessed from term-by-term identification of the forcing terms at the second order. The nonlinear second-order terms are

$$\begin{aligned}\mathbf{F}_{(\varepsilon^2)}\equiv&\sum_{j,k=0}^{2}(a_ja_k\mathbf{N}(\hat{\mathbf{q}}_j,\hat{\mathbf{q}}_k)e^{-i(m_j+m_k)\theta}e^{-i(\omega_j+\omega_k)t}+\text{ c.c.})\\ &+\sum_{j,k=0}^{2}(a_j\bar{a}_k\mathbf{N}(\hat{\mathbf{q}}_j,\bar{\hat{\mathbf{q}}}_k)e^{-i(m_j-m_k)\theta}e^{-i(\omega_j-\omega_k)t}+\text{ c.c.})\\ &+\sum_{\ell=0}^{2}\Delta\eta_\ell\mathbf{G}(\mathbf{Q}_0,\mathbf{e}_\ell),\end{aligned} \quad (64)$$

where $\mathbf{e}_\ell$ is an element of the orthonormal basis of $\mathbb{R}^{N_p}$, a vector composed of zeros except at the position ℓ where it is equal to unity. Since no quadratic combination of elements in Eq. (62) results in resonant terms, the second-order term can be expanded as

$$\mathbf{q}_{(\varepsilon^2)}\equiv\sum_{\substack{j,k=0\\k\leqslant j}}^{2}(a_ja_k\hat{\mathbf{q}}_{j,k}+a_j\bar{a}_k\hat{\mathbf{q}}_{j,-k}+\text{ c.c. })+\sum_{\ell=0}^{2}\Delta\eta_\ell\mathbf{Q}_0^{(\eta_\ell)}, \quad (65)$$

with the rules $\hat{\mathbf{q}}_{j,k}=\hat{\mathbf{q}}_{k,j}$ and $\hat{\mathbf{q}}_{-j,-k}=\bar{\hat{\mathbf{q}}}_{j,k}$. Note the slight abuse of notation with $\hat{\mathbf{q}}_{-0}=\bar{\hat{\mathbf{q}}}_0$. Terms $\hat{\mathbf{q}}_{j,j}$ are harmonics of the flow, $\hat{\mathbf{q}}_{j,k}$ with $j\neq k$ are coupling terms, $\hat{\mathbf{q}}_{j,-j}$ are harmonic base flow modification terms, and $\mathbf{Q}_0^{(\eta_\ell)}$ are base flow corrections due to the assumed departure of the parameter $\Delta\eta_\ell=\eta_{\ell_c}-\eta_\ell$ from the critical point measured by ε. Finally, the second-order terms are computed by solving the following

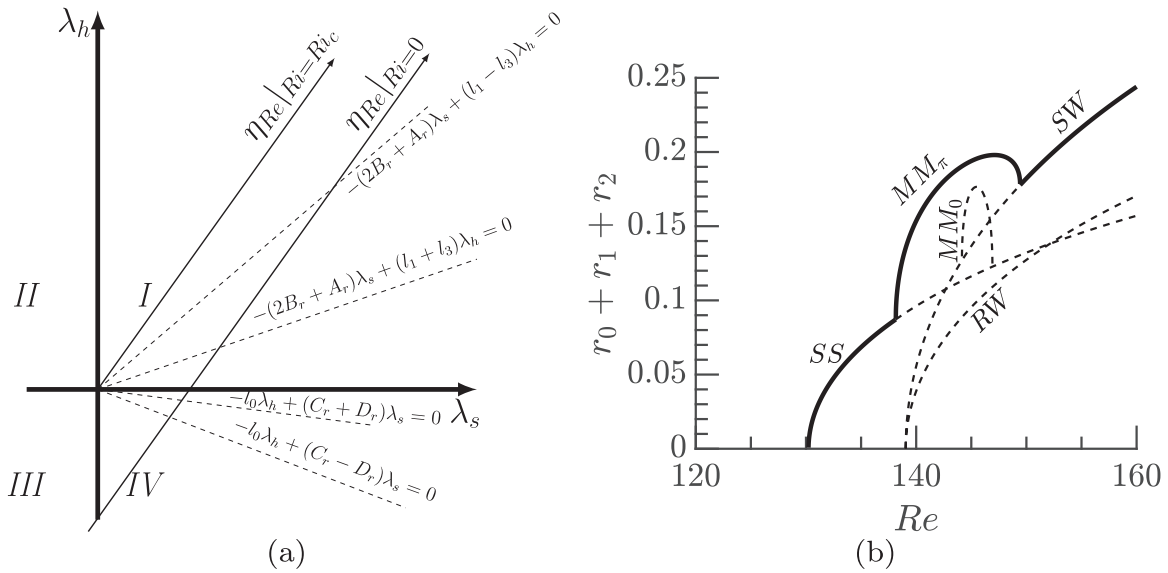

FIG. 22. Construction of the stability diagram for the WFA-MC problem with a fixed disk of aspect ratio $\chi = 10$. (a) The unfolding plane (λ_s, λ_h). Dashed lines indicate the loci of bifurcations from SS and SW to $MM_{0,\pi}$. The paths labeled $\eta_{Re}|_{Ri=Ri_c}$ and $\eta_{Re}|_{Ri=0}$ are the paths followed in this plane for $Ri = Ri_c$ and $Ri = 0$, respectively. For this case $Ri_c < 0$ and so increasing Ri destabilizes the system. (b) Bifurcation diagram corresponding to the $\eta_{Re}|_{Ri=0}$ path. See Sec. VIII B for details.

nonresonant system of equations,

$$\mathbf{J}_{(\omega_j+\omega_k, m_j+m_k)}\hat{\mathbf{q}}_{j,k} = \hat{\mathbf{F}}^{(j,k)}_{(\varepsilon^2)}, \tag{66}$$

where $\hat{\mathbf{F}}^{(j,k)}_{(\epsilon^2)} \equiv \mathbf{N}(\hat{\mathbf{q}}_j, \hat{\mathbf{q}}_k) + \mathbf{N}(\hat{\mathbf{q}}_k, \hat{\mathbf{q}}_j)$ and

$$\mathbf{J}_{(0,0)}\mathbf{Q}_0^{(\eta_\ell)} = \mathbf{G}(\mathbf{Q}_0, \mathbf{e}_\ell). \tag{67}$$

4. Order ε^3

At third order resonant terms are generated, and these lead to secular (nonperiodic) terms in the expansion. We eliminate these terms by imposing a solvability condition on the system via the Fredholm alternative. This condition determines the required normal form at third order in ε. Specifically, the linear terms λ_s and λ_h are determined as follows:

$$\lambda_s = \frac{\langle \hat{\mathbf{q}}_0^\dagger, \hat{\mathbf{F}}^{(a_0)}_{(\epsilon^3)}\rangle}{\langle \hat{\mathbf{q}}_0^\dagger, \mathbf{B}\hat{\mathbf{q}}_0\rangle}, \quad \lambda_h = \frac{\langle \hat{\mathbf{q}}_1^\dagger, \hat{\mathbf{F}}^{(a_1)}_{(\epsilon^3)}\rangle}{\langle \hat{\mathbf{q}}_1^\dagger, \mathbf{B}\hat{\mathbf{q}}_1\rangle} = \frac{\langle \hat{\mathbf{q}}_2^\dagger, \hat{\mathbf{F}}^{(a_2)}_{(\epsilon^3)}\rangle}{\langle \hat{\mathbf{q}}_2^\dagger, \mathbf{B}\hat{\mathbf{q}}_2\rangle}, \tag{68}$$

while the (real) cubic coefficients l_i for $i = 0, 1, 2, 3$ are given by

$$l_0 = \frac{\langle \hat{\mathbf{q}}_0^\dagger, \hat{\mathbf{F}}^{(a_0|a_0|^2)}_{(\epsilon^3)}\rangle}{\langle \hat{\mathbf{q}}_0^\dagger, \mathbf{B}\hat{\mathbf{q}}_0\rangle}, \quad l_3 = \frac{\langle \hat{\mathbf{q}}_0^\dagger, \hat{\mathbf{F}}^{(\bar{a}_0 a_1 \bar{a}_2)}_{(\epsilon^3)}\rangle}{\langle \hat{\mathbf{q}}_0^\dagger, \mathbf{B}\hat{\mathbf{q}}_0\rangle},$$

$$l_1 - il_2 = \frac{\langle \hat{\mathbf{q}}_0^\dagger, \hat{\mathbf{F}}^{(a_0|a_1|^2)}_{(\epsilon^3)}\rangle}{\langle \hat{\mathbf{q}}_0^\dagger, \mathbf{B}\hat{\mathbf{q}}_0\rangle}, \quad l_1 + il_2 = \frac{\langle \hat{\mathbf{q}}_0^\dagger, \hat{\mathbf{F}}^{(a_0|a_2|^2)}_{(\epsilon^3)}\rangle}{\langle \hat{\mathbf{q}}_0^\dagger, \mathbf{B}\hat{\mathbf{q}}_0\rangle}. \tag{69}$$

Finally, the complex coefficients A, B, C, and D are given by

$$B = \frac{\langle \hat{\mathbf{q}}_1^\dagger, \hat{\mathbf{F}}^{(a_1|a_1|^2)}_{(\epsilon^3)}\rangle}{\langle \hat{\mathbf{q}}_1^\dagger, \mathbf{B}\hat{\mathbf{q}}_1\rangle}, \quad A + B = \frac{\langle \hat{\mathbf{q}}_1^\dagger, \hat{\mathbf{F}}^{(a_1|a_2|^2)}_{(\epsilon^3)}\rangle}{\langle \hat{\mathbf{q}}_1^\dagger, \mathbf{B}\hat{\mathbf{q}}_1\rangle},$$

$$C = \frac{\langle \mathbf{q}_1^\dagger, \hat{\mathbf{F}}^{(a_1|a_0|^2)}_{(\epsilon^3)}\rangle}{\langle \hat{\mathbf{q}}_1^\dagger, \mathbf{B}\hat{\mathbf{q}}_1\rangle}, \quad D = \frac{\langle \mathbf{q}_1^\dagger, \hat{\mathbf{F}}^{(a_0^2 a_2)}_{(\epsilon^3)}\rangle}{\langle \hat{\mathbf{q}}_1^\dagger, \mathbf{B}\hat{\mathbf{q}}_1\rangle}. \tag{70}$$

The forcing terms associated with the solvability conditions in Eqs. (68), (69), and (70) are detailed in Appendix A 1.

VIII. CONSTRUCTION OF BIFURCATION DIAGRAMS

We now explain how the results derived in the previous section can be used to construct consistent bifurcation diagrams. The method is similar to that used in Hirschberg and Knobloch [29] and is explained in Fig. 22. As illustrated in this figure, the conditions for the occurrence of the various bifurcations can be interpreted as lines in the (λ_s, λ_h) plane. For example, the primary steady-state bifurcation occurs along the line $\lambda_s = 0$, which is the horizontal axis in this representation. Similarly, the primary Hopf bifurcation occurs along the line $\lambda_h = 0$, which is the vertical axis. The conditions relevant to the birth of mixed modes also correspond to straight lines, as displayed in the figure. For both the wake problem (WFA or WFA-MC) and the TCF problem, variation of the base-flow parameters defines a path in the (λ_s, λ_h) plane. The bifurcation diagram can then be constructed by considering the successive crossings of this path with the lines defining the bifurcations.

Let us consider first the bifurcation scenario of the WFA-MC case as a function of the parameters η_{Re} and η_{Ri}, at a constant distance in terms of the second parameter from the organizing center. We denote by $\eta_{Re}|_{Ri=Ri_c}$ the path followed at a constant Richardson number equal to that at which the unsteady and steady modes become simultaneously unstable. Similarly, we denote by $\eta_{Re}|_{Ri=0}$ the straight line path from quadrant III (defined by $\lambda_s < 0$, $\lambda_h < 0$), traversing quadrant IV ($\lambda_s > 0$, $\lambda_h < 0$), and then crossing into quadrant I ($\lambda_s > 0$, $\lambda_h > 0$). This path is relevant to the wake problem (WFA) for increasing Reynolds number if we assume a linear dependence of the form (13). When following this path, the first bifurcation is the primary bifurcation leading to the SS mode. There are two possible secondary bifurcations on this

branch, leading to MM_0 and MM_π, and these occur along the lines $-l_0\lambda_h + (C_r \pm D_r)\lambda_s = 0$ with positive sign for MM_0 and negative sign for MM_π. The sign of D_r indicates which of these bifurcations occurs first along the given path. For example, if $D_r < 0$, as displayed in the figure, the bifurcation to MM_π occurs first. Moreover, if $\Delta_- > 0$ (as assumed in the figure), this bifurcation is supercritical and gives rise to a stable branch. The bifurcation from SS to MM_π may occur subsequently, as found in the figure, but the branch born at this bifurcation is necessarily unstable, according to the considerations in Sec. IV C.

Similarly, the lines $-(2B_r + A_r)\lambda_s + (l_1 \pm l_3)\lambda_h = 0$ indicate secondary bifurcations from SW to MM_0 (positive sign) and MM_π (negative sign). Starting from the pure SW mode and following the prescribed path backward, the sign of l_3 lets us distinguish which of these lines will be crossed first. For example, if $l_3 < 0$, as displayed in the figure, the bifurcation to MM_π occurs first, leading to a stable branch if $\Delta_- > 0$.

Figure 22(b) exhibits the case corresponding to $l_3 < 0$, $D_r < 0$, $\Delta_+ > 0$, $\Delta_- > 0$, the situation relevant to wake flow past a fixed disk. The figure displays the bifurcation diagram for a disk of aspect ratio $\chi = 10$. For details, see Sec. VIII B.

In the following, we analyze the predicted transition behavior of the flow past a fixed sphere and a fixed disk. In some figures, we use the lift coefficient to illustrate the bifurcation diagram; this is defined as $C_L = \frac{L}{\frac{1}{2}\rho_\infty U_\infty^2 D}$, with L the lift force, ρ_∞ and U_∞ the density and velocity in the far field (assumed equal to unity), respectively, and D the diameter of the object.

A. Mixed convection in the flow past a sphere

Let us revisit the problem of pattern formation behind a sphere falling through a thermally stratified fluid. In our formulation the sphere is held fixed, with upward flow past it (the WFA-MC problem). Specifically, a sphere of diameter D is held at a constant temperature T_b subject to upward flow characterized by a constant velocity U_∞ and temperature T_∞ far from the body. The problem is specified by the Reynolds number as $\mathrm{Re} = \frac{U_\infty D}{\nu}$ and the Richardson number $\mathrm{Ri} = -\frac{\beta(\mathbf{e}_{U_\infty}\cdot\mathbf{g})(T_b - T_\infty)D}{U_\infty^2}$. This problem has many practical applications in engineering such as cooling, heating [26], sedimentation [54], melting [55], combustion [56], and vaporization [57]. A hot sphere represents a heat source embedded within the physical domain, where the solid body is subjected to forces of hydrodynamic and thermal origin. There are two main cases of interest. The case of a hot falling sphere where the fluid within the wake is accelerated with respect to the spherical body is called the *assisting* case and is characterized by a positive Richardson number ($\mathrm{Ri} > 0$). The opposite case, where the wake of a hot ascending spherical particle is decelerated by buoyancy effects, is referred to as the *opposing* case and corresponds to a negative Richardson number ($\mathrm{Ri} < 0$). Kotouc *et al.* [26] studied numerically both configurations for two Prandtl numbers, $\mathrm{Pr} = 0.72$ and $\mathrm{Pr} = 7$. The assisting flow case displays an organizing center of Hopf-Hopf type with azimuthal wave numbers $m = 1$ and $m = 2$.

The opposing flow configuration exhibits instead a point in the $(\mathrm{Re}, \mathrm{Ri})$ parameter space where a steady-state mode and a pair of unsteady modes with azimuthal wave number

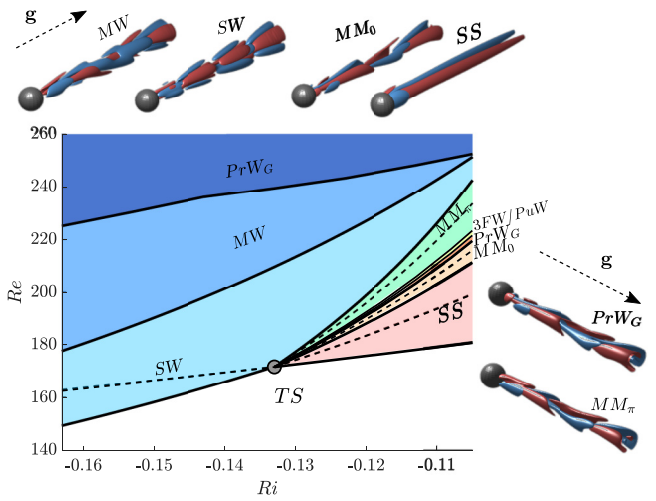

FIG. 23. Predicted flow patterns for flow past a hot sphere (the opposing case of mixed convection) in parameter space. Snapshots of the reconstructed states are included. The direction of gravity $\boldsymbol{g}$ is represented by a dashed line parallel to the axis of revolution and points from the sphere towards the wake when $T_b - T_\infty > 0$.

$m = \pm 1$ are simultaneously unstable; cf. Figs. 23 and 24. The opposing flow case at $\mathrm{Pr} = 0.72$ displays a large variety of patterns. The codimension-two point at $(\mathrm{Re}_c, \mathrm{Ri}_c)$ point (see Tables XII and XIII) splits the parameter space in the following sense: for $\mathrm{Ri}_c < \mathrm{Ri} < 0$ the primary bifurcation breaks the axisymmetry of the steady-state solution, i.e., it corresponds to a steady-state mode (state I in Kotouc *et al.* [26]); for $\mathrm{Ri} < \mathrm{Ri}_c$ the primary branch is a standing wave (state XIV in Kotouc *et al.* [26]), i.e., a solution with mean-zero lift force preserving the symmetry plane. For Richardson numbers $\mathrm{Ri} < \mathrm{Ri}_c$ the observed transition to more complex spatio-temporal patterns is explained by the interaction between the unsteady pair of modes. In this regime the cubic truncation is degener-

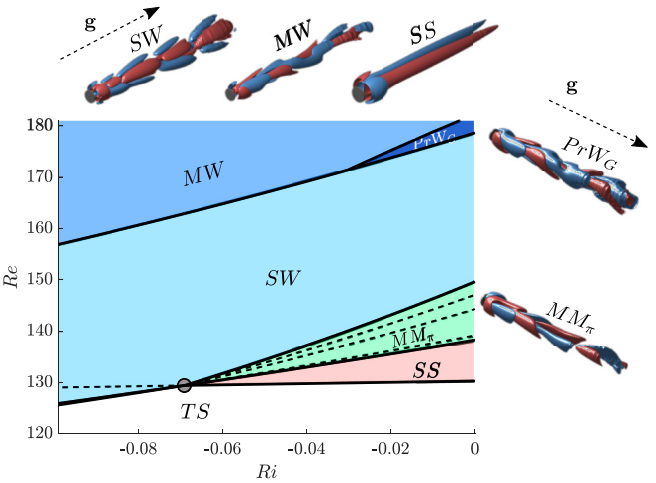

FIG. 24. Predicted flow patterns for flow past a hot disk with $\chi = 10$ (the opposing case of mixed convection) in parameter space. Snapshots of the reconstructed states are included. The direction of gravity $\boldsymbol{g}$ is represented by a dashed line parallel to the axis of revolution pointing from the disk towards the wake when $T_b - T_\infty > 0$.

TABLE XII. Location of the codimension-two point at Pr = 0.72 and the corresponding Strouhal number (Sr_c) at unsteady onset, together with the linear coefficients in the normal form for the WFA-MC flow past a sphere or a disk.

Case	Re_c	Ri_c	Sr_c	λ_s	λ_h
Sphere	172	−0.13	8.5×10^{-2}	$86.7\cdot\eta_{\mathrm{Re}}+0.82\cdot\eta_{\mathrm{Ri}}$	$(84.7-67.9i)\cdot\eta_{\mathrm{Re}}+(2.19-3.31i)\cdot\eta_{\mathrm{Ri}}$
Disk $\chi=10$	129.4	−0.069	1.07×10^{-1}	$76.8\cdot\eta_{\mathrm{Re}}+0.057\cdot\eta_{\mathrm{Ri}}$	$(66.0-25.2i)\cdot\eta_{\mathrm{Re}}+(0.52-1.10i)\cdot\eta_{\mathrm{Ri}}$
Disk $\chi=3$	152.9	−0.079	9.5×10^{-2}	$95.3\cdot\eta_{\mathrm{Re}}+0.37\cdot\eta_{\mathrm{Ri}}$	$(92.5-40.0i)\cdot\eta_{\mathrm{Re}}+(1.10-1.48i)\cdot\eta_{\mathrm{Ri}}$

ate, as already explained, and in order to lift the degeneracy between the modulated wave states MW and IMM (these states are labeled XX in Kotouc *et al.* and not distinguished) one must either include higher order terms in the normal form or introduce terms that break the O(2) symmetry; see Appendix B. These modulated wave states then bifurcate further, generating general Precessing Waves. In the study of Kotouc *et al.* [26], the authors did not observe PrW_G, and instead identified aperiodic states, i.e., states that did not display any particular spatiotemporal symmetry. This finding could be explained by a subsequent bifurcation towards a 3FW, although this is not taken into account in the normal form.

When $\mathrm{Ri}>\mathrm{Ri}_c$ a large variety of states exist. The axisymmetric steady state loses stability with respect to a nonaxisymmetric steady-state mode, thereby losing axisymmetry. The resulting SS state then transitions into a mixed mode MM_0 that preserves reflection symmetry and is associated with a nonzero mean lift. The MM_0 state further transitions into a general precessing wave PrW_G, i.e., a state without a symmetry plane and slowly rotating mean lift, which in turn bifurcates into a 3FW and finally to a pulsating wave state. These three states are located within small regions of the parameter space. However, they have been numerically determined: PrW_G was numerically observed by Kotouc *et al.* [26] for $\mathrm{Ri}>-0.1$ (state XIII) and the 3FW (or PuWs) state was identified for $\mathrm{Ri}\approx-0.1$ (state XIX), which is a state that displays a temporary symmetry plane and at least two frequency components. The pulsating wave state eventually transitions into MM_π, i.e., a mixed mode without a symmetry plane (see also state XIII in [26]). This series of bifurcations is followed either by SW or MW (or a precessing wave), in qualitative accordance with the study of Kotouc *et al.*

B. Mixed convection in the flow past a disk

Let us now examine the transition scenario for axisymmetric wake flow past a disk, focusing again on the *opposing flow* case under mixed convection conditions. This problem depends on three control parameters, the Reynolds number Re, the Richardson number Ri, and the aspect ratio of the disk χ, where $1/\chi$ is the dimensionless thickness.

TABLE XIII. Cubic and quintic coefficients of the normal form for the WFA-MC flow past a sphere for Pr = 0.72.

l_0	l_1	l_2	l_3	p^1_Δ
−10.57	−4.57	−0.078	0.27	−201.1
A	B	C	D	p^2_N
$1.07+0.75i$	$-2.8+3.54i$	$-3.78+3.02i$	$0.79-1.0i$	−18.10

The WFA problem for $\mathrm{Ri}=0$ and $1/\chi\approx0$ has already been studied by Fabre *et al.* [13] using numerical simulations and normal form coefficients fitted from the simulations. The case $\chi=3$ was studied in detail by Auguste *et al.* [14]. A more rigorous study via multiple-scale analysis was performed by Meliga *et al.* [27]. Later Chrust *et al.* [15] explored the flow dependence on the parameters (Re, χ) using numerical simulations and proposed a classification of the patterns observed. These studies demonstrated the importance of the disk thickness on the transition scenario. Chrust *et al.* observed that, when the thickness $1/\chi$ is large, for instance, $\chi=1$, the symmetry plane is preserved for large values of the Reynolds number, i.e., only SS and MM_0 (possibly with modulated mixed modes or precessing waves) are observed before spatio-temporal chaos appears. In the limit of zero thickness, when $1/\chi\approx0$, we will see that the transition scenario starts with the formation of a SS pattern followed by the breaking of the symmetry plane, leading to a MM_π mode and eventually to standing waves SW. At intermediate values of the thickness, a large variety of spatio-temporal patterns may be observed, as highlighted by the study of Auguste *et al.* In the present study, we shall look for the connections between the *opposing flow* case in mixed convection and the situation at $\mathrm{Ri}=0$, in terms of the spatio-temporal patterns observed in the flow.

Figure 25 displays the location of the codimension-two point corresponding to the Hopf–steady-state bifurcation, obtained by varying $1/\chi\in[0,1]$. The top panels show the corresponding temperature distribution in space and the growing extent of the recirculation bubble in the steady states associated with two distinct values of the aspect ratio χ of the disk. In the range of aspect ratios considered here, the critical Reynolds number grows linearly with the thickness $1/\chi$ of the disk, as previously observed by Fernandes *et al.* [18]. In addition, the critical Richardson number displays a maximum around $1/\chi\approx0.1$ followed by a linear decrease. In the following, we shall discuss in detail the two cases $\chi=10$ and $\chi=3$. The case $\chi=10$ corresponds to a case with a relatively simple transition scenario, similar to that explained by Meliga *et al.* [27]. On the other hand, the case $\chi=3$ displays a larger number of spatio-temporal structures and is qualitatively similar to the case of the sphere discussed in Sec. VIII A.

The coefficients of the normal form for $\chi=10$ at the codimension-two point are listed in Table XIV, and the parameter space summarizing the normal form predictions is displayed in Fig. 24. In this case, to the left of the codimension-two point (gray point in the diagram), the trivial steady-state transitions to standing waves and the subsequent bifurcations are uniquely explained by the unsteady modes. To

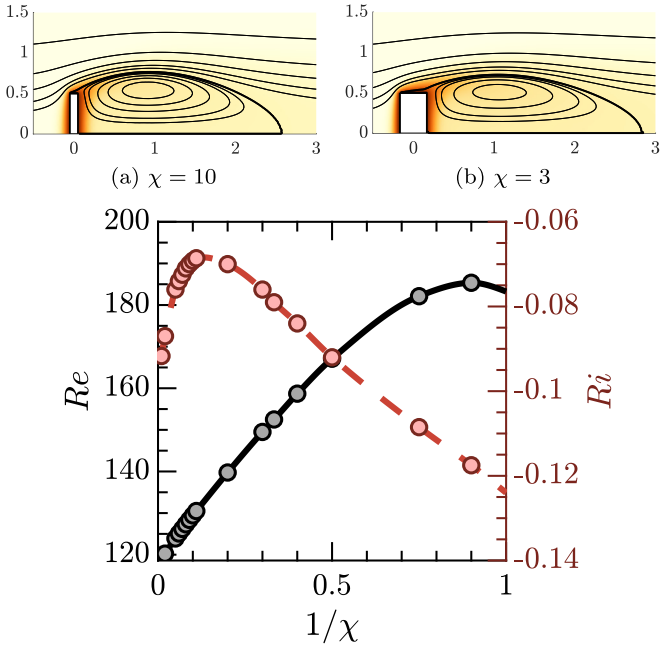

FIG. 25. Location of the codimension-two Hopf–steady-state bifurcation in the (Re, Ri) plane as a function of the aspect ratio χ of the disk (Re: black line; Ri: red line). The color-coded symbols refer to the points obtained in numerical computations. Top: Temperature distribution in the trivial steady state at (a) $1/\chi = 0.1$ (Re ≈ 130, Ri ≈ -0.068) and (b) $1/\chi \approx 0.33$ (Re ≈ 150, Ri ≈ -0.078).

the right of the codimension-two point the primary bifurcation breaks the axisymmetry of the steady state, i.e., it generates the SS state, followed by a periodic state with no reflection symmetry and nonzero mean lift, i.e., the MM_π state. The mixed mode MM_π state eventually bifurcates into a standing wave solution, which finally bifurcates to MW via the effect of higher order terms.

The dynamics near the organizing center for the flow past a disk with thickness $1/\chi = 1/3$ is richer. As in the previous cases, to the left of the organizing center the transition scenario is based on the initial formation of standing waves, followed by modulated waves and a possible tertiary bifurcation, not taken into account in the normal form, leading to temporal chaos. To the right of the organizing center, the transition scenario is qualitatively similar to that of the sphere (compare Figs. 23 and 26), although in the present case the codimension-two point is sufficiently close for the theory to provide quantitative predictions of the transition scenario. The coefficients of the normal form are listed in Table XV. In other words, the transition scenario in the simple WFA problem

TABLE XIV. Cubic and quintic coefficients of the normal form for the WFA-MC flow past a disk with $\chi = 10$ for Pr $= 0.72$.

l_0	l_1	l_2	l_3	p^1_Δ
-4.45	-5.94	0.92	-2.28	-50
A	B	C	D	p^2_N
$0.1 - 1.29i$	$-2.14 + 1.69i$	$-0.64 - 2.35i$	$-1.05 + 1.10i$	-1

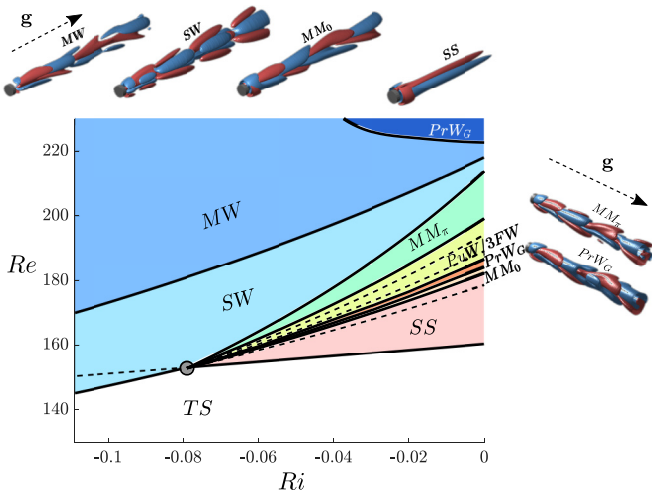

FIG. 26. Predicted flow patterns for flow past a hot disk with $\chi = 3$ (the opposing case of mixed convection) in parameter space, at Pr $= 0.72$. Snapshots of the reconstructed states are included. The direction of gravity $\boldsymbol{g}$ is represented by a dashed line parallel to the axis of revolution pointing from the disk towards the wake when $T_b - T_\infty > 0$.

of the disk with aspect ratio $\chi = 3$ is constrained by the dynamical structures emanating from the organizing center at Ri $\neq 0$, something that is not the case for the sphere; see Kotouc *et al.* [26, Fig 4]. Figure 27 displays the reconstruction of the lift coefficient from the normal form at Ri $= 0$, in comparison to the results obtained numerically by Auguste *et al.* in [14]. It distinguishes five regions, with the Knit-Knot (KK) region among them. The transition begins at Re ≈ 159.4 (Re ≈ 159.8 [14]) via the formation of a steady-state pattern (SS), which eventually bifurcates into a mixed mode (MM_0) at around Re ≈ 182.5 (Re ≈ 179.9 in [14]). The MM_0 state loses stability at around Re ≈ 184.5. Quantitatively, up to this point, the sequence of bifurcations is reasonably well predicted with regard to the data reported in [14]. The Knit-Knot region in our analysis covers a large variety of states with similar characteristics in terms of the frequency components (at least two) and the lift coefficient C_L. Auguste *et al.* [14] identified this motion as temporally quasiperiodic motion resulting from spontaneously broken reflection symmetry. The temporal dynamics of the KK state may be described as the composition of a state with frequency ω_h and a low-frequency state, whose frequency experiences large variation within its region of existence (from $T_p \approx 96\frac{2\pi}{\omega_h}$ at Re $= 185$ to $T_p \approx 48\frac{2\pi}{\omega_h}$ at Re $= 187$ and then to $T_p \approx 54\frac{2\pi}{\omega_h}$ at Re $= 190$; cf. Fig. 28). This bifurcation sequence is followed by the appearance of the MM_π state, estimated to be around Re ≈ 198.5

TABLE XV. Cubic and quintic coefficients of the normal form for the WFA-MC flow past a disk with $\chi = 3$ for Pr $= 0.72$.

l_0	l_1	l_2	l_3	p^1_Δ
-6.19	-4.86	0.47	-2.76	-50
A	B	C	D	p^2_N
$0.56 - 0.38i$	$-2.3 + 2.3i$	$-1.7 + 0.32i$	$0.79 + 0.52i$	-6

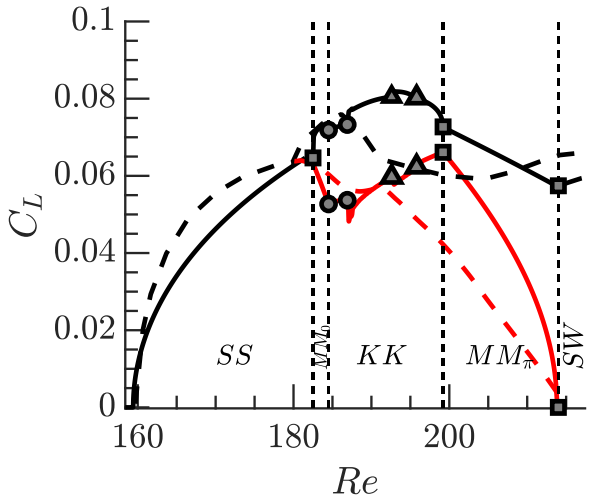

FIG. 27. Bifurcation diagram for a disk with $\chi = 3$ in terms of the lift coefficient C_L for the WFA problem (Ri = 0). Solid lines were computed from the normal form, dashed lines were extracted from [14]. Black lines denote $C_{L,\max}$ and red lines denote the average of C_L. See legend in Fig. 29 for a description of the markers.

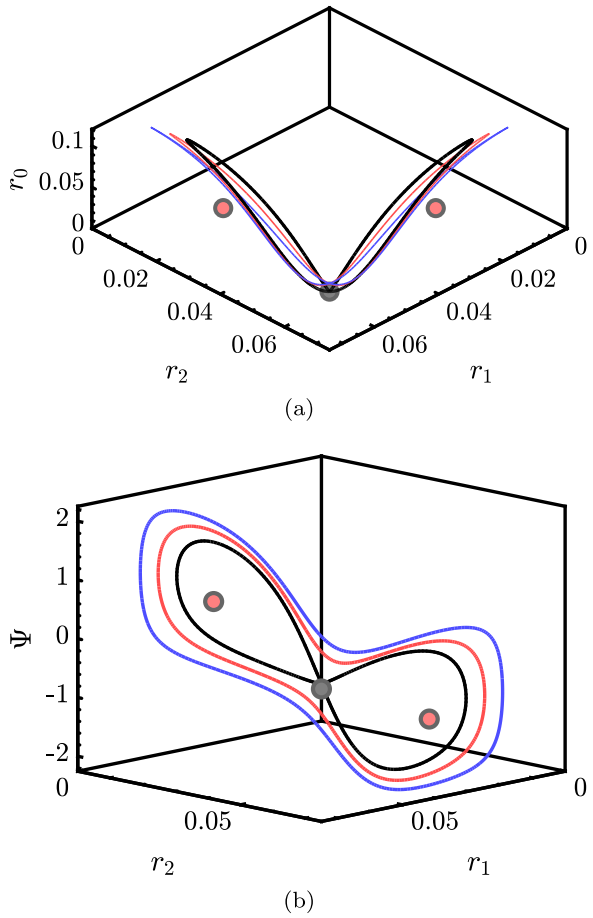

FIG. 28. Homoclinic orbit $\mathrm{Re}^{\mathrm{Hom}}_{MM_0}$ (gray line) at Re = 186.4 of Fig. 29. The gray dot is the location of MM_0, and the red markers indicate the location of the PrW_G states. The red and blue trajectories represent limit cycles for higher values of Re; the period of these states diverges logarithmically as Re → 186.4 from above (not shown).

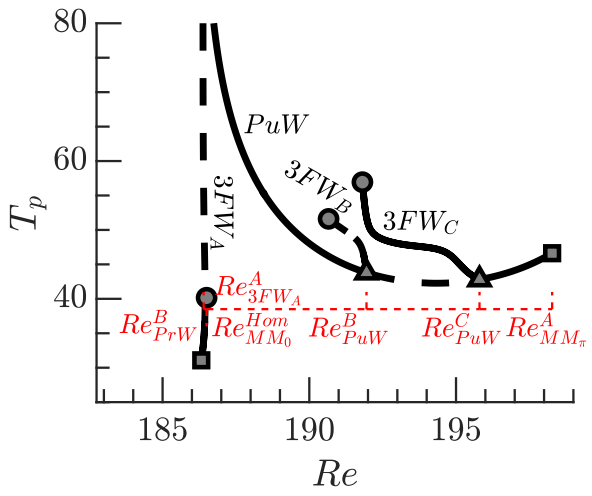

FIG. 29. Bifurcation diagram in the Knit-Knot region of Fig. 27 in terms of the period T_p of the low-frequency modulation. Square markers: Hopf bifurcation; circles: saddle-node bifurcation; triangles: Neimark-Sacker bifurcation.

(Re ≈ 190.4 in [14]), which connects to the standing wave branch at around Re ≈ 214 (Re ≈ 215.2 in [14]). According to theory, this sequence of bifurcations should be followed by the formation of a modulated wave branch and precessing waves. However, we do not discuss these patterns here due to the lack of simulation data to compare with and because these patterns can be described only using the fifth-order normal form whose coefficients we have not computed. For more information, see Fig. 26.

Let us return to the discussion of the Knit-Knot region. In our more detailed analysis, this state is actually composed of several simpler states; see Fig. 29. The MM_0 bifurcates into a precessing wave PrW_G at Re ≈ 184.5. This precessing wave is stable up to Re ≈ 186.3, where a saddle-node bifurcation takes place leading to a 3FW, denoted as $3FW_A$ in Fig. 29. The three-frequency wave is observable only in a small interval, however, and eventually reconnects to a pulsating wave via a global homoclinic bifurcation at around Re ≈ 186.9. This pulsating wave is stable up to around Re ≈ 191.9. At this stage, we can observe two other bifurcations leading to three-frequency waves with $3FW_B$ (unstable) and $3FW_C$ (stable); both of these branches reconnect to the main branch (PuWs) following a saddle-node bifurcation of limit cycles. The pulsating wave state finally reconnects with the symmetry-breaking mixed mode (MM_π) branch.

IX. DISCUSSION AND CONCLUSION

In this article, we have analyzed the properties of the normal form and the bifurcation scenario relevant to the bifurcations observed in axisymmetric wakes described by the Navier-Stokes equation. We have shown that near the onset of instability, it is possible to reduce the dynamics via center manifold reduction to a normal form, i.e., an ordinary differential equation, whose unfolding fully captures the local behavior of the Navier-Stokes equation. Such normal forms inherit the discrete and continuous symmetries of the system, in the present case O(2) symmetry. We have shown that this

approach, carried out in the vicinity of a steady-state–Hopf-mode interaction, suffices to predict much of the observed behavior.

Our analysis of the generic steady-state–Hopf-mode case relied on a reduction to polar coordinates. The fixed point solutions of the normal form, e.g., the pure modes and the mixed modes, have been observed in a variety of fluid flows, including Taylor-Couette and wake flows. Here we have attempted to provide a complete description of the fixed point solutions of the normal form, as well as the possible bifurcations to periodic solutions of the polar normal form corresponding to two- and three-frequency waves.

Particularly noteworthy is our discovery of robust, potentially attracting, heteroclinic cycles in this mode interaction. In previous studies [58,59], self-sustained processes have been related to a three-step process involving rolls advecting streamwise velocity, leading to streaks which once unstable lead to wavy perturbations whose nonlinear interaction with itself feeds the rolls. In terms of the mode interaction, the self-sustained cycle described by Dessup *et al.* [58] corresponds to a $\mathrm{Het}_{\mathrm{SS-SW}}$ cycle or to an orbit that shadows it. In this sense, one could expect that other, more complex dynamics, for instance, a $\mathrm{Het}_{\mathrm{Pr}W_A}$ cycle, may also be observed in the bifurcation scenario of real fluid systems. We mention that the indefinite increase in period associated with the approach to an attracting robust heteroclinic cycle cannot in general be seen in numerical integration of the normal form, on account of rounding error. Instead, the solution trajectory settles into a statistical limit cycle with a finite mean period [60]. This is even more so for partial differential equations [61] and in experiments where the presence of noise prevents approach to such a cycle [62]. This fact points to the importance of fluctuations in applications of the theory to fluid dynamics problems, as also emphasized in [48] in connection with the SNIPER bifurcation.

We have applied here the general theory to several distinct fluid flows and used it to explore the bifurcation scenario of wake flows behind a sphere or disk falling through either a constant density fluid or a vertically stratified fluid (problems WFA and WFA-MC, respectively). In particular, in Sec. VII we determined the normal form coefficients for these problems on the assumption that each object is held fixed, and used these results in Sec. VIII to construct consistent stability diagrams for these flows, comparing the predicted bifurcation scenarios for mixed-convection flow past a fixed axisymmetric object, a disk or a sphere, with the results of direct numerical simulations of these flows. These results enabled us to rationalize the results of previous numerical studies including those in the complicated Knit-Knot region of Auguste *et al.* [14] for the WFA problem for a disk of thickness $\chi = 3$ and the WFA-MC problem for a sphere of Kotouč *et al.* [26], states XIII or XIX, thereby demonstrating the utility of our bifurcation-theoretic approach. Unfortunately, neither of these cases predicts the presence of structurally stable heteroclinic cycles, although such states may arise for other parameter values.

ACKNOWLEDGMENT

The work of E.K. was supported in part by the National Science Foundation under Grant No. DMS-1908891.

APPENDIX A: NORMAL FORM REDUCTION

1. Third-order forcing terms

The third-order forcing terms are obtained from the substitution of the ansatz (58) into $\mathbf{F}(\mathbf{q}, \boldsymbol{\eta})$. The general expression of the third-order forcing term $\mathbf{F}_{(\varepsilon^3)}$ is as follows:

$$\begin{aligned}\mathbf{F}_{(\varepsilon^3)} \equiv & \sum_{\substack{j=-2\\k,\ell=-2}}^{2} a_j a_k a_\ell [\mathbf{N}(\hat{\mathbf{q}}_j, \hat{\mathbf{q}}_{k,\ell}) + \mathbf{N}(\hat{\mathbf{q}}_{k,\ell}, \hat{\mathbf{q}}_j)] e^{-im_n\theta} e^{-i\omega_n t} \\ & + \sum_{j=-2,\ell=0}^{2} a_j \Delta\eta_\ell \big[\mathbf{N}\big(\hat{\mathbf{q}}_j, \mathbf{Q}_0^{(\eta_\ell)}\big) + \mathbf{N}\big(\mathbf{Q}_0^{(\eta_\ell)}, \hat{\mathbf{q}}_j\big)\big] \\ & \times e^{-im_j\theta} e^{-i\omega_j t} \\ & + \sum_{j=-2,\ell=0}^{2} a_j \Delta\eta_\ell \mathbf{G}(\hat{\mathbf{q}}_j, \mathbf{e}_\ell) e^{-im_j\theta} e^{-i\omega_j t}, \end{aligned} \tag{A1}$$

with a slight abuse of notation such that $\hat{\mathbf{q}}_j = \overline{\hat{\mathbf{q}}}_{-j}$, $\hat{\mathbf{q}}_{k,j} = \overline{\hat{\mathbf{q}}}_{-k,-j}$, and $a_j = \overline{a}_{-j}$. Therefore, the azimuthal wave number and the frequency associated with a negative index are both considered to be of the opposite sign, i.e., $\omega_{-j} = -\omega_j$ and $m_{-j} = -m_j$. Finally, ω_n and m_n are defined by the relations $\omega_n = \omega_j + \omega_k + \omega_\ell$, $m_n = m_j + m_k + m_\ell$, where $n = j + k + \ell$. Resonant terms are those for which (ω_n, m_n) is equal to either $(0, m_0)$, (ω_1, m_1) or $(\omega_1, -m_1)$ (plus the complex conjugate pairs). The remaining terms play a role only in higher-order truncations. Hierarchically, the first class of third-order forcing terms consists of those that are linear with respect to the amplitudes a_j for $j = 0, 1, 2$,

$$\hat{\mathbf{F}}_{(\varepsilon^3)}^{(a_j)} \equiv \sum_{\ell=0}^{2} \Delta\eta_\ell \big(\big[\mathbf{N}\big(\hat{\mathbf{q}}_j, \mathbf{Q}_0^{(\eta_\ell)}\big) + \mathbf{N}\big(\mathbf{Q}_0^{(\eta_\ell)}, \hat{\mathbf{q}}_j\big)\big] + \mathbf{G}(\hat{\mathbf{q}}_j, \mathbf{e}_\ell)\big). \tag{A2}$$

The second type of resonant forcing terms are those used to compute the real coefficients l_j for $j = 0, 1, 2, 3$. These are proportional to the cubic terms in the first equation of the complex normal form (8) and are given by

$$\begin{aligned}\hat{\mathbf{F}}_{(\varepsilon^3)}^{(a_0|a_0|^2)} \equiv & [\mathbf{N}(\hat{\mathbf{q}}_0, \hat{\mathbf{q}}_{0,-0}) + \mathbf{N}(\hat{\mathbf{q}}_{0,-0}, \hat{\mathbf{q}}_0)] \\ & + [\mathbf{N}(\hat{\mathbf{q}}_{-0}, \hat{\mathbf{q}}_{0,0}) + \mathbf{N}(\hat{\mathbf{q}}_{0,0}, \hat{\mathbf{q}}_{-0})], \end{aligned} \tag{A3}$$

with the notation $\hat{\mathbf{q}}_{-0} = \overline{\hat{\mathbf{q}}}_0$. Similarly, the terms $\hat{\mathbf{F}}_{(\varepsilon^3)}^{(a_0|a_j|^2)}$ for $j = 1, 2$ are given by

$$\begin{aligned}\hat{\mathbf{F}}_{(\varepsilon^3)}^{(a_0|a_j|^2)} \equiv & [\mathbf{N}(\hat{\mathbf{q}}_0, \hat{\mathbf{q}}_{j,-j}) + \mathbf{N}(\hat{\mathbf{q}}_{j,-j}, \hat{\mathbf{q}}_0)] \\ & + [\mathbf{N}(\hat{\mathbf{q}}_{-j}, \hat{\mathbf{q}}_{0,j}) + \mathbf{N}(\hat{\mathbf{q}}_{0,j}, \hat{\mathbf{q}}_{-j})] \\ & + [\mathbf{N}(\hat{\mathbf{q}}_j, \hat{\mathbf{q}}_{0,-j}) + \mathbf{N}(\hat{\mathbf{q}}_{0,-j}, \hat{\mathbf{q}}_j)], \end{aligned} \tag{A4}$$

while $\hat{\mathbf{F}}_{(\varepsilon^3)}^{(\overline{a}_0 a_1 \overline{a}_2)}$ is expressed as

$$\begin{aligned}\hat{\mathbf{F}}_{(\varepsilon^3)}^{(\overline{a}_0 a_1 \overline{a}_2)} \equiv & [\mathbf{N}(\hat{\mathbf{q}}_{-0}, \hat{\mathbf{q}}_{1,-2}) + \mathbf{N}(\hat{\mathbf{q}}_{1,-2}, \hat{\mathbf{q}}_{-0})] \\ & + [\mathbf{N}(\hat{\mathbf{q}}_1, \hat{\mathbf{q}}_{-0,-2}) + \mathbf{N}(\hat{\mathbf{q}}_{-0,-2}, \hat{\mathbf{q}}_1)] \\ & + [\mathbf{N}(\hat{\mathbf{q}}_{-2}, \hat{\mathbf{q}}_{-0,1}) + \mathbf{N}(\hat{\mathbf{q}}_{-0,1}, \hat{\mathbf{q}}_{-2})]. \end{aligned} \tag{A5}$$

The third class of forcing terms are those used for the computation of the complex coefficients A, B, C, and D. These are $\hat{\mathbf{F}}^{(a_j|a_j|^2)}_{(\varepsilon^3)}$ for $j = 1, 2$:

$$\begin{aligned}\hat{\mathbf{F}}^{(a_j|a_j|^2)}_{(\varepsilon^3)} \equiv\ & [\mathbf{N}(\hat{\mathbf{q}}_j, \hat{\mathbf{q}}_{j,-j}) + \mathbf{N}(\hat{\mathbf{q}}_{j,-j}, \hat{\mathbf{q}}_j)] \\ & + [\mathbf{N}(\hat{\mathbf{q}}_{-j}, \hat{\mathbf{q}}_{j,j}) + \mathbf{N}(\hat{\mathbf{q}}_{j,j}, \hat{\mathbf{q}}_{-j})], \end{aligned} \tag{A6}$$

$\hat{\mathbf{F}}^{(a_j|a_k|^2)}_{(\varepsilon^3)}$ for $j = 1, 2$ and $k = 0, 1, 2$ with $j \neq k$,

$$\begin{aligned}\hat{\mathbf{F}}^{(a_j|a_k|^2)}_{(\varepsilon^3)} \equiv\ & [\mathbf{N}(\hat{\mathbf{q}}_j, \hat{\mathbf{q}}_{k,-k}) + \mathbf{N}(\hat{\mathbf{q}}_{k,-k}, \hat{\mathbf{q}}_j)] \\ & + [\mathbf{N}(\hat{\mathbf{q}}_{-k}, \hat{\mathbf{q}}_{j,k}) + \mathbf{N}(\hat{\mathbf{q}}_{j,k}, \hat{\mathbf{q}}_{-k})] \\ & + [\mathbf{N}(\hat{\mathbf{q}}_k, \hat{\mathbf{q}}_{j,-k}) + \mathbf{N}(\hat{\mathbf{q}}_{j,-k}, \hat{\mathbf{q}}_k)]. \end{aligned} \tag{A7}$$

Finally, the term $\hat{\mathbf{F}}^{(a_0^2 a_2)}_{(\varepsilon^3)}$ is expressed as

$$\begin{aligned}\hat{\mathbf{F}}^{(a_0^2 a_2)}_{(\varepsilon^3)} \equiv\ & [\mathbf{N}(\hat{\mathbf{q}}_0, \hat{\mathbf{q}}_{0,2}) + \mathbf{N}(\hat{\mathbf{q}}_{0,2}, \hat{\mathbf{q}}_0)] \\ & + [\mathbf{N}(\hat{\mathbf{q}}_2, \hat{\mathbf{q}}_{0,0}) + \mathbf{N}(\hat{\mathbf{q}}_{0,0}, \hat{\mathbf{q}}_2)]. \end{aligned} \tag{A8}$$

APPENDIX B: MODULATED WAVE MODE

The modulated wave mode is a degenerate solution of the normal form (8) truncated at third order. Crawford and Knobloch [33] analyzed the unfolding of the three simplest degeneracy conditions: (1) $A_r + 2B_r = 0$, (2) $B_r = 0$, and (3) $A_r = 0$. Here we briefly summarize some of their results and list sufficient conditions for the branching and stability of the modulated wave solution. The existence of the MW solution is subject to the following conditions:

$$\begin{aligned} & p^1\big(0, r_1^2 + r_2^2, \big(r_2^2 - r_1^2\big)^2, 0, 0, \lambda\big) \equiv 0, \\ & p^2\big(0, r_1^2 + r_2^2, \big(r_2^2 - r_1^2\big)^2, 0, 0, \lambda\big) \equiv 0. \end{aligned} \tag{B1}$$

Hill and Stewart [63] observed that the condition $p^2 \equiv 0$ is a degeneracy condition if one evaluates the polynomial p^2 at the origin, i.e., $p^2(0, 0, 0, 0, 0, 0) \equiv A_r$. Since, to fifth order,

$$\begin{aligned} & p^1\big(0, r_1^2 + r_2^2, \big(r_2^2 - r_1^2\big)^2, 0, 0, \lambda\big) \\ & \quad \equiv \lambda_h + \big(\tfrac{1}{2}A_r + B_r\big)\big(r_1^2 + r_2^2\big) \\ & \qquad + p^1_\Delta\big(r_2^2 - r_1^2\big)^2 + p^1_N\big(r_1^2 + r_2^2\big)^2, \\ & p^2\big(0, r_1^2 + r_2^2, \big(r_2^2 - r_1^2\big)^2, 0, 0, \lambda\big) \\ & \quad \equiv \tfrac{1}{2}A_r + p^2_N\big(r_1^2 + r_2^2\big) + p^2_\Delta\big(r_2^2 - r_1^2\big)^2, \end{aligned} \tag{B2}$$

the $\{r_1, r_2\}$ evolution is given by

$$\begin{aligned} \dot{r}_1 =\ & r_1\big[\lambda_h + B_r r_1^2 + (A_r + B_r) r_2^2 \\ & + \big(p^1_\Delta + p^1_{N^2} - p^2_N\big) r_1^4 + \big(p^1_\Delta + p^1_{N^2} + p^2_N\big) r_2^4 \\ & + 2\big(p^1_{N^2} - p^1_\Delta\big) r_2^2 r_1^2 + p^2_\Delta\big(r_2^2 - r_1^2\big)^3\big], \\ \dot{r}_2 =\ & \kappa \cdot \dot{r}_1, \end{aligned} \tag{B3}$$

where $\kappa \cdot \dot{r}_1$ stands for the action of the reflection symmetry, defined in Eq. (6), and $p^2_\Delta = 0$ to restrict the equation to fifth order. Inspection of Eq. (B3) shows that the fixed points r_a, r_b satisfy

$$\begin{aligned} r_a^2 &= \frac{1}{2}\left[-\frac{A_r}{2p^2_N} - \sqrt{\frac{\chi}{4p^2_N p^1_\Delta}}\right], \\ r_b^2 &= \frac{1}{2}\left[-\frac{A_r}{2p^2_N} + \sqrt{\frac{\chi}{4p^2_N p^1_\Delta}}\right], \end{aligned} \tag{B4}$$

where the symbol χ, which is a function of the parameter λ_h, is defined in Table VI. Evidently, the MW states exist when $A_r/p^2_N < 0$ and $0 < \chi/(p^2_N p^1_\Delta) < A_r^2/(p^2_N)^2$. The stability within the MW subspace, i.e., with respect to perturbations in $\{r_1, r_2\}$ only, can be analyzed in terms of the determinant and trace of the Jacobian stability matrix restricted to this subspace:

$$\det(M^{\mathrm{MW}}) = 32 p^2_N p^1_\Delta r_a^2 r_b^2 (r_a - r_b)^2 (r_a + r_b)^2, \tag{B5a}$$

$$\begin{aligned} \mathrm{tr}(M^{\mathrm{MW}}) =\ & \frac{A_r}{p^2_N}\left[\frac{A_r p^1_{N^2}}{p^2_N} - \frac{1}{2}(A_r + 2B_r)\right] \\ & + \big(r_a^2 - r_b^2\big)^2\big(4p^1_\Delta - 2p^2_N\big), \end{aligned} \tag{B5b}$$

In view of Eq. (B5a), the determinant vanishes when $r_a r_b = 0$ corresponding to the rotating wave branch and when $r_a = r_b$ corresponding to the standing wave branch. Therefore, the modulated wave branch connects the branches of rotating and standing waves. The standing wave changes stability when $\sigma_{\mathrm{SW}} \equiv -2r^2_{\mathrm{SW}}(A_r + 4r^2_{\mathrm{SW}} p^2_N)$ changes sign, which can happen if $A_r p^2_N < 0$. The corresponding standing wave amplitude is given by $r^2_{\mathrm{SW}} = -\frac{A_r}{4p^2_N}$. The standing wave emerges as a stable (resp. unstable) solution within the $\{r_1, r_2\}$ subspace if $A_r > 0$ (resp. $A_r < 0$), and it becomes unstable (resp. stable) when $r^2_{\mathrm{SW}} = -\frac{A_r}{4p^2_N}$. The stability of the rotating wave within the $\{r_1, r_2\}$ subspace is determined by the eigenvalue $\sigma_{\mathrm{RW}} \equiv -r^2_{\mathrm{RW}}(A_r - 2r^2_{\mathrm{RW}} p^2_N)$, which is stable (resp. unstable) if $A_r < 0$ (resp. $A_r > 0$). The corresponding amplitude is $r^2_{\mathrm{RW}} = -\frac{A_r}{2p^2_N}$.

The conditions on the determinant show that the MW branch does not experience steady bifurcations, except at the two end points. The MW solution is stable if $\det(M^{\mathrm{MW}}) > 0$, that is, $p^2_N p^1_\Delta > 0$, and the trace is negative. It is sufficient to ensure that the trace is negative at the end points, a condition equivalent to $A_r > 0$, $p^2_N < 0$, $p^1_\Delta < 0$ and $B_r + A_r < 0$. Otherwise, the MW branch may experience a Hopf bifurcation leading to a 3FW.

Let us now focus on the stability of the MW branch with respect to perturbations in the variable r_0. We see that the MW can bifurcate into a precessing wave solution whenever

$$\lambda_s - l_1 \frac{A_r}{p^2_N} \geqslant 0.$$

In the supercritical case, the PrW connects in parameter space a mixed mode with a modulated wave. Finally, a possible scenario for a bifurcation from PrW towards a three-frequency wave arises whenever Eq. (9d) does not possess a fixed point.

[1] M. Golubitsky and M. Roberts, A classification of degenerate Hopf bifurcations with $O(2)$ symmetry, J. Diff. Equ. **69**, 216 (1987).

[2] J. D. Crawford and E. Knobloch, Symmetry and symmetry-breaking bifurcations in fluid mechanics, Annu. Rev. Fluid Mech. **23**, 341 (1991).

[3] M. Golubitsky and W. Langford, Pattern formation and bistability in flow between counterrotating cylinders, Physica D **32**, 362 (1988).

[4] P. Chossat and G. Iooss, *The Couette-Taylor Problem*, Applied Mathematical Sciences, Vol. 102 (Springer-Verlag, New York, 1994).

[5] M. Golubitsky, J. Swift, and E. Knobloch, Symmetries and pattern selection in Rayleigh-Bénard convection, Physica D **10**, 249 (1984).

[6] J. Sierra, D. Fabre, V. Citro, and F. Giannetti, Bifurcation scenario in the two-dimensional laminar flow past a rotating cylinder, J. Fluid Mech. **905**, A2 (2020).

[7] D. Ormières and M. Provansal, Transition to turbulence in the wake of a sphere, Phys. Rev. Lett. **83**, 80 (1999).

[8] K. Gumowski, J. Miedzik, S. Goujon-Durand, P. Jenffer, and J. E. Wesfreid, Transition to a time-dependent state of fluid flow in the wake of a sphere, Phys. Rev. E **77**, 055308(R) (2008).

[9] R. Natarajan and A. Acrivos, The instability of the steady flow past spheres and disks, J. Fluid Mech. **254**, 323 (1993).

[10] B. Ghidersa and J. Dušek, Breaking of axisymmetry and onset of unsteadiness in the wake of a sphere, J. Fluid Mech. **423**, 33 (2000).

[11] A. G. Tomboulides and S. A. Orszag, Numerical investigation of transitional and weak turbulent flow past a sphere, J. Fluid Mech. **416**, 45 (2000).

[12] J. Sierra-Ausín, M. Lorite-Diez, J. Jimenez-Gonzalez, V. Citro, and D. Fabre, Unveiling the competitive role of global modes in the pattern formation of rotating sphere flows, J. Fluid Mech. **942**, A54 (2022).

[13] D. Fabre, F. Auguste, and J. Magnaudet, Bifurcations and symmetry breaking in the wake of axisymmetric bodies, Phys. Fluids **20**, 051702 (2008).

[14] F. Auguste, D. Fabre, and J. Magnaudet, Bifurcations in the wake of a thick circular disk, Theor. Comput. Fluid Dyn. **24**, 305 (2010).

[15] M. Chrust, G. Bouchet, and J. Dušek, Parametric study of the transition in the wake of oblate spheroids and flat cylinders, J. Fluid Mech. **665**, 199 (2010).

[16] P. Ern, F. Risso, D. Fabre, and J. Magnaudet, Wake-induced oscillatory paths of bodies freely rising or falling in fluids, Annu. Rev. Fluid Mech. **44**, 97 (2012).

[17] P. Fernandes, P. Ern, F. Risso, and J. Magnaudet, On the zigzag dynamics of freely moving axisymmetric bodies, Phys. Fluids **17**, 098107 (2005).

[18] P. C. Fernandes, F. Risso, P. Ern, and J. Magnaudet, Oscillatory motion and wake instability of freely rising axisymmetric bodies, J. Fluid Mech. **573**, 479 (2007).

[19] P. C. Fernandes, P. Ern, F. Risso, and J. Magnaudet, Dynamics of axisymmetric bodies rising along a zigzag path, J. Fluid Mech. **606**, 209 (2008).

[20] F. Auguste, J. Magnaudet, and D. Fabre, Falling styles of disks, J. Fluid Mech. **719**, 388 (2013).

[21] M. Chrust, S. Goujon-Durand, and J. E. Wesfreid, Loss of a fixed plane symmetry in the wake of a sphere, J. Fluid Struct. **41**, 51 (2013).

[22] J. Tchoufag, D. Fabre, and J. Magnaudet, Global linear stability analysis of the wake and path of buoyancy-driven disks and thin cylinders, J. Fluid Mech. **740**, 278 (2014).

[23] J. Tchoufag, D. Fabre, and J. Magnaudet, Weakly nonlinear model with exact coefficients for the fluttering and spiraling motion of buoyancy-driven bodies, Phys. Rev. Lett. **115**, 114501 (2015).

[24] J. Tchoufag, J. Magnaudet, and D. Fabre, Linear instability of the path of a freely rising spheroidal bubble, J. Fluid Mech. **751**, R4 (2014).

[25] P. Bonnefis, D. Fabre, and J. Magnaudet, When, how, and why the path of an air bubble rising in pure water becomes unstable, Proc. Natl. Acad. Sci. USA **120**, e2300897120 (2023).

[26] M. Kotouč, G. Bouchet, and J. Dušek, Transition to turbulence in the wake of a fixed sphere in mixed convection, J. Fluid Mech. **625**, 205 (2009).

[27] P. Meliga, J.-M. Chomaz, and D. Sipp, Global mode interaction and pattern selection in the wake of a disk: A weakly nonlinear expansion, J. Fluid Mech. **633**, 159 (2009).

[28] M. Golubitsky, I. Stewart, and D. G. Schaeffer, *Singularities and Groups in Bifurcation Theory: Volume II*, Vol. 69 (Springer Science & Business Media, 2012).

[29] P. Hirschberg and E. Knobloch, Zigzag and varicose instabilities of a localized stripe, Chaos **3**, 713 (1993).

[30] P. Hirschberg and E. Knobloch, A robust heteroclinic cycle in an O(2) $\times Z_2$ steady-state mode interaction, Nonlinearity **11**, 89 (1998).

[31] G. Mougin and J. Magnaudet, Path instability of a rising bubble, Phys. Rev. Lett. **88**, 014502 (2001).

[32] D. Rand, Dynamics and symmetry. Predictions for modulated waves in rotating fluids, Arch. Ration. Mech. Anal. **79**, 1 (1982).

[33] E. Knobloch, On the degenerate Hopf bifurcation with $O(2)$ symmetry, Contemp. Math. **56**, 193 (1986).

[34] S. A. van Gils and J. Mallet-Paret, Hopf bifurcation and symmetry: Travelling and standing waves on the circle, Proc. R. Soc. Edinburgh A **104**, 279 (1986).

[35] A. S. Landsberg and E. Knobloch, Direction-reversing traveling waves, Phys. Lett. A **159**, 17 (1991).

[36] J. D. Crawford, M. Golubitsky, and W. F. Langford, Modulated rotating waves in $O(2)$ mode interactions, Dyn. Stabil. Syst. **3**, 159 (1988).

[37] M. J. Field, Equivariant dynamical systems, Trans. Am. Math. Soc. **259**, 185 (1980).

[38] J. Guckenheimer and P. Holmes, Structurally stable heteroclinic cycles, Math. Proc. Cambr. Philos. Soc. **103**, 189 (1988).

[39] M. Krupa and I. Melbourne, Asymptotic stability of heteroclinic cycles in systems with symmetry, Ergodic Theor. Dyn. Syst. **15**, 121 (1995).

[40] M. Krupa and I. Melbourne, Asymptotic stability of heteroclinic cycles in systems with symmetry II, Proc. R. Soc. Edinburgh A **134**, 1177 (2004).

[41] I. Melbourne, P. Chossat, and M. Golubitsky, Heteroclinic cycles involving periodic solutions in mode interactions with $O(2)$ symmetry, Proc. R. Soc. Edinburgh A **113**, 315 (1989).

[42] E. Knobloch and M. Silber, Oscillatory convection in a rotating layer, Physica D **63**, 213 (1993).

[43] D. A. Weinberg, Canonical forms for symmetric tensors, Linear Algebra Appl. **57**, 271 (1984).
[44] J. Porter and E. Knobloch, New type of complex dynamics in the 1:2 spatial resonance, Physica D **159**, 125 (2001).
[45] J. Porter and E. Knobloch, Complex dynamics in the 1:3 spatial resonance, Physica D **143**, 138 (2000).
[46] A. Dhooge, W. Govaerts, and Ya. Kuznetsov, MATCONT: A MATLAB package for numerical bifurcation analysis of ODEs, ACM Trans. Math. Softw. **29**, 141 (2003).
[47] M. K. S. Yeung and S. H. Strogatz, Nonlinear dynamics of a solid-state laser with injection, Phys. Rev. E **58**, 4421 (1998).
[48] F. Pétrélis, S. Fauve, E. Dormy, and J.-P. Valet, Simple mechanism for reversals of Earth's magnetic field, Phys. Rev. Lett. **102**, 144503 (2009).
[49] L. P. Shil'nikov, A case of the existence of a countable number of periodic motions, Soviet Math. Doklady **6**, 163 (1965).
[50] P. Glendinnning and C. Sparrow, Local and global behaviour near homoclinic orbits, J. Stat. Phys. **35**, 645 (1984).
[51] L. P. Shilnikov and A. Shilnikov, Shilnikov bifurcation, Scholarpedia **2**, 1891 (2007), revision no. 194931.
[52] E. Knobloch, D. R. Moore, J. Toomre, and N. O. Weiss, Transitions to chaos in double-diffusive convection, J. Fluid Mech. **166**, 409 (1986).
[53] E. Knobloch and D. R. Moore, Minimal model of binary fluid convection, Phys. Rev. A **42**, 4693 (1990).
[54] H. Gan, J. Chang, J. J. Feng, and H. H. Hu, Direct numerical simulation of the sedimentation of solid particles with thermal convection, J. Fluid Mech. **481**, 385 (2003).
[55] P. Mcleod, D. S. Riley, and R. S. J. Sparks, Melting of a sphere in hot fluid, J. Fluid Mech. **327**, 393 (1996).
[56] S. S. Sadhal, P. S. Ayyaswamy, and J. N. Chung, *Transport Phenomena with Drops and Bubbles* (Springer Science & Business Media, 2012).
[57] C. H. Chiang and W. A. Sirignano, Interacting, convecting, vaporizing fuel droplets with variable properties, Int. J. Heat Mass Transf. **36**, 875 (1993).
[58] T. Dessup, L. S. Tuckerman, J. E. Wesfreid, D. Barkley, and A. P. Willis, Self-sustaining process in Taylor-Couette flow, Phys. Rev. Fluids **3**, 123902 (2018).
[59] Y. Bengana and L. S. Tuckerman, Spirals and ribbons in counter-rotating Taylor-Couette flow: Frequencies from mean flows and heteroclinic orbits, Phys. Rev. Fluids **4**, 044402 (2019).
[60] F. H. Busse, Transition to turbulence in Rayleigh-Bénard convection, in *Hydrodynamic Instabilities and the Transition to Turbulence* (Springer-Verlag, Berlin, 1981), pp. 97–137.
[61] I. Mercader, J. Prat, and E. Knobloch, Robust heteroclinic cycles in two-dimensional Rayleigh-Bénard convection without Boussinesq symmetry, Intl. J. Bifurcat. Chaos **12**, 2501 (2002).
[62] E. Stone and P. Holmes, Random perturbations of heteroclinic attractors, SIAM J. Appl. Math. **50**, 726 (1990).
[63] A. Hill and I. Stewart, Hopf-steady-state mode interactions with $O(2)$ symmetry, Dyn. Stabil. Syst. **6**, 149 (1991).